HIGH-PERFORMANCE MICRO-FABRICATED GAS CHROMATOGRAPHY COLUMNS FOR COMPLEX MIXTURE ANALYSIS

by

Shaelah M. Reidy

A dissertation submitted in partial fulfillment
of the requirement for the degree of
Doctor of Philosophy
(Chemistry)
in The University of Michigan
2009

Doctoral Committee:

Professor Richard D. Sacks, Co-Chair (Deceased)
Professor Mark E. Meyerhoff, Co-Chair
Franklin L. Dorman, Restek Corporation, Co-Chair
Professor Robert T. Kennedy
Professor Kensall D. Wise

“Good luck with that”

Dedication

This work is dedicated to Professor Richard D. Sacks, without whom this work could not be possible. His energy, enthusiasm and passion for science inspired and motivated his students. He was an advisor, a teacher, a colleague, and a friend and will be sincerely missed by not only his students and colleagues, but by the entire scientific community. He has taught us all how to be card carrying analytical chemists.

Acknowledgements

I've learned that science is not done in a vacuum, there needs to be influence and inspiration from outside sources. There have been many people who have helped me reach the point I am at today, and for that I am forever grateful.

I would first like to thank my family, who believed I could accomplish this even when I wasn't certain myself. I may not have always expressed it, but I do appreciate the constant questions. I would also like to thank Meghan, Patrick, Ariele, Bailey, Sara, Jen, Hillary, Maggie and everyone else at my home away from home. Thank you for always being there and offering support when I needed it.

Next, I would like to thank all of the past and remaining Sacks lab members for creating a completely unforgettable graduate school experience. We have gone through some of the hardest times together, but I know we all came out stronger and better scientists. I would specifically like to thank Amy Payeur, Cory Fix, Randy Lambertus, Joshua Whiting, Megan McGuigan, PT Stevens, Mark Libardoni, Dr. Shai Kendler, Dr. Juan Sanchez. It definitely wasn't all work and no play. I also offer my sincerest thank you to the members of the μGC team. First to Katharine Beach and Robert Gordenker, you have both been a huge help in helping my finish. Also, Dr. Masuoud Agah, Dr. Willie Steinecker, Becki Veeneman, Dr. Hanseup Kim, with whom I have worked closely, as well as all the members of the WIMS-ERC at the University of Michigan.

I would like to thank the Chemistry Department staff, specifically Aiko Nakatani, especially for always having the full candy bowl. I would also like to thank U of M

Electronics Shop, Don George, the U of M Machine Shop, and Rich Giszczak for all their invaluable advice and assistance.

I would like to acknowledge the University of Michigan- Department of Chemistry, the National Science Foundation Engineering Research Center for Wireless Integrated Microsystems, and NASA for financial support and funding.

I would especially like to thank my graduate committee for all their helpful advice, and guidance especially under such unique circumstances. I thank all those that took me under their wings, Dr. Kensall Wise, Dr. Frank Dorman, and Dr. Mark Meyerhoff, and offered such wonderful support when I needed it the most. I would like to thank Dr. Michael Morris and Dr. Robert Kennedy for their direction.

Lastly, I would like to thank Dr. Richard Sacks, who made all of this work possible. You are missed each and every day.

Table of Contents

Dedication ii
Acknowledgements.....iii
List of Figures vii
List of Tables.....xiii
Chapter
Chapter 1 — Introduction.....1
Introduction.....1
Microfabricated Columns.....7
Theory.....15
Tunable Selectivity.....26
High-Speed Temperature Programming.....31
Comprehensive Two-Dimensional Gas Chromatography.....33
Statement of Purpose.....35
References.....37

Chapter 2 — Static Coated, High Performance Silicon/Glass Micro-Fabricated Columns for Gas Chromatography.....46
Introduction.....46
Experimental.....48
Results and Discussion.....53
Conclusions.....69
References.....71

Chapter 3 — Temperature Programmed Gas Chromatograph using Silicon Microfabricated Columns with Integrated Heaters and Temperature Sensors ….74
Introduction.....74
Experimental.....76
Results and Discussion.....81
Conclusions.....89
References.....91

Chapter 4 — Separation Enhancement by Thermal Tuning using Silicon Microfabricated Columns with Integrated Heaters and Temperature Sensors ….94
Introduction.....94
Experimental.....96
Results and Discussion.....99
Conclusions.....108
References.....110

Chapter 5 - Evaluation and Optimization of Micro-Fabricated Testbed System.112
Introduction……..112
Experimental…….....115
Results and Discussion.....116
Conclusions……..125
References……127

Chapter 6 —Microfabricated GCxGC Development …….....129
Introduction……..129
Experimental…….....134
Results and Discussion.....139
Conclusions……..149
References……152

Chapter 7 —Conclusions…….....156

List of Figures

Figure

1.1 Scanning electron micrographs of 3-m-long channels in a 3.2 cm by 3.2 cm silicon chip: (a) entire chip with connection capillaries drawn in; (b) detail of gas flow turnaround at center of chip; (c) detail of etched-channel structure……..13

1.2 WIMS micro-GC block diagram, the solid arrows indicated the flow path during sampling, the dashed arrows indicated flow path during analysis. (Diagram courtesy of Prof. Edward Zellers)…….15

1.3 Plot of H, B, C_g, and C_s for rectangular cross-section columns (150-μm wide by 250 μm deep and 3-m long) assuming a film thickness of 1 μm using (a) Golay's model and (b) Spangler's model for band dispersion using air carrier gas.....23

1.4 Plot of H, B, C_g, and C_s for rectangular cross-section columns (150-μm wide by 250 μm deep and 3-m long) assuming a film thickness of 0.1 μm using (a) Golay's model and (b) Spangler's model for band dispersion using air carrier gas.....25

1.5 Instrument schematic of dual column ensemble with adjust pressure source at junction point between the two columns. CG, carrier gas; C_1, column 1; C_2, column 2; EPC, electronic pressure controller; P, pressure gauge……30

2.1 Photograph of silicon on glass micro-fabricated columns……..50

2.2 System used for static coating of silicon MEMS columns. Top shows filling configuration, and bottom shows solvent removal configuration…….....…..……..51

2.3 Plots of height equivalent to a theoretical plate versus average carrier gas (air) velocity for a 3-m-long static coated column. 1, plot from equation 1; 2, plot from equation 2.3, 3, plot for experimental data using n-octane at 40^{o}C; 4 and 5, plots 1 and 2 corrected for extra-column band broadening using experimental data and equation 2.4 respectively.....57

2.4 Plots of height equivalent to a theoretical plate versus average carrier gas (air) velocity for a 3-m long static-coated column showing Plot 5 (a) and Plot 3 (b) from Figure 2.3 resolved into the individual band-broadening sources. *B*, longitudinal diffusion; C_g, gas-phase non-equilibrium effects; C_s, stationary-phase non-equilibrium effects; *D*, extra-column band broadening. In (a), the sum of C_g and C_s is shown. In (b) only the sum is shown.....60

2.5 Test chromatograms of a 15-component mixture separated isothermally at 30°C using a 0.5-m (a), 1.0-m (b) and 3.0-m long static-coated columns. Peak numbers correspond to compound numbers in Table 2.2.....62

2.6 Temperature-programmed chromatograms of an n-C_5 to n-C_{12} mixture of normal alkanes using a 3.0-m long column (a) and a 0.25-m long column (b). For (a), programming rates were 30 °C/min (A), 20 °C/min (B) and 10 °C/min (C). For (b), the programming rates were 50 °C/min (A), 30 °C/min (B) and 10 °C/min (C). In all cases, the starting temperature was 30°C and the final temperature was 180°C.....65

2.7 Plots of cumulative peak capacity nc versus retention time for the temperature-programmed separation of a n-C_5 to n-C_{12} normal alkane mixture using a 3.0-m (a) and a 0.25-m (b) long static-coated column. Numbers next to plots give temperature-programming rates in °C/min. In all cases, the starting temperature was 30°C and the final temperature was 180 °C.....66

2.8 Temperature-programmed chromatograms of an air-phase petroleum hydrocarbon mixture (a) using a 3.0-m long column and a mixture chemical warfare and explosive agent markers (b) using a 0.25-m long column. Chromatogram (a) had an initial hold at 30°C for 2 min and then ramped to 180°C at 30°C/min. Chromatogram (b) was ramped at 30°C/min from 40-180°C.....68

3.1 Photograph of 3.0-m long column chip mounted on a substrate and wire bonded to solder terminals. Insets show photomicrographs of integrated heaters and RTD sensors.....78

3.2 Left, diagram of the proportional integral controller used for heating the silicon MEMS columns; right, photographs of the 0.25-m long column wire-bonded to solder terminals on a phenolic support and the control board used for column heating.....80

3.3 Thermal images of 3-m long columns with only one heater operating (right) and with all four heaters operating (left). Temperatures are shown on the gray scales to the right of each image. The two gray scales are not the same.....81

3.4 Temperature versus time plots for the 3-m long column using the proportional integral controller showing simple temperature ramps (a), complex ramps with isothermal intervals (b) and the superimposition of five similar ramps (c). Numbers on plots give the ramp rates in ^{o}C/min.....83

3.5 Chromatograms of an n-C_5 to n-C_{15} mixture using the 3-m long column temperature programmed at 20 ^{o}C/min. (a), 40 ^{o}C/min. (b), and 60 ^{o}C/min (c)....84

3.6 Chromatogram of a 30-component mixture obtained with the 3-m long column temperature programmed at 20 ^{o}C/min. Peak numbers correspond to compound numbers in Table 3.1.....85

3.7 Temperature versus time plots for the 0.25-m long column using the proportional integral controller showing simple temperature ramps (a), complex ramps with isothermal intervals (b) and the superimposition of five similar ramps (c). Numbers on plots give the ramp rates in ^{o}C/min.....87

3.8 Chromatograms of an n-C_5 to n-C_{15} mixture using the 0.25-m-long-column temperature programmed at 100^{o}C/min. (a), 300^{o}C/min. (b) and 1000^{o}C/min (c)89

4.1 A band trajectory plot and chromatogram of a 5-compound isothermal separation on a single three-meter-nonpolar microfabricated column.....100

4.2 A temperature programmed separation of a 10-compound mixture. The column was temperature programmed at 60°C/min. An accompanying band trajectory plot for 9 of the 10 compounds shows good correlation between predicted retention times and actual retention times.....101

4.3 Instrument schematic of thermal tuning system. Sample is injected into a split/splitless inlet (I), and introduced onto the first column (C_1) a 50-cm-nonpolar column, which is temperature programmed using a micro-controller (MC). After separation on the first column, components are separated on the second column (C_2), a 50-cm-polar column and are detected by a flame ionization detector (D).....102

4.4 Band trajectory plot, band position versus time, of a two-component co-elution. Both columns were temperature programmed at the same rate.....104

4.5 Thermally tuned separation of C_{12} and acetophenone. The first column was temperature programmed from 30-70°C at 100°C/min and held at 70°C for 60s and then from 70-100°C at 100°C/min. The second column was temperature programmed from 30-100°C at 100°C/min.....105

4.6 A 14-component multifunctional mixture on a single (a) polar and (b and c) nonpolar column. (a and b) Separation temperature programmed at 100°C/min from 30-100°C with multiple co-elutions on both columns. (c) Separation on nonpolar column temperature programmed from 30-100°C with an isothermal hold at 70°C for 60s.....106

4.7 Temperature programmed separation of 14-component mixture (a) when both columns temperature programmed at the same rate and (b) when there is a 60s isothermal hold at 70°C.....108

5.1 Block diagram of μGC layout with all component parts. Operation is described below.....113

5.2 Photograph of Gen 0.6 system with all of the components that have been evaluated.....117

5.3 Golay plot Gen 0.6 system with a nonpolar column, polar column and fluidic substrate. Optimal velocity was found to be approximately 16 cm/s yielding a minimum plate height of 0.0612 cm. This plate height gives a maximum number of 9800 plates on the system.....118

5.4 Three separations illustrating column performance with the fluidic substrate. Detection is obtained using a commercial FID. All separations are temperature programmed,;separations (b&c) are temperature programmed at the same rate.119

5.5 A 20-component mixture using a μPCF injector, dual columns and fluidic substrate. Detection was obtained using a commercial FID.....121

5.6 Golay plots of dual column system with fluidic substrate and chemiresistor sensor array. The bottom square plot shows the results from just the sensor array. The top diamond plot is from the FID as connected to the tail pipe of the sensor array. Due to the finite response time of the sensor array, there is some band broadening that occurs. The middle plot, is the original Golay plot.....123

5.7 Chromatograms of ten component mixture separated under isothermal conditions. The top plot is the chromatogram from the FID as connected to the tail pipe of the sensor array. The bottom four chromatograms are from the different channels of the sensor array.....124

6.1 Instrument schematics of GCxGC systems. (a) Pneumatic modulation system. First dimension column is a 3-m nonpolar microfabricated column and the second dimension column is a 1-m polar microfabricated column. Modulation is obtained by opening and closing the junction point valve. (b) Thermal modulation system. First dimension column, is a 3-m nonpolar microfabricated column, and the second dimension column is a 0.25-m polar microfabricated column. Modulation is obtained by resistively heating capillary. Details of modulator in text.....136

6.2 Components of thermal modulator housing and modulator cartridge. Photo courtesy of Bruce Block.....137

6.3 One-dimensional separation of a thirteen component mixture separated on two micro-columns. There are multiple co-elutions that occur, compounds 2:4, 5:6:7, 8:9, and 12:13.....140

6.4 GCxGC separation as collected at the detector. A second dimension separation is taking place every 20.5 seconds. Inset shows four second dimension separation slices of three components that would co-elute in one-dimensional GC, but are separated on the second column.....141

6.5 Contour plot of 13-component separation. All 13 components are separated over the separation plane. Peak intensity is illustrated by color.....142

6.6 A thermally modulated one-dimensional chromatogram of the separation of normal alkanes, C_6-C_{10}, and ketones, C_3-C_7. Inset shows the separation of pentanone and n-nonane. When this separation is not modulated these two components would perfectly co-elute.....144

6.7 Contour plot of a thermally modulated separation. The contour plot shows the structure that result from a GCxGC separation. The peaks along the bottom are the nonpolar alkanes, and along the top are the polar ketones.....145

6.8 Column performance at different channel dimensions. All columns have the equivalent internal diameter of 100μm i.d. column. The narrower the column width, the better the column performance.....147

6.9 A plot of pressure versus number of theoretical plates at different column dimensions. The best column has the narrowest width, and the worst column is the current column configuration.....148

List of Tables

Table

1.1 Models for band dispersion in gas phase separations.....22

2.1 Column properties for the different column lengths.....49

2.2 List of compounds for 15 component chromatograms.....52

2.3 Component list for applications chromatograms and their boiling points (in °C).68

3.1 Component list for 30-component separation.....86

4.1 Components from 14-component mixtures and their boiling points (in °C).....107

5.1 Components from 11 component separation and their boiling points (in °C).....119

5.2 Components from the 20 component mixture and their boiling points (in °C)...121

5.3 Components from the 10 component mixture and their boiling points (in °C)...125

6.1 List of thirteen components and their boiling points (in °C).....140

Chapter 1

Introduction

Introduction

Gas chromatography (GC) is the most widely used technique for the separation and quanitification of volatile and semi-volatile organic compounds. Volatile and semi-volatile organic compounds (VOCs and SVOCs) are of concern for numerous reasons, including indoor and ambient air quality, climate change (global warming), industrial emissions control, and breath analysis. Measurements of these pollutants are essential to assessing sources, sinks, and transport pathways as well as their effects on environments and their inhabitants. Where the characterization of complex VOC mixtures is necessary, a separation step is required.

There has been increasing interest in the development of field portable GC systems which require faster analysis times. With conventional GC, there is the major disadvantage of long analysis times. Extended sample analysis time, which is common for industrial and contract laboratories, results in decreased sample throughput and increased sample analysis cost. High speed gas chromatography (HSGC) has become and important tool for the rapid analysis of relatively simple mixtures of organic

compounds. The application of HSGC to field portable instrumentation would allow for the decrease in analysis times while maintaining quality separations.

Investigation of capillary columns for HSGC applications began shortly after the advent of the wall coated open tubular column by Golay in 1957[1]. There has been an increasing focus on higher sample throughput for GC. Relative to packed columns, wall coated open tubular columns allowed for exchanging separation resolution for faster analyses. A major milestone in the push toward faster analyses was the introduction of microbore columns[2,3], leading to use of shorter columns operated with higher linear velocities to reduce analysis times[4,5].

HSGC Inlets

More recent improvements in high speed separations have focused on generating narrow injection plugs[6,7,8], enhancing selectivity using dual column systems[5,9,10,11,12,13,14], and increasing temperature programming rates[15,16,17]. Due to the drastically increased effects of inlet and detector dead times in high speed separation systems, research has been dedicated to the development of inlet devices capable of generating narrow injection plugs. High-speed diaphragm valves in series with conventional split/splitless injectors have generated ~20 ms injection plugs[18,19,20].

In the "load" position a 1-µL sample loop on the six-port valve fills with effluent from the split/splitless inlet on the GC, while exhaust from the loop passes to a vent. In the "inject" position, the sample loop volume is delivered to the column using an auxiliary helium carrier gas supply operating at a very high volumetric flow rate. The valve remains in the inject position for 20 ms before rotating back to the "load"

position[21]. This valve based injection system was later modified to a synchronized dual-valve injection that can generate injection plug widths of 3.3 ms. The instrument uses the same configuration as the previous work, with the second high-speed diaphragm valve being connected downstream of the first. After actuation of the first valve, the 20 ms plug enters the sample loop of the second valve where the valve is set to the "load" position for only a portion of this 20 ms, resulting in much narrower injection plugs[21].

Many of the analytes of interest in environmental surveillance are present at trace levels and a sample preconcentration step may be necessary for detection. The growing demand for on-site environmental monitoring is driving the development of field-portable instrumentation that can reduce analysis times as well as the risks of sample loss and contamination during transport and storage associated with conventional methods involving separate sampling and laboratory analysis steps. Sorption based preconcentrators for the collection of organic compounds from large-volume vapor samples address many of these issues[22,23,24,25,26,27]. Sorption traps often use a graded series of carbon-based adsorbents arranged so that during sampling, gas flow is in the direction from the lowest to the highest surface area adsorbent, pulling out components based on their boiling point. Prior to thermal desorption and injection onto the chromatographic column, gas flow in the trap is reversed. Injection plug widths vary from 0.7 s for pentane to several seconds for higher boiling point components[25,26]. By evaluating the effects of trap heating rates and carrier gas flow rates, injection band widths for pentane and undecane were reduced to 89 and 520 ms, respectively[28]. Carrier gas flow rates through the trap are varied by introducing a downstream split vent that decreased transport time between the trap and the column, thus reducing injection plug

band widths. The use of cryogenic cooling on a bare metal traps or the head of the column to refocus the desorbed injection plug has been shown to reduce injection plug band widths to as low as ~6 ms[29,30,31] unfortunately the consumption of cryogenic gases prevents the development of field-portable instrumentation using these types of inlets.

HSGC Separation Enhancements

Methods of compensating for losses in column resolution associated with shorter columns and higher carrier gas flow rates include tunable and programmable column selectivity. Column selectivity can be tuned through either the use of mixed stationary phases[32,33], or by coupling in-series two wall coated open tubular columns with differing stationary phases[10,11,12,13, 14,15,34]. The relative contribution of each stationary phase in the column ensemble can be adjusted by varying the column lengths, film compositions and thicknesses, or by changing the hold-up time for each of the columns. The hold-up times for each of two columns in an ensemble can be altered using an electronic pressure controller at the junction point of the two columns. By changing the pressure at this point, the pressure drop along each of the columns changes, shifting the carrier gas flow rates and altering the fractional contribution of each column in the ensemble to the overall separation.

An alternative to pneumatic selectivity enhancement is application of differential thermal pulsing[35]. Traditionally, power constraints have limited this type of selectivity enhancement to laboratory applications. More recently however, column heating structures have been designed that allow for temperature programming rates greater than 20°C/s while consuming far less power than standard convection ovens[36,37,38]. These

low-thermal-mass column structures also enable rapid cool down, reducing cycle times. The relative contribution of two columns connected in series can be altered by rapidly heating the second column just before a targeted component enters it. The increase in temperature reduces component retention, increasing band migration velocities for components on the second column. The second column must be rapidly cooled before the second component of a targeted set crosses the junction point. The cooler temperature experienced by the second component will reduce its band migration velocity and introduce a time window in the ensemble retention times of the targeted pair without significantly affecting other components in the mixture. This work led to the introduction of a band acceleration device (BAD), where only the first segment of the second column is heated and cooled. Here, a metal sheath surrounds the segment allowing for rapid heating, while compressed air is used for cooling[39].

Detectors

With relatively short columns and fast analysis, analyte bands eluting from a chromatographic column are significantly narrower than with conventional GC, requiring fast detectors and data acquisition. Most laboratory high-speed GC has been done with flame ionization detection (FID), that typically has a response time of less than a few milliseconds. Dead volumes from FIDs are also negligible. The gold standard in high-speed detection has been the time-of-flight mass spectrometer (TOF-MS). The instrument has extremely high spectral acquisition rates, at least several hundred full-mass-range spectra per second, which allow for tracking of narrow chromatographic peaks[40]. It also offers spectral continuity, referring to the fact that ion abundance ratios

are the same for all points on the peak. These constant ion abundances allow for changes in the ratios, to act as the basis for spectral deconvolution for overlapping peaks, thus taking some of the separation burden off of the column[41].

The increasing effort in recent years for the miniaturization of analytical instruments has brought forth significant contributions in the development of field-portable and microfabricated detectors. Due to their ability to scale well, simplicity and ease of fabrication, micro-fabricated thermal-conductivity detectors (TCD) have been developed. Temperature constraints and poor minimum detectable limits, however, can be problematic for some applications[42,43,61]. TCD's are also not suitable for operation in air due to the similarity in the thermal conductivity of air and that of most organic compounds.

Selective detection to provide enhanced component identification, and in some cases, to provide for deconvolution of overlapping peaks in targeted analysis applications has received considerable attention to increase the utility of micro-fabricated columns. Notably, micro-fabricated arrays of polymer-coated surface acoustic-wave (SAW) devices[5,44,45,46] and chemiresistor devices[47,48,49,50] have been used as detectors for GC. Identification is based on the relative sensitivities of each sensor in the array to each component[48].

The development of field-portable instrumentation not only calls for reductions in size and power, but also for reductions in the amounts of consumables required for operation. Portable GC systems have been highly dependent on carrier gas tanks or hydrogen generators to supply transport gas. Work has been done using vacuum outlet GC with atmospheric pressure air as the carrier gas to relieve instruments of these bulky

tanks, enabling long-term operation without the need to replenish consumables[5,51,52,53,54,55].

Many current field portable GCs suffer from poor selectivity and resolution, lack speed, and are power hungry, resulting in inadequate analyses. Transferring current separation strategies from bench-top instruments to portable and microfabricated systems is a demanding task. Previous work integrating these strategies in portable systems has led to drastic losses in peak capacity, resolving power, and powers of detection resulting in unsatisfactory analyses.

Microfabricated GC Columns

The miniaturization of analytical systems as a means of reducing instrumentation and analysis costs and for the development of novel applications which benefit from small instrument size has been ongoing for nearly 30 years. The work presented in this dissertation builds on those previous efforts. It is important not only to realize that parallel projects on similar work exist, but to draw from them and to learn from their results. A review covering the development of micro-GC is presented below, including significant contributions and pitfalls.

The earliest reports of a microfabricated gas chromatograph are by Angell and Terry[56,57] at Stanford University, who proposed an instrument the size of a box of matches. The instrument they developed fit on a single 5-cm diameter silicon wafer, and consisted of an etched silicon column, gas sample loop, thermoconductivity detector, and valve seats. The end product was an instrument with poor column performance, which led to the replacement of the microfabricated column with a conventional fused-silica

capillary column. Commercial instruments based on this prototype are still being marketed[58,85].

The development of various aspects of miniaturized vapor analysis instruments has been explored at several national laboratories and universities[4,59, 60,61,62,63,64,65,66], and several portable systems are commercially available[58,67,68]. Traditionally, miniaturized instruments have relied on relatively short columns and are designed for specialized applications such as hazardous substance analysis[60,62,63,65], chemical process monitoring[4,59], and clinical diagnostics[64]. Microfabricated columns etched in silicon, metal, or polymer substrates have been explored. Etching processes have included deep reactive ion etching[60,62,63] wet chemical etching[59,61], and high energy laser etching[66]. In most cases the columns have had relatively low resolving power, and were inadequate for complex mixture analysis.

Kolesar and Reston reported on a microfabricated GC system interfaced with a miniature sample injector[61]. Their methods were unique in that column stationary phase deposition took place before bonding the glass cover plate to the etched silicon substrate. They used conventional patterning techniques to deposit a thin layer of copper phthalocyanine along a 300-µm wide by 10-µm deep, 0.9-m long micromachined column. A miniature sample injector incorporating a 10 µL sample loop and a dual detector scheme using a copper phtalocyanine chemiresistor and a thermal conductivity detector bead were used in a single cavity. Separations of ammonia and nitrogen dioxide used helium carrier gas and required 30 minutes. Overall system resolution was extremely poor and separation speeds were an order of magnitude slower than desired.

More recent work on microfabricated vapor analysis systems derives from a Micro Gas Analyzer (MGA) DARPA initiative (http://www.darpa.mil/mto/mga/) and two European start-up companies, SLS Micro Technology (http://www.sls-micro-technology.de/) and C2V (Concept to Volume, http://www.c2v.nl/). The MGA project is currently funding research at Sandia National Labs, Honeywell, and the University of Illinois. The instruments being developed are designed for the detection of chemical warfare agents in military applications. Work has not been published from either the Illinois or the Honeywell efforts.

Sandia's micro-GC design incorporates a microfabricated sample pre-concentrator based on a resistively heated sol-gel coated membrane that can heat to 200°C in 4 ms, while generating ~200 ms wide desorption bands[63]. Concentration factors of 100-500 for dimethyl methyl phosphonate (DMMP) have been achieved with this device, showing preferential selectivity over interfering compounds of a factor of 25[69]. Their chromatographic column is a spiral channel fabricated in a silicon substrate with dimensions of 100-µm wide by 400-µm deep. The columns are typically 86-cm long and fit on a 1.44 cm^2 silicon chip. Separations of 6 components in less than 1 minute have been shown using these columns with FID[63]. They have done a significant amount of work on surface acoustic wave sensors due to their high sensitivity and unique response patterns[62,63,69].

Work by Overton at Louisiana State University ties into the Sandia MGA effort. The LSU effort focuses on the fabrication and evaluation of high aspect ratio nickel GC columns. The columns are fabricated using a LIGA process and are 30-50µm wide by 400-650 µm deep and range in length from 0.5 -2 m[70]. The columns were integrated with

a microFast GC (Analytical Specialists, Baton Rouge, Louisiana) and separations of 7 chemical warfare agent simulants and interferents in less than 4 s have been demonstrated[71]. The microFast GC platform is about the size of a shoebox and weighs ~12 pounds. Sample injection is accomplished using either syringe or valve inlets, where it is delivered to an adsorbent trap for preconcentration. The sample is then injected to dual 100 μm i.d., 1-m long capillary columns with at-column heating capability before reaching dual FIDs. The instrument consumes 50mL/min hydrogen and requires 100 W average power at 24 volts dc[72].

SLS Micro Technology incorporates a 9 x 6 cm etched silicon fluidic substrate with a sliding valve based sample injection loop for 500 nL injection volumes. A thermal conductivity detector with a response time of less than 200 nsec and a sensitivity of 7ppm for propane in helium is fabricated on-chip. The separation columns are ~1-m long with a cross-section equivalent to a 60-μm i.d. round capillary column, and can be heated to 200°C within 20 s using 5 W average power. The columns are coated using plasma enhanced vapor deposition with a range of siloxane backbone stationary phases, and have been shown to baseline resolve methane and ethane[73]. The instrument has an on-board carrier gas supply, with an estimated consumption of 100μL/min. It operates using a 12-V supply and requires 10 W of power on average. The instrument is not designed for field applications. Recently, work developing a packed separation column using carbon nano-tubes for the separation of fixed gases was initiated[74]. Using a 50-mm long carbon nano-tube coated column, SLS has demonstrated the separation of methane and carbon dioxide.

Concept to Volume (C2V) markets a micro-GC module that acts as a fluidic integration platform. The module includes a microvalve based injection, a commercial 50-μm i.d. capillary column, a thermal conductivity detector, and has a total volume of ~250cm^3. The instrument operates on 3 W average power and uses an on-board carrier gas supply with no micro-pump. This instrument is being developed as a portable GC for fast analysis of toxic industrials chemicals and chemical warfare agents. Performance of the module has been demonstrated with separations of natural gas and BTEX samples in less than 20s with injection plug widths of less than 200ms[75]. The instrument is however, limited to isothermal operation, limiting the boiling point range of components that can be separated during a single analysis.

The Engineering Research Center (ERC) for Wireless Integrated MicroSystems (WIMS) at the University of Michigan is currently working to develop a completely microfabricated gas chromatograph for environmental monitoring[47,76,77]. The instrument uses preconcentration[78,79,80], separation[5,12,13,14,16,17,24,53,54], and gas sensing[48,49] technologies that were developed by members of the WIMS μ-GC team. The instrument is designed for autonomous operation using ambient air as the carrier gas and a micro-fabricated pump[81,82] to drive the separation. A critical part of this ongoing initiative is the development of the microfabricated separation columns. Adequate resolving power to separate 30-50 volatile organic compounds per analysis and low thermal mass for low-power temperature programming are performance goals set for the analytical columns. The entire instrument, including the columns, relies on silicon microelectromechanical systems (MEMS) technologies.

The microfabricated columns are made using a deep reactive ion etching (DRIE) process that creates a 150-μm wide by 240-μm deep rectangular cross section channel for column lengths of 25 cm, 50 cm, 1 m, and 3 m. Images of the 3-m long columns are shown in Figure 1.1. A double square spiral geometry with two parallel channels connected at the center of the chip by a flow direction turnaround help to minimize chip surface area (Figure 1.1 (b)). Columns (3-m long) are etched on a 3.2-cm by 3.2-cm section of a standard 4-in. silicon wafer, with four columns being fabricated simultaneously. Ports for fused silica connecting lines are etched at opposite ends of each column with dimensions of 350-μm wide by 300-μm high to accommodate 100-μm i.d., 245-μm o.d. deactivated fused silica connecting lines. After etching the channel in silicon it is sealed with a Pyrex 7740 wafer by low pressure anodic bonding at 400 °C with a force of ~200 N[83,84,85,86]. A 4-mm silicon edge around the column allows for attachment of fluidic connection lines, integration of heaters and pressure and temperature sensors, and electrical connections to the chip. The heaters and temperature sensors are simple electrical resistors created by evaporating and patterning 250Å/500Å Ti/Pt on the back of the silicon wafer. A single heater is patterned on all four sides of the column to suppress any temperature gradient created by the location of the heaters. The high thermal conductivity of silicon helps to ensure high temperature uniformity over the surface area of the column[85].

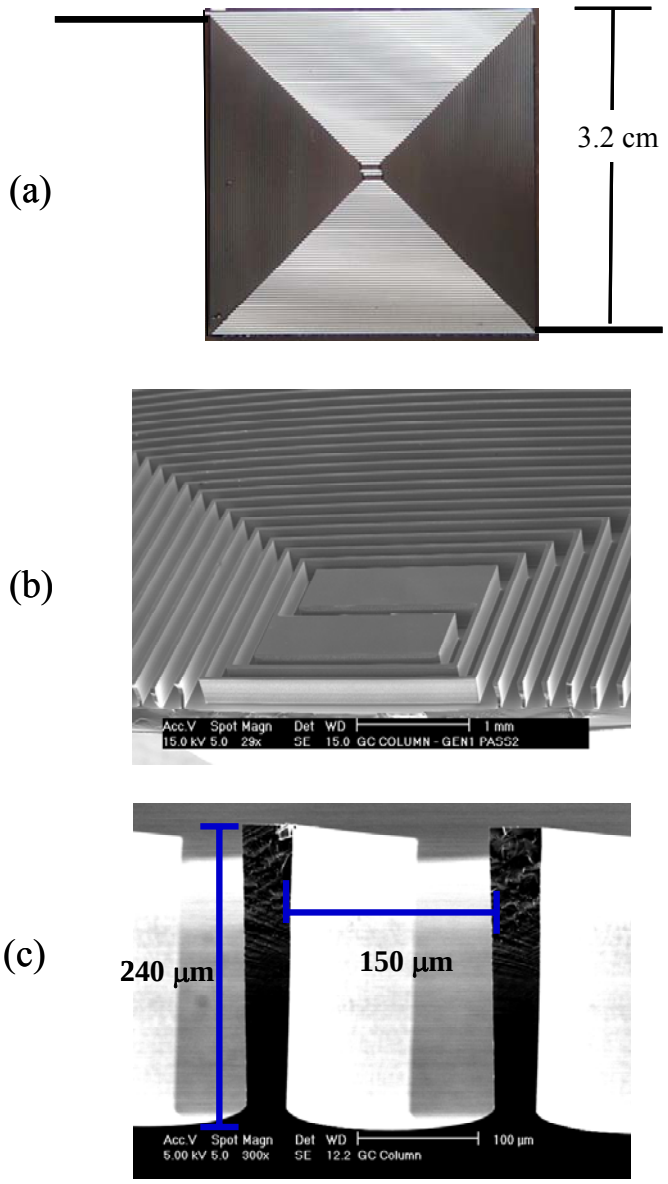

Figure 1.1 Scanning electron micrographs of 3-m-long channels in a 3.2 cm by 3.2 cm silicon chip: (a) entire chip with connection capillaries drawn in; (b) detail of gas flow turnaround at center of chip; (c) detail of etched-channel structure.

In addition to power constraints of the battery-powered autonomous instrument, modeling of the MEMS vacuum pump that will be used to drive the separation suggests that the maximum pressure drop along the column will be about 0.5 atm[87]. This constraint coupled with the relatively high viscosity of air limits the pneumatic restriction

of the channel to relatively small values if adequate carrier-gas velocities and volumetric flow rates are to be achieved.

Figure 1.2 shows a simplified block diagram of the most recent version of the fluidic substrate for the 10 year vision of the WIMS micro-GC. In the sampling mode (solid arrows), the microfabricated valves[88] are flipped by an electrostatic peristaltic micropump[81,82] to the appropriate positions to allow organic compounds in large volume air samples to flow through the particle filter[89]. The manually packed, three-stage μPCF will quantitatively capture components on a series of three porous, carbon-based adsorbents, arranged in order of increasing specific surface areas[78,79,80]. The internal standard is designed to generate vapor at a constant rate by passive diffusion from a liquid reservoir. Analysis of this standard provides the means to compensate for aging, drift, or other factors that might affect analytical performance[90].

In the analysis mode (dashed arrows), the valves switch to redirect the flow path through a series coupled ensemble of microfabricated columns. A second particle filter now acts to protect the vacuum pump. The PCF is rapidly heated to thermally desorb the sample as a narrow injection plug. A pneumatic restriction in the gas flow path towards the inlet splits the sample as it enters the separation column, further narrowing the injection plug width.

The two 1-m-long MEMS columns use different stationary phases and have independent temperature control providing for several modes of programmable selectivity. The stop-flow bypass valve are used to nearly stop the carrier gas flow in C_1 for short intervals in order to enhance the separation of sample component pairs that are separated by the first column but coelute from the column ensemble. This will be

described in detail. Column C_1 uses a non-polar PDMS stationary phase, and C_2 uses a moderately polar trifluoropropylmethyl polysiloxane phase.

An integrated array of eight chemiresistors is used as the μGC detector. The chemiresistors are designed to produce a set of partially selective responses to components eluting from the column ensemble. It employs interfacial films of Au-thiolate monolayer-protected nanoclusters whose resistances shift upon sorbing vapors[48,49,91]. The response patterns are combined with column retention times to identify the specific vapor, and the magnitude of the responses from the sensors is used for quantitative analysis[24,48,49].

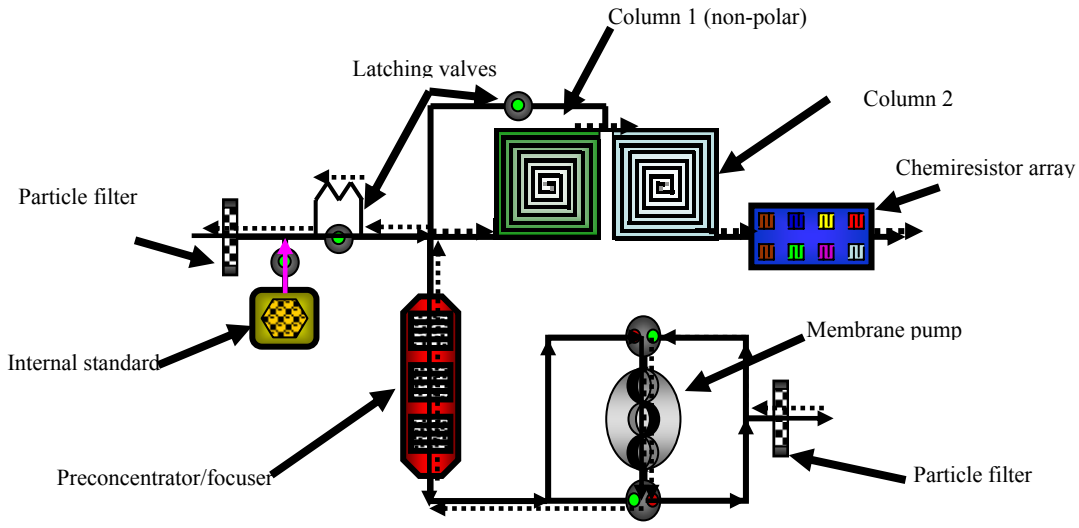

Figure 1.2 WIMS micro-GC block diagram, the solid arrows indicate the flow path during sampling, the dashed arrows indicate flow path during analysis. (Diagram courtesy of Prof. Edward Zellers)

Theory

Column Resolution. In general, the short column lengths associated with micro-fabricated GC systems reduce chromatographic efficiency. Column efficiency is defined

as the length of column required to obtain a separation equivalent to that occurring under equilibrium conditions in a separatory funnel for a specified distribution ratio (ratio of the concentration of the analyte in the stationary phase over the concentration of the analyte in the mobile phase) and phase volume ratio (ratio of the volume of the mobile phase to the volume of the stationary phase). This length of column is termed the height equivalent to a theoretical plate, *H*, smaller values of *H* are associated with greater column efficiency.

Although *H* defines column efficiency, the number of plates *N* in a column defines the resolving power of the column and is related to *H* as follows[92]:

$$N = \frac{L}{H} \tag{1.1}$$

where *L* is the length of the column. It can also be determined from an isothermal analysis using equation 1.2[92]

$$N = 5.545\left(\frac{t_r}{w_{1/2}}\right)^2 \tag{1.2}$$

where t_r is the retention time for a component and $w_{1/2}$ is the full width at half height for the component peak.

The most frequently used measure of separation quality is the resolution, *R*, defined as the ratio of the separation of the peak apexes to the average base width (4σ) for two adjacent peaks. For an isothermal separation *R* is defined by the Pernell Equation (equation 1.3)[93]

$$R = \left(\sqrt{\frac{N}{16}}\right)\frac{\Delta K}{K_a}\frac{k_a}{k_a + 1} \tag{1.3}$$

where ΔK is the difference in the distribution ratios for the two components, K_a is the average of the distribution ratios, and k_a is the average retention factor. A retention factor in chromatography is the ratio of the amount of time a component spends in the stationary phase relative to the amount of time it spends in the mobile phase, and defines the rate of migration of a component through a column. The first term of Equation 1.3 takes into account the resolving power of the column, indicating the need to maximize the number of theoretical plates on the column. The second term reflects the need for a large enough difference in distribution ratios. The third them shows the necessity to operate in a temperature regime where k_a+1 is significantly different from k_a ($k_a \sim$ 1-10). Column temperature effects on analyte retention factors are described by the van't Hoff relation. Plots are relatively linear over a limited temperature range, and a general rule is that a 15-20°C increase in column temperature results in a twofold decrease in analyte retention factors[94].

Peak Capacity. Shorter columns can lead to significant reductions in peak capacity, limiting the ability to do complex mixture analysis. Peak capacity n_p is defined as the number of perfectly spaced peaks that will fit in an isothermal chromatogram with a specified resolution R_s,[94]

$$n_p = 1 + \left(\frac{1}{4R_s}\right)\left(\sqrt{\frac{L}{H}}\right)\ln\left(\frac{t_{rl}}{t_m}\right) \qquad (1.4)$$

where t_m is the time it takes an unretained peak to elute from the column, and t_{rl} is the elution time of the last eluting component. The analysis time for an isothermal separation is determined by t_{rl},[95]

$$t_{rl} = \frac{L}{u}(k+1) \qquad (1.5)$$

where u is average linear carrier gas velocity. A reduction in column length of an order of magnitude in a microfabricated instrument can produce a corresponding order of magnitude reduction in overall analysis time.

Column Efficiency. It is important to note that the peak capacity expression assumes H is constant over the length of the separation, which holds true only for isothermal separations. H for round-cross-section wall coated open tubular capillary columns is given by the expanded Golay equation[96],

$$H = \frac{2D_g}{u} f_1 f_2 + \frac{1+6k+11k^2}{24(k+1)^2} \frac{r^2}{D_g} \frac{f_1}{f_2} u + \frac{2}{3} \frac{k}{(k+1)^2} \frac{{d_f}^2}{D_s} u + \frac{\Delta t^2 u^2}{L(k+1)^2} \qquad (1.6)$$

where D_g is the binary diffusion coefficient in the gas phase, f_2 is the Martin-James gas compression coefficient, f_1 is the Golay-Giddings gas compression coefficient, r is column radius, d_f is stationary phase film thickness, D_s is the binary diffusion coefficient in the stationary phase, Δt is instrumental dead time and accounts for dead volumes in the inlet, connection lines, and detector, the finite time required to produce the analyte vapor in the inlet, and the time required to measure and receive the detector signal. The shortened form of the Golay equation is:

$$H = \frac{B}{u} f_1 f_2 + (C_g \frac{f_1}{f_2} + C_s) u + D_{ec} u^2 \qquad (1.7)$$

where the B term, accounts for band broadening due to longitudinal diffusion during the time spent in the separation column; the C_g and C_s terms account for band broadening due to resistance to mass transport in the gas and stationary phases, respectively; the C_g term is related to the distance in the gas phase traveled by an average analyte molecule while another molecule is in the stationary phase; and the D_{ec} term accounts for all extra-column sources of band broadening.

The gas compression factors f_1 and f_2 are defined in equations 1.8 and 1.9 respectively, where P is the ratio of the column inlet pressure to the outlet pressure[94].

$$f_1 = \frac{9}{8}\frac{\left(P^4 - 1\right)\left(P^2 - 1\right)}{\left(P^3 - 1\right)^2} \tag{1.8}$$

$$f_2 = \frac{3}{2}\frac{\left(P^2 - 1\right)}{\left(P^3 - 1\right)} \tag{1.9}$$

The average linear carrier gas velocity, u, is defined by equation 1.10,

$$u = u_o f_2 \tag{1.10}$$

where u_o is the carrier gas velocity at the outlet of the column, defined by equation 1.11[94].

$$u_o = \frac{r^2 p_o \left(P^2 - 1\right)}{16\eta L} \tag{1.11}$$

Here p_o is the outlet pressure and η is the carrier gas viscosity at the column temperature.

The dead times of the inlet and the detector are a function of their respective dead volumes and the local carrier gas flow rate given by equation 1.12

$$\Delta t = \frac{V_z}{F_z} = \frac{V_z}{u_z A_z} \tag{1.12}$$

where V_z is the dead volume at position z along the analyte flow path, F_z is the volumetric flow rate at position z, and A_z is the cross sectional area..

The dead volume of the detector is only a problem for closed cell detectors like photoionization and sensor array detectors, where a finite volume must be flushed before a response is produced. One of the main contributors to extra column band broadening in microfabricated instruments tends to be the inlet. The effects of dead volumes in injection systems in microfabricated systems are magnified due to the use of short columns and short analysis times. Electronic contributions to the D_{ec} term arise from

electrometer and detector time constants, and are not usually large contributors to system dead time.

The two critical parameters of a separation column are the minimum plate height (maximum resolution), H_{min}, and the optimal operating velocity, u_{opt}. Neglecting the C_s and D terms and f_1, differentiation of Equation 1.6 gives[94].

$$H_{\min} = r\sqrt{\frac{1+6k+11k^2}{3(k+1)^2}} \tag{1.13}$$

$$u_{opt} = \frac{D_g f_2}{r}\sqrt{\frac{48(k+1)^2}{1+6k+11k^2}} \tag{1.14}$$

Equation 1.13 and 1.14 clearly illustrate the importance of smaller diameter columns for high efficiency and fast analysis. Note that H_{min} is independent of the choice of carrier gases for thin films where the C_s term is negligible. Large u_{opt} values are important for high speed analysis since they allow for higher carrier gas flow rates without losses in column efficiency. The dependence of u_{opt} on the choice of carrier gas is shown in equation 1.14 by the inclusion of the diffusion coefficient, and reflects the preference for the lighter molecular weight gases like hydrogen or helium.

A critical design parameter in the development of field-portable instrumentation is the choice of carrier gas. Atmospheric air is not a popular choice as a carrier gas for GC, but is necessary for the development of a completely autonomous instrument. The major benefit of using atmospheric air as a carrier gas is that it alleviates the system of bulky hydrogen or helium tanks. The drawback is that some stationary phases rapidly deteriorate in air, limiting the maximum operating temperature of the chromatographic columns. Previous studies have shown that the PDMS and trifluoropropylmethyl polysiloxane stationary phases used here are stable in air to 200°C[97]. Another

disadvantage of using air carrier gas is the high viscosity and relatively small binary diffusion coefficients for organic compounds in air that result in low optimum carrier gas velocities and rapid loss of efficiency at gas velocities higher than optimum. Using air carrier gas under high-speed conditions, H is shown to increase rapidly with increasing average linear carrier gas velocity, resulting in a loss of resolution at operating velocities substantially above u_{opt}.

Golay modified his work in 1981 to accommodate rectangular channels such as those created by deep reactive ion etching[98]. Equation 1.6 is modified to,

$$H = \frac{2D_g}{u} f_1 f_2 + \frac{(1 + 9k + 25.5k^2)}{105(1+k)^2} \frac{uw^2}{D_g} \frac{f_1}{f_2} + \frac{2}{3} \frac{k}{(k+1)^2} \frac{(w+h)^2 d_f^{\,2}}{D_s h^2} + \frac{\Delta t^2 u^2}{L(k+1)^2} \quad (1.15)$$

where w is the channel width, and h is the channel depth. This equation was derived using an elliptical approximation to estimate u and closely resembles the round-cross-sectional form of the Golay equation (Equation 1.6) with the differences illustrated in Table 1.1.

More recently Spangler[99] analyzed the same problem using an approximate velocity profile and derived a solution similar to that of Golay for H in rectangular cross section channels. He later derived a simplified equation for high-aspect-ratio (h>>w) columns[100]. Giddings derived a model for band dispersion in rectangular columns using a liquid mobile phase. The model was later modified[101] for gas phase separations by adding gas compression terms to account for the pressure drop along the column.

Modeling of band dispersion in micro-channels for gas-phase separations is still ongoing and several variations of these models can be found in the literature[102,103,104]. The work here will rely on comparisons of experimental data to the Golay and Spangler models for band dispersion in rectangular channels.

Table 1.1 Models for band dispersion in gas phase separations.

Reference	B term	C_g term	C_s term	D term
Golay[96] (round)	$2D_g$	$\frac{1+6k+11k^2}{24(k+1)^2}\frac{r^2}{D_g}$	$\frac{2}{3}\frac{k}{(k+1)^2}\frac{{d_f}^2}{D_s}$	$\frac{\Delta t^2}{L(k+1)^2}$
Golay[98] (rect.)	$2D_g$	$\frac{(1+9k+25.5k^2)}{105(1+k)^2}\frac{w^2}{D_g}$	$\frac{2}{3}\frac{k}{(k+1)^2}\frac{(w+h)^2{d_f}^2}{D_s h^2}$	$\frac{\Delta t^2}{L(k+1)^2}$
Spangler[99] (rect.)	$2D_g$	$\frac{(0.9+2k+35k^2)}{96(k+1)^2}\frac{w^2}{D_g}$	$\frac{2}{3}\frac{k}{(k+1)^2}\frac{{d_f}^2}{D_s}$	$\frac{\Delta t^2}{L(k+1)^2}$
Giddings[101] (rect.)	$2D_g$	$\frac{(1+9k+25.5k^2)}{105(k+1)^2}\frac{w^2}{D_g}$	$\frac{2}{3}\frac{k}{(k+1)^2}\frac{{d_f}^2}{D_s}$	$\frac{\Delta t^2}{L(k+1)^2}$

The contributions to band dispersion for the Golay and Spangler models are presented in Figure 1.3 using air carrier gas for the column dimensions (150 μm-wide by 250 μm-deep and 3-m long). The *B, C_g,* and C_s terms are shown as well as *H* for (a) the Golay model and (b) the Spangler model assuming a stationary phase film thickness of 1.0 μm. There are several key differences highlighted by these plots. Most notably, the Spangler model predicts the efficiency of the column (H_{min}) to be greater, 14000 theoretical plates compared to the Golay theory, 12000 theoretical plates, nearly a ~14% difference. The Golay model also predicts the u_{opt} value to be slightly lower than the Spangler model, 13.5 compared to 15.0 cm/s, a difference of ~10%. It is also important to point out that the relative contributions of the C_g and C_s terms differ drastically. Under thick-film conditions (film thickness/column i.d. >1/1000), the Golay model attributes

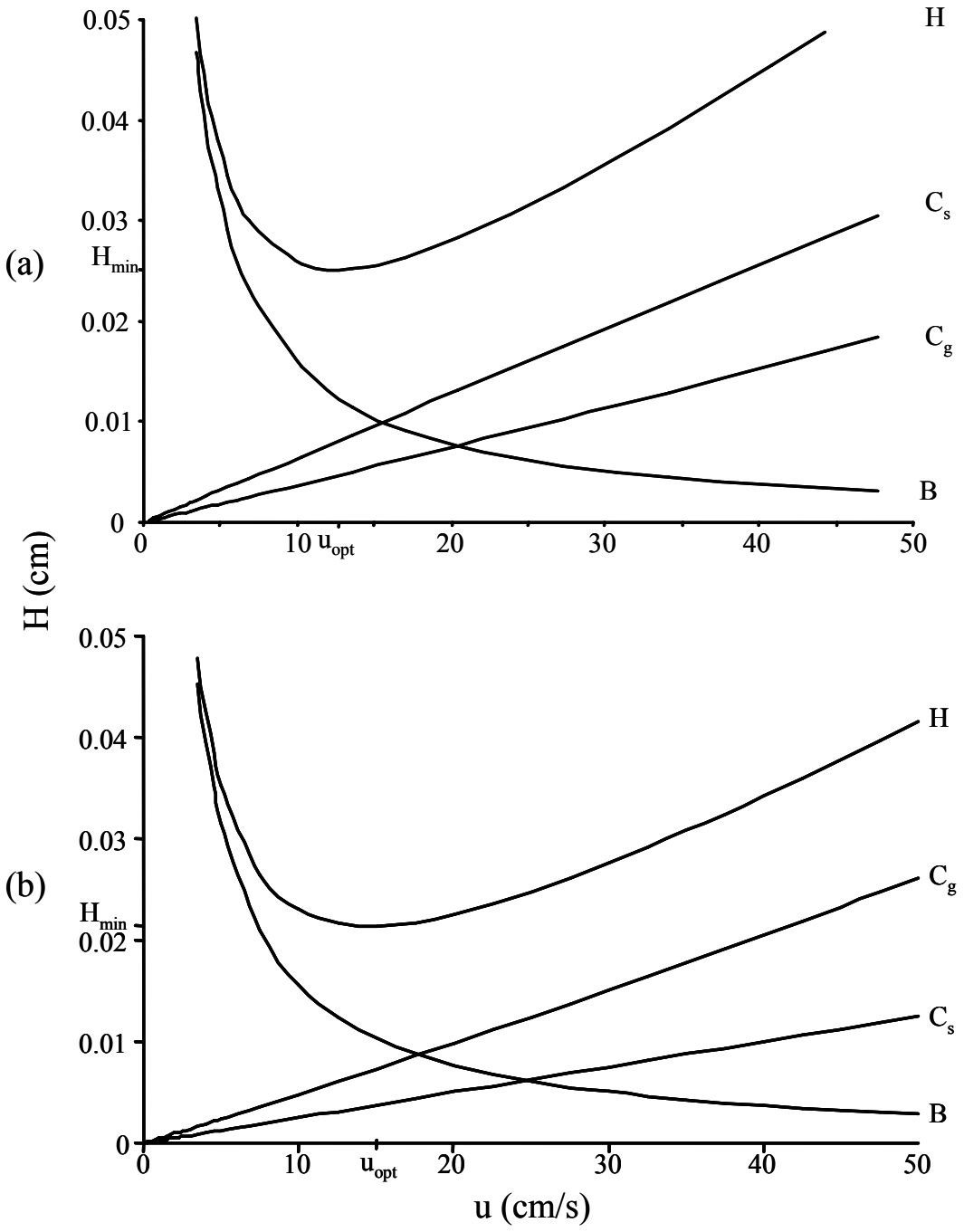

Figure 1.3 Plots of H, B, C_g, and C_s for rectangular cross-section columns (150-µm wide by 250-µm deep and 3-m long) assuming a film thickness of 1 µm using (a) Golay's model and (b) Spangler's model for band dispersion using air carrier gas.

significantly more band dispersion to mass transport in the stationary phase C_s, while Spangler attributes more dispersion to the mass transport in the gas phase term C_g.

Figure 1.4 shows how the two models compare under thin-film conditions. With thin films, the contribution to band broadening from mass transport in the stationary phase becomes negligible. Under these conditions the Golay model predicts greater column efficiencies for the assigned column dimensions, 19600 relative to 17200 theoretical plates for the Spangler model, a difference of ~13%. Notice the increase in column resolution for both models compared to a thick-film column, this is due to the lack of contributions to band dispersion from the C_s term. The u_{opt} values for both models also show significant improvement compared to thick film columns, with the Golay model and Spangler model predicting u_{opt} values of 20.5 and 17.6 cm/s, respectively. In general, thin-film columns allow for higher resolution separations with shorter analysis times, but are not as useful for highly volatile components that have better retention characteristics for thick films.

Because of the short columns used in field-portable and microfabricated GC instruments, low peak capacities limit analyses to relatively simple mixtures. Through an understanding of band dispersion in round cross-section capillary columns, models for band dispersion in rectangular cross-section columns have been derived. By applying these models to the microfabricated columns being evaluated here, improvements in column efficiency and peak capacity can be measured. These improvements lead to higher resolution columns, with higher u_{opt} values, and make complex mixture analysis a viable option.

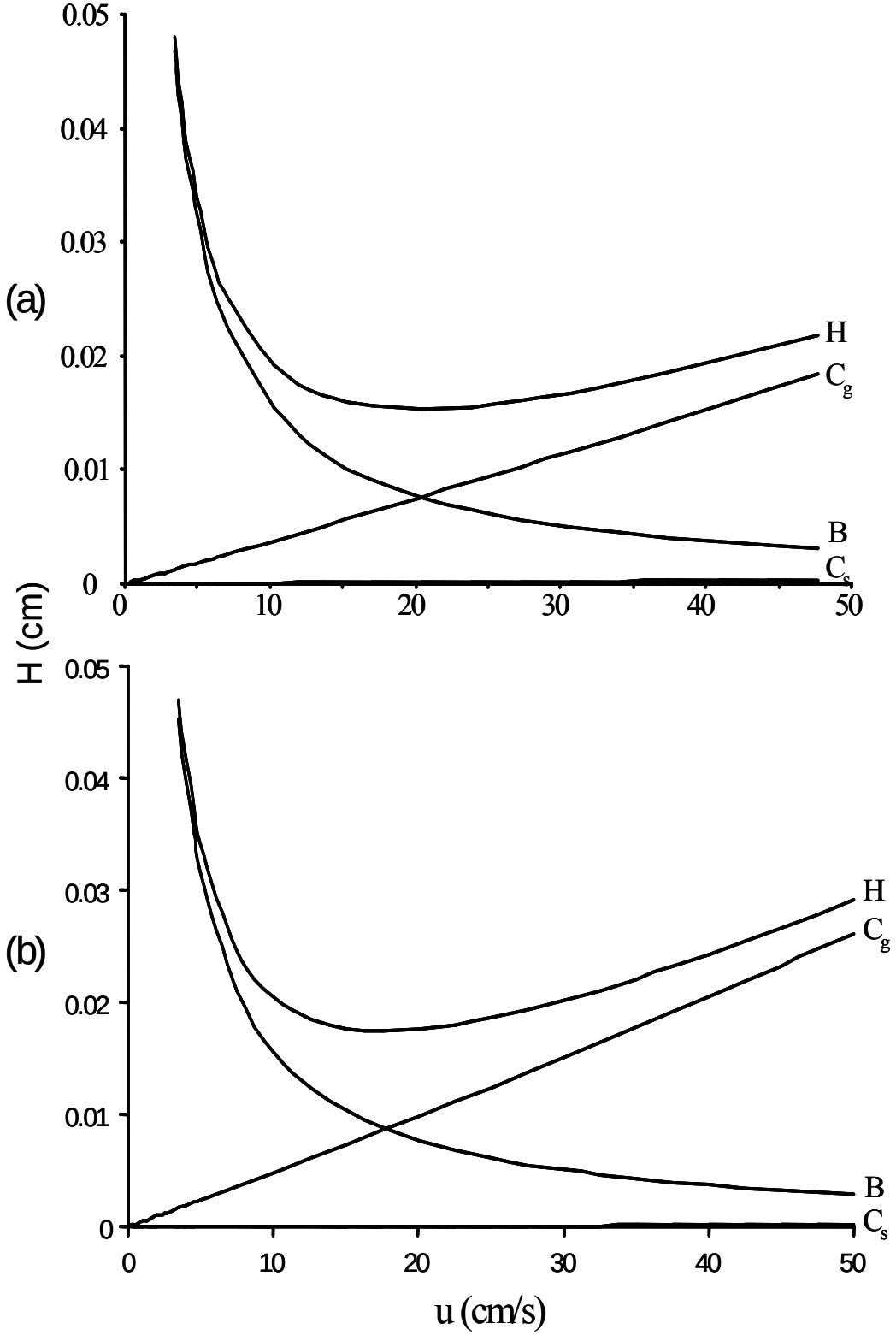

Figure 1.4 Plots of H, B, C_g, and C_s for rectangular cross-section columns (150-μm wide by 250-μm deep and 3-m long) assuming a film thickness of 0.1 μm using (a) Golay's model and (b) Spangler's model for band dispersion using air carrier gas.

Tunable Selectivity

As mentioned previously, peak capacity is the number of perfectly spaced peaks with a specified resolution that can fit in an isothermal separation. Consequently, peak capacity is an ideal number, which can not be realized. It has been shown that relative to the peak capacity for a separation, a chromatogram of random components will never contain more than 37% of its potential peaks[105]. Furthermore it has been shown that a chromatogram must be 95% empty to yield a 90% probability that a given component will appear as an isolated peak. To illustrate the point, for a column with a peak capacity of 100 peaks, a 50 component mixture will yield only 18 single-component peaks[105]. To combat losses in peak capacity, traditionally a chromatographer would increase the length of the separation column. Doubling the length of the column will lead to a factor of two increase in peak capacity[94]. For high-speed applications including field-portable and microfabricated instruments, lengthening the separation column is not practical. Tunable selectivity using dual column ensembles has been shown to allow for better utilization of the available peak capacity in high-speed separations. These techniques generally use dual column ensembles with two columns of differing stationary phases. The differing selectivities of the two stationary phases will provide distinct retention characteristics for each component on the ensemble. Here selectivity refers to the pattern of peaks as they elute from an individual column. By manipulating the relative contribution of each column in the ensemble, peaks can be "tuned" to empty spaces in the chromatogram, thus utilizing the available peak capacity.

Previous studies have demonstrated the use of pressure-tunable dual-column ensembles using conventional fused silica capillary columns[10,11,12,13,14]. Dual column systems take advantage of different analyte-stationary phase interactions generated from stationary phases of different polarities. Retention characteristics of a combination of stationary phases used in a dual column system are additive if retention for each component in the mixture is expressed as its retention factor for each individual stationary phase. This idea is expressed in equation 1.16,

$$k_e = f_A k_A + f_B k_B \tag{1.16}$$

where k_e is ensemble retention factor, f_A and f_B are the fractional contributions of each column to the ensemble hold-up time, and k_A and k_B are the retention factors for the compounds on each respective stationary phase. The fractional contribution of each column is calculated as a function of the hold-up time on each column, t_{mA} and t_{mB}, compared to the ensemble hold-up time t_{me}.

$$f_A = \frac{t_{mA}}{t_{me}} \tag{1.17}$$

$$f_B = \frac{t_{mB}}{t_{me}} \tag{1.18}$$

By adjusting individual column lengths[106,107], hold-up times[10,12,13], column temperatures[35], or stationary phase film thickness, the fractional contribution of each column can be altered. This can shift component ensemble retention times to the extent that overall elution order can change.

A flexible approach to enhanced selectivity is the use of a series coupled column ensemble with an adjustable carrier gas supply at the junction point between the two columns, shown in Figure 1.5. Transient changes in the junction point pressure produce

differential changes in the carrier gas velocity in the two columns. An increase in the junction point pressure reduces carrier gas velocity on the first column and increases carrier gas velocity on the second column. Changing the hold-up time of an individual column changes the residence time of components on that column, altering the influence of the stationary phase on each column to the overall separation. Reducing the junction point pressure has the opposite effect, in that residence time on the second column is increased and residence time on the first column is decreased, making the second column a larger contributor to the overall separation. This can only be done by splitting the first column effluent between the second column and a vent line at the junction point[53]. As shown in Figure 1.5, a detector can also be used at the junction point to monitor the elution of components off the first column. If no single set junction point pressure results in complete separation, the junction point pressure can be controlled electronically[12,13,16,17,53]. With pressure-programmable selectivity, the ensemble junction point pressure is initially set to provide for the best separation of early eluting components. After these components migrate across the junction point into the second column, the pressure can be changed without affecting the ensemble elution order of the early eluting components. This adjustment of the junction point pressure provides for more favorable conditions for the separation of the next group of components. This procedure can be repeated several times to enhance the separation of a complex mixture under positive pressure[108,109] and vacuum outlet conditions[71,54].

More recently the use of short stop-flow pulses has been explored under positive pressure and vacuum outlet conditions[55] as an alternate method for enhancing selectivity. In this case, a stop-flow pulse is used to selectively separate a single pair of components

with little effect on the retention of other mixture components. For stop-flow, the system utilizes a pneumatic valve connected directly from the inlet to the junction point between the two columns. This technique requires adequate resolution from the first column to separate components that coelute from the column ensemble. After the first component crosses the junction point, and prior to the second component crossing the junction point, the valve is opened. The pressure at the junction point rapidly equilibrates with the inlet pressure, nearly stopping the migration of the second component on the first column, while increasing the migration rate of the first component on the second column. The overall effect of a stop-flow pulse is enhanced separation of the two components in the ensemble chromatogram without significant changes to the resolution of other components. An advantage to this technique over using simple pressure pulses[13] (but not stop-flow) is that there will be no sample flow into any portion of the valving apparatus, thus preventing sample loss or contamination during a stop-flow pressure pulse. It also alleviates the need for an electronic pressure controller.

Another method of selectively enhancing separations has been achieved by rapid heating of the second column in the ensemble relative to the first column[35]. For component pairs that are separated by the first column but co-elute from the ensemble, the second column can be rapidly heated when one of the targeted components is in the second column and the other component is still in the first column. During the pulse, migration rates of bands in the second column increase.

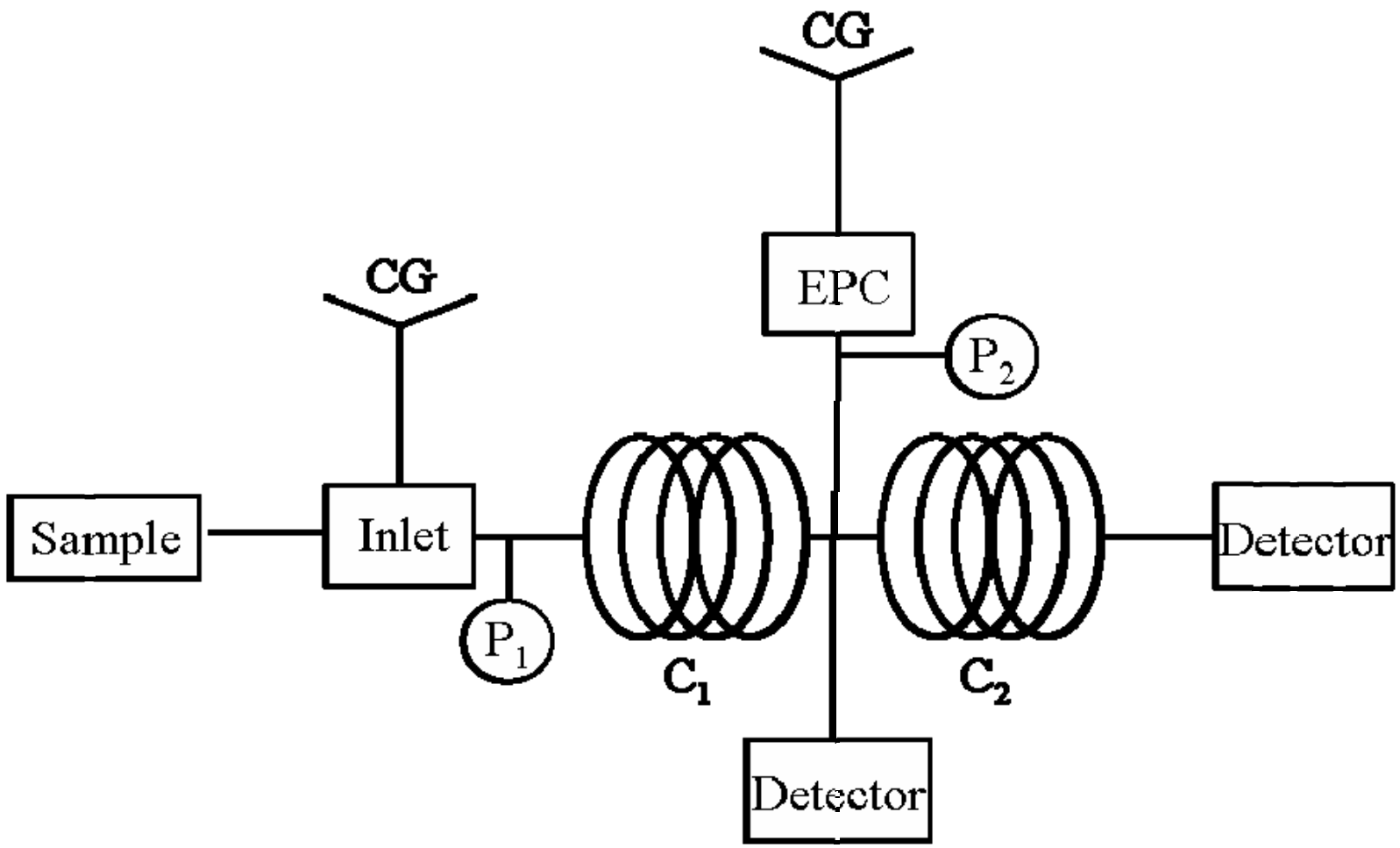

Figure 1.5 Instrument schematic for a dual column ensemble with an adjustable pressure source at the junction point between the two columns. CG, carrier gas; C_1, column 1; C_2, column 2; EPC, electronic pressure controller; P, pressure gauge.

If the second column, is cooled prior to the second component arriving at the junction point of the ensemble, enhanced separation of the targeted peak pair will be achieved. Since technology limits the heating rate of conventional GC ovens to maximum linear range of 50-100°C/min and a minimum cooling time of 200ws for a 250°C temperature differential, the application of temperature pulses for programmable selectivity requires the use of specially made columns. Also, having independent temperature control of the two columns allows for co-eluting pairs to be tuned apart by varying the temperature programming ramp on one column independent of the other. By varying the temperature programming ramp, the columns contribution to the overall separation is altered. By increasing the ramp rate, there is a decrease in column influence on the total separation.

High-Speed Temperature Programming

Temperature programming is necessary for efficient GC analysis of mixtures containing VOCs with a wide range of boiling points. Programming rates of up to 20°C/min are commonly reported. Laboratory GC instruments with conventional convection ovens typically have available maximum linear programming ramps of about 50°C/min. Faster programming rates than can be provided by conventional ovens are needed to accommodate high speed separations. Also, the lengthy cool-down period of a convection oven limits the cycle time of the analysis. Recent advances in high speed temperature programming[129,110] have led to significant reductions in separation times. Methods for high-speed heating of fused-silica capillary columns using resistance heating of a metal sleeve surrounding the column have been described[36,37]. This has resulted in

robust field portable instruments[6] and laboratory applications[15]. Temperature control is achieved through sensing the electrical resistance of the metal column sleeve, or by a sensor wire contained within the sleeve. An electronic switch is used to connect the column jacket to a dc power supply as needed based on a feedback loop from the temperature sensors. Temperature programming rates greater than 1000°C/min can be achieved using commercially available technology[36,37].

For isothermal separations, H is used as the measurement of column resolving power. For temperature programmed separations, the Trennzhal number (TZ), defined as the number of peaks that will fit between a consecutive pair of n-alkanes with a resolution of 1.18, is a useful measure of column resolving power[111]. The TZ value gives a measure of local peak capacity[112],

$$TZ = [\frac{\Delta t_R}{\Sigma W_{1/2}}] - 1 \qquad (1.19)$$

where Δt_R is the difference in retention times for the two reference peaks, and $\Sigma W_{1/2}$ is the sum of their full widths at half height. The peak capacity of a larger chromatographic region is given by the sum of the TZ values for several adjacent pairs of n-alkanes and adding the previously unaccounted for reference peaks. This defines a total peak capacity $(n_p)_{x,y}$ between reference alkanes x and y.

$$(n_p)_{x,y} = \Sigma_{x,y}(TZ + 1) \qquad (1.20)$$

By plotting peak capacity versus retention time of the second reference peak for each adjacent pair of alkanes, the effects of temperature programming rate on solute volatility range, peak capacity, and analysis time are illustrated.

Comprehensive Two-Dimensional Gas Chromatography

The development of two-dimensional gas chromatography was pioneered in the early 1990's by John Phillips[113]. Since its inception, its application as a powerful resolving technique has been exemplified by its use on complex mixtures in the petroleum and fragrance industries as well as environmental applications. The need for GCxGC is justified by the extent of peak overlap in one-dimensional GC. In GCxGC, the entire chromatogram eluting from the primary column is diced in two segments, typical 2-12 s in width, and each segment is focused and sequentially injected as a narrow plug into the secondary column for a second orthogonal separation. The resulting two-dimensional chromatogram has peaks scattered about a plane rather than along a line. The peak capacity becomes the product of the two dimensions. Therefore, component identification is potentially more reliable because each substance has two identifying retention measures rather than one. Separations are likely to be more structured in two dimensions leading to more recognizable patters that are characteristic of the mixture components.

Using two columns of different selectivity allows for very large peak capacities to be achieved. At the forefront of this technology is comprehensive two-dimensional gas chromatography (GCxGC). This technique begins by generating a slow chromatogram on the first column producing large elution bandwidths. The effluent from the first column is collected and focused by a thermal modulator and every few seconds the modulator injects a narrow plug into the second dimension column for high-speed analysis. The second column is usually a polar microbore column using a thin film of stationary phase and length no greater than a few meters. For a set of compounds,

GCxGC chromatograms are displayed on a two-dimensional plan and this can yield very large peak capacities.

By using two columns with different selectivity in the same oven and a very slow temperature programming rate (~3-5°C/min), the two dimensions are assumed to be orthogonal. That is the first dimension separation is based on volatility and the second on polarity. Within the limit of completely uncorrelated retention patterns from the two columns, the available peak capacity becomes the product of the peak capacities of the two individual separations. In addition to the large available capacity, GCxGC is a favorable chromatographic method for complex mixtures because of its structured chromatograms and increased sensitivity.

The modulator is the in-line interface between the first and second separation dimensions in GCxGC, and its continued development is paramount to the overall success of the technology. An efficient modulator that traps the effluent from the first column and releases sharply focused fractions into the second column, is an essential feature of instruments developed for GCxGC. A slotted, rotating heater that sweeps material trapped in the modulator as sharp pulses into the second column[114], a moveable cold zone[115], and a modulation by pulsing cold and hot jets of gas onto the modulator capillary[116] have all been successfully used for this purpose. While successful results have been achieved by each of these designs, the inability to precisely heat and cool the device, the lack of robustness and need for large amounts of cryogenic gasses has limited their popularity. Although thermal modulators have been under investigation over the past twenty years[117], the immaturity of GCxGC offers considerable room for improved modulator design and performance.

The goal of this research is to improve column performance. Previous micro-fabricated columns have lacked sufficient separating powers and with these columns many of the separation goals of the WIMS center were unobtainable.

Statement of Purpose

The work described in this dissertation is towards the development of high performance micro-fabricated columns for gas chromatography. The previous columns were limited to mixtures with limited vapor pressure ranges due to the fact that they are restricted to temperature programming in the GC oven and had thick stationary phases. There was a need for the improvement in column performance. Chapter 2 describes the development of a static coating procedure. Columns with thinner stationary phases can be obtained. These columns are capable of separating the most complex mixtures ever reported with micro-fabricated columns.

The micro-fabricated columns have been designed with heaters and temperature sensors. Chapter 3 utilizes these sensors; temperature programming can be achieved without the need for a large convection oven. By eliminating this need, there are separations possible that could not be obtained previously. This can be achieved through faster temperature programming rates, thermal tuning and micro-fabricated testbed systems.

Conventional temperature programming rates are limited to the heating rates of the oven. Even with the current state of the art technology the heating rates are limited to 70°C/min. With the at-column heating capabilities of the micro-columns temperature

programming rates up to 1500°C/min have been achieved. For high-speed separations, fast flow rates and fast temperature programming rates are necessary.

Thermal tuning requires independent temperature programming of two columns with differing stationary phases. Chapter 4 describes this separation enhancement technique. It has been achieved with micro-fabricated columns and aides in the separation in complex mixtures without the need for additional mechanical parts.

Chapter 5 describes the use of these micro-fabricated columns in a micro-fabricated testbed system. This system uses not only micro-fabricated columns, but also micro-fabricated inlets and detector. This testbed allows for the determination of final system requirements.

The columns have also been integrated into a GCxGC system. Chapter 6 uses these columns with both thermal and pneumatic modulation. These preliminary results set the groundwork for system development and determination of system parameters.

References

[1]Golay, M.J.E. In Gas Chromatography 1957 (East Lansing Symposium); Coates, V.J.; Noebels, H.J.; Fagerson, I.S., Eds; Academic Press; New York, **1958**; pp 1-13.

[2] Van Es, A.; Janssen, J.; Bally, R.; Cramers, C.; Rijks, J. *J. High Resolut. Chromatogr*. **1987**, 10, 273.

[3] Gonnord, M. F.; Guiochon, G.; Onsuka, F. L. *Anal. Chem***. 1983**, 55, 2115.

[4] Overton, E.; Carney, K.; Roques, N.; Dharmasema, H. *Field Anal. Chem. Tech*. **2001**, 5, 97.

[5] Whiting, J.; Lu, C.; Zellers, T.; Sacks, R. *Anal. Chem*. **2001**, 73, 4668.

[6] Nowak, M.; Gorusch, A.; Smith, H.; Sacks, R. *Anal. Chem*. **1998**, 70, 2481.

[7] Gaspar, Gyula; Arpino, Patrick; Guiochon, Georges. *Journal of Chromatographic Science* **1977**, 15(7), 256.

[8] Nowak, M.; Gorusch, A.; Smith, H.; Sacks, R.; *Anal. Chem*. **1993**, 65, 2516.

[9] Sandra, P.; David, F.; Prood, M.; Diricks, G.; Verstappe, M.; Verzele, M. *J. High Resolut. Chromatogr. & Chromatogr. Commun*. **1985**, 8, 782.

[10] Akard, M.; Sacks, R. *Anal. Chem*. **1995**, 67, 2733.

[11] Hinshaw, J.V.; Ettre, L.S. *Chromatographia* **1986**, 21, 561.

[12] Veriotti, T.; Sacks, R. *Anal. Chem*. **2001**, 7, 3045.

[13] Veriotti, T.; McGuigan, M; Sacks, R. *Anal. Chem*. **2001**, 73, 279.

[14] Lu, C. J.; Whiting. J. J.;Sacks, R. D.; Zellers, E. T. *Anal. Chem*. **2003**, 75, 1400.

[15] MacDonald, S. J.; Wheeler, D. *American Laboratory* **1998**, 30(22), 27.

[16] Grall, A.; Leonard, C.; Sacks, R. *Anal. Chem*. **2000**, 72, 591.

[17] Leonard, C.; Grall, A. J.; Sacks, R. D. *Anal. Chem*. **1999**, 71, 2123.

[18] Hope, J. L.; Johnson, K. J.; Cavelti, M. A.; Prazen, B. J.; Grate, J. W.; Synovec, R. E. *Analytica Chimica Acta* **2003**, 490, 223.

[19] Bruckner, C. A.; Prazen, B. J.; Synovec, R. E. *Anal. Chem.* **1998**, *70*, 2796-2804.

[20] Sinha, A. E.; Johnson, K. J.; Prazen, B. J.; Lucas, S. B.; Fraga, C. G.; Synovec, R. E. J. Chromatogr., A **2003**, 983, 195.

[21] Gross, G. M.; Prazen, B. J.; Grate, J. W.; Synovec, R. E. *Anal. Chem.* **2004**; *76*(13), 3517.

[22] Lu, C. J.; Zellers, E. T., *Anal. Chem*. **2001**, 73, 3449.

[23] Lu, C. J.; Zellers, E. T., *Analyst* **2002**, 127, 1061.

[24] Lu, C. J.; Whiting, J.; Sacks, R. D.; Zellers, E. T., *Anal. Chem*. **2003**, 75, 1400.

[25] Sanchez, J. M.; Sacks, R. D., *Anal. Chem*. **2003**, 75, 2231.

[26] Sanchez, J. M.; Sacks, R. D., *Anal. Chem*. **2003**, 75, 978.

[27] Sanchez, J. M.; Sacks, R. D., *J. Sep. Sci*. **2005**, 28, 22.

[28] Whiting, J. J.; Sacks, R. D. *Journal of Separation Science* **2006**, 29(2), 218.

[29] Graydon, J. W.; Grob, K., *J. Chromatogr*. **1983**, 254, 265.

[30] Klemp, M. A.; Akard, M. L.; Sacks, R. D., *Anal. Chem*. **1993**, 65, 2516.

[31] Borgerding, A. J.; Wilkerson, C. W. *Anal. Chem*. **1996**, *68*,701.

[32] Pilgrim, G.; Keller, R. *J. Chromatogr*. **1973**, 11, 206.

[33] Laub, R.; Purnell, J. *J. Chromatogr*. **1975**, 112, 71.

[34] Purnell, J.; Williams, P. *J. Chromatogr*. **1984**, 292, 197.

[35] Whiting, J. J.; Sacks, R. D. *Anal. Chem*. **2003**, 75, 2215.

[36] Gras, R. L.; Luong, J. C.; Mustacich, R. V.; Shearer, R. L. *Journal of ASTM International* **2005**, 2(7).

[37] Sloan, K. M.; Mustacich, R. V.; Eckenrode, B. A. *Field Anal Chem and Tech*. **2001**, 5, 288.

[38] Rounbehler, D.; Bedford, E. High-Speed Detection of Vapors of Specific Compounds. U.S. Patent 5,092,155, **1992**.

[39] Libardoni, M,; McGuigan, M.; Yoo, Y. J.; Sacks, R. D. *J. Chromatogr. A*. **2005**, 1086 (1-2), 151.

[40] Erickson, E.; Enke, C.; Holland, J.; Watson, J. *Anal. Chem*. **1990**, *62*, 1079.

[41] Leonard, C.; Sacks, R. *Anal. Chem*. **1999**, *71*, 5177.

[42] Wu, Y. E.; Chen, K.; Chen, C. W.; Hsu, K. H. *Sensors and Actuators A*. **2002**, *100,* 37.

[43] Chen, K.; Wu, Y. E. *Sensors and Actuators A*. **2000**, *79*, 211.

[44] Bender, F.; Barie, N.; Romoudis, G.; Voigt, A.; Rapp, M. Sensors *and Actuators B*. **2003**, *93*, 135.

[45] Manginell, R. P.; Lewis, P. R.; Adkins, D. R.; Kottenstette, R. J.; Wheeler, D.; Sokolowski, S.; Trudell, D.; Byrnes, J.; Okandan, M.; Bauer, J. M.; Manley, R. G. Proceedings of SPIE-The International Society for Optical Engineering **2004**, 5591, 44.

[46] Park, J.; Zellers, E. T. *Analyst* **2000**, 125(10), 1775.

[47] Lu, C-J.; Steinecker, W. H.; Tian, W-C.; Oborny, M. C.; Nichols, J. M.; Agah, M.; Potkay, J. A.; Chan, H. K. L.; Driscoll, J.; Sacks, R. D.; Wise, K. D.; Pang, S. W.; Zellers, E. T**.** *Lab on a Chip* **2005**, 5(10), 1123.

[48]Steinecker, W. H.; Rowe, M. P.; Matzger, A. J.; Zellers, E. T. "Chemiresistor array with nanocluster interfaces as a micro-GC detector." In *Proceedings of the 12th*

International Conference on Solid-State Sensors, Actuators and Microsystems Transducers '03, Boston, MA, June 8-12, **2003**; p 1343.

[49] Cai, Q-Y.; Zellers, E. T. *Anal. Chem*. **2002**, 74(14), 3533.

[50] Cai, Q-Y.; Zellers, E. T. **"**Chemiresistor vapor sensor array employing monolayer-encapsulated metal (MenM) nanoclusters**."** Proceedings - Electrochemical Society **2001**, 408.

[51] Smith, H.; Zellers, E. T.; Sacks, R. D. *Anal. Chem*. **1999**, 71, 1610.

[52] Grall, A. J.; Sacks, R. D. *Anal. Chem*. **1999**, 71, 5199.

[53] Grall, A.; Sacks, R. D. *Anal. Chem*. **2000**, 72, 2507.

[54] Grall, A.; Zellers, E.T.; Sacks, R. *Environ. Sci. Technol*. **2001**, 35, 163.

[55] Whiting, J.; Sacks, R. *Anal. Chem*. **2002**, 74(1), 246.

[56] Terry, S. C.; Jerman, J. H.; Angell, J. B. *IEEE Transactions on Electron Devices* **1979**, 26, 1880.

[57] Angell, J. B.; Terry, S. C.; Barth, P. W. *Sci. Am*. **1985**, 248, 44.

[58] http://www.chem.agilent.com/Scripts/PCol.asp?lPage=180

[59] Yu. C. M.; Lucas, M.; Koo, C.; Stratton, P.; DeLima, T.; Behymer, E. *Micro-Electro-Mechanical Systems (MEMS)* **1998**, *DSC-Vol. 66*, 481.

[60] Noh, H.; Hesketh, P. J.; Frye-Mason, G. C. *J. Microelectromech. Syst*. **2002**, *11 (6)*, 718.

[61] Kolesar, E. D.; Reston, R. R. IEEE Trans. Components, Packaging, and Manufacturing Tech. **1998**, 21 (4), 324.

[62] Manginell, R. P.; Okandan, M.; Bauer, J. M.; Manley, R. G.; Trudell, D.; Kottenstette, R. J.; Lewis, P. R.; Adkins, D.; Heller, E. J.; Stewart, H.; Shul,

R. J. Micro Total Anal. Syst. 2004-íTAS '04 **2005**, 2 (297), 61-63.

[63] Manginell, R. P.; Lewis, P. R.; Adkins, D. R.; Kottenstette, R .J.; Wheeler, D.; Sokolowski, S.; Trudell, D.; Byrnes, J.; Okandan, M.; Bauer, J. M.; Manley, R. G. "Recent Advancements in the Gas-Phase MicroChemLab," SPIE Optics East Lab-on-a-chip Conference, SPIE Proceedings Vol 5591, Philadephia, PA, 2004, 44.

[64] Lorenzelli, L.; Benvenuto, A.; Adami, A.; Guarinieri, V.; Margesin, B.; Mulloni, V.; Vincenzi, D. *Biosensors and Bioelectronics*. **2005**, 20, 1968.

[65] Bhushan, A.; Challa, V.; McKeon, J.; Yemane, D.; Overton, E. B.; Murphy, M. C.; Goettert, J. *TMS Lett*. **2004**, *1* (7), 145-146.

[66] Ngan, M. L.; Lee, K. C.; Cheah, K. W. *J. Appl. Phys*. **1998**, 83, 1637.

[67] http://www.varianinc.com/cgi-bin/nav?products/chrom/gc/microgc/mgc4900&cid=JKMMJJMJFP

[68] http://www.microfastgc.com/

[69] Manginell, R. P.; Frye-Mason, G. P.; Kottenstette, R. J.; Lewis, P. R.; Wong, C. C. "Microfabricated Planar Preconcentrator," *Tech. Digest 2000 Sol.-State Sensor and Actuator Workshop*, **2000**, 179.

[70] Bhushan, A.; Challa, V.; McKeon, J.; Yemane, D.; Overton, E. B.; Murphy, M. C.; Goettert, J. "Application of Scanning Acoustic Microscopy in Characterizing Metal Micro Gas Chromatograph Columns," *TMS Letters*, 1 (7), **2004**, 145.

[71] Bhushan, A.; Yemane, D.; Goettert, J.; Overton, E. "LiGA Fabricated High Aspect Ratio Nickel Gas Chromatograph Columns as a Step Towards a Portable and Fast GC Instrument," 5th Workshop on Harsh-Environment Mass Spectrometry, Sarasota, Fl. **2005**.

[72] http://www.microfastgc.com/

[73] http://www.sls-micro-technology.de/

[74] Lehmann, U.; Sussiek, M.; Muller, J. "A packed column realized on a 1 cm^2 sized silicon glass chip for permanent gas separation," Pittcon, Orlando, FL, **2005**.

[75] http://www.c2v.nl/

[76] Lu, C. J.; Tian, W. C.; Steinecker, W. H.; Guyon, A.; Agah, A.; Oborny, M. C.; Sacks, R. D.; Wise, K. D.; Pang, S. W.; Zellers, E. T. "Functionally integrated MEMS micro gas chromatograph subsystem," *Proceedings of the Seventh International Confernece on Miniaturized Chemical and Biochemical Analysis Systems* - μTAS '03, Squaw Valley, CA, October 5-9, **2003**, 411.

[77] Zellers, E. T.; Steinecker, W. H.; Lambertus, G. R.; Agah, M. Lu, C. J.; Chan. H. K. L.; Potkay, J. A.; Oborny, M. C.; Nichols, J. M.; Astle, A.; Kim, H. S.; Rowe, M. P.; Kim, J.; de Silva, L. W.; Zheng, J.; Whiting, J. J.; Sacks, R. D.; Pang, S. W.; Kaviany, M.; Bergstrom, P. L.; Matzger, A. J.; Kurdak, C.; Bernal, L. P.; Najafi, K.; Wise, K. D. "A Versatile MEMS Gas Chromatograph for Determinations of Environmental Vapor Mixtures," *Solid-State Sensors, Actuators and Microsystems Workshop*, Hilton Head Island, South Carolina, June 6-10, **2004**, 61-66.

[78] Lu, C. J.; Zellers, E. T. *Analyst* **2002**, 127, 1061.

[79] Tian, W.; Pang, S. W.; Lu, C. J.; Zellers, E. T. *J. Microelectromech. Syst*. **2003**, 12 (3), 264.

[80] Chan, H. K. L.; Takei, M.; Pang, S. W.; Veeneman, R. A.; Zellers, E. T. "Microfabricated preconcentrator for quantitative analysis of low concentration organic

compounds," *Proc. 13th Int. Conf. Solid-State Sensors,* Actuators, and Microsystems, Transducers 05, vol. 2, Seoul, Korea, June **2005**, 2091.

[81] H. Kim, W. Steinecker, G. Lambertus, A. Astle, K. Najafi, E. Zellers, L. Bernal, and K. Wise, "Integrated high-pressure 4-stage micro gas pump for high-speed micro gas chromatography", in *Proc.* 10*th Int. Conf. on Miniaturized Systems for Chemistry and Life Sciences (μTAS '06)*, pp. 1037-1039, Tokyo, Japan, Nov. 5-9, 2006

[82] Kim, H.; Najafi, K. "Characterization of Parylene-assisted wafer bonding: Long-term stability and influence of process chemicals," *13th International Conference on Solid-State Sensors, Actuators, and Microsystems* (*Transducers '05*), Seoul, Korea, Jun. 5-9, 2005.

[83] Potkay, J. A.; Driscoll, J. A.; Agah, M.; Sacks, R. D.; Wise, K. D. *Proc. of the 16th Annual IEEE Conference on Micro-Electro-Mechanical Systems (MEMS)*, Kyoto, Japan, January 19-23, **2003**, 395.

[84] Agah, M.; Potkay, J. A.; Driscoll, J. A.; Sacks, R. D.; Kaviany, M.; Wise, K. D. "Thermal Behavior of High-Performance Temperature-Programmed Microfabricated Gas Chromatography Columns," *Technical Digest of the 12th International Conference on Solid-State Sensors, Actuators and Microsystems*, Boston, Massachusetts, USA, June 8-12, **2003**, pp. 1339-1342.

[85] Agah, M.; Lambertus, G. R.; Sacks, R. D.; Wise, K. D. "High-Speed MEMS-based Gas Chromatography," Displays, Sensors, and MEMS, San Francisco, CA, Nov. **2004**.

[86] Agah, M., Potkay, J. A., Lambertus, G. R**.**, Sacks, R. D., Wise, K. D. "High-performance Temperature-Programmed Microfabricated Gas Chromatography Columns," *IEEE J. Microelectromech. Systems,* **2005**, 14(5), 1039.

[87] Astle, A. A.; Bernal, L. P.; Najafi, K.; **Kim**, H.; Washabaugh, P. D. "Modeling, Design, and Fabrication of a High Frequency Micro Vacuum Pump", ASME '03, Washington D.C., USA, Nov. 15-21, **2003**.

[88] Potkay, J. A.; Wise, K. D. "An Electrostatically Latching Thermopneumatic Microvalve with Closed-Loop Position Sensing," *Proceedings of the Eighteenth Annual IEEE Conference on Micro Electro Mechanical Systems (MEMS)*, Miami, Florida, USA, January **2005**, 415.

[89] Zheng, J.; Christophersen, M.; Bergstrom, P. L. Extended Abstracts 4th Int. Conf. on Porous Semicon. Sci. Tech., Valencia, Spain, March 14–19th, **2004**, 42.

[90] Oborny, M. C.; Zheng, J.; Nichols, J. M.; Lu, C.-J.; Bergstrom, P. L.; Manginell, R. P.; Frye-Mason G. C.; Zellers, E. T. Proceedings of the Seventh International Conference on Miniaturized Chemical and Biochemical Analysis Systems – μTAS '03, Squaw Valley, CA, October 5–9, 2003, 1243.

[91] Wohltjen, H.; Snow, A. W. *Anal. Chem*., **1998**, 70, 2856.

[92] Martin, A. J. P.; Synge, R. L. M. *J. Biochem*. **1941**, *35*, 1359.

[93] J. H. Purnell, *J. Chem. Soc*. **1960,** 1268**.**

[94] Grob, R. L.; Barry, E. F. *Modern Practice of Gas Chromatography* 2004; John Wiley & Sons, Inc.; Hoboken, NJ, 232.

[95] Giddings, J. C. *Anal. Chem*. **1969**, 39, 1027.

[96] Golay, M. J. E. *Theory of Chromatography in Open and Coated Tubular Columns with Round and Rectangular Cross-Sections. Gas Chromatography.* New York:Academic Press; **1958**, 36-55.

[97] Grall, A. J.; Sacks, R. D. *Anal. Chem*. **1999**, 71, 5199.

[98] Golay, M. J. E. *J Chromatogr. A*. **1981**, 216, 1.

[99] Spangler, G. E. *Anal. Chem*. **1998**, 70, 4805.

[100] Spangler, G. E. *J. Micro-column Sep*. **2001**, 13, 285.

[101] Giddings, J. C.; Chang, J. P.; Myers, M. N.; Davis, J. M.; Caldwell, K. D. *J. Chromatogr*. **1983**, 255, 359.

[102] Ahn, H.; Brandani, S. *American Institute of Chemical Engineers* **2005**, *51*, 1980.

[103] Poppe, H. *J Chromatography A* **2002**, *948*, 3.

[104] Lapizo-Encinas, B. H.; Pinto, N .G. *Separation Science and Technology* **2002**, *37*, 2745.

[105] Davis. J. M.; Giddings, J. C. *Anal. Chem*. **1983**, *55*, 418.

[106] Freeman, R. R; Kukla, D. *J. Chromatogr. Sci*. **1986**, 24, 392.

[107] Purnell, J.H.; Rodriquez, M.; Williams, P.S. *J. Chromatogr*. **1986**, 358, 39.

[108] Smith, H.; Sacks, R. D. *Anal. Chem*. **1997**, 69, 5159.

[109] Coutant, C.; Sack, R. D. *Anal. Chem*. **1999**, 71, 5501.

[110] Sacks, R.; Smith, H.; Nowak, M. *Anal. Chem*. **1998**, 70, 29A.

[111] Grob, K., Jr.; Grob, K.J. *Chromatogr*. **1981**, 207, 291.

[112] Kaiser, R. *Chromatographie in der Gasphase*. 2nd ed.; Bibliografisches Institut: Mannheim, Germany. **1966**; Vol. 2.

[113] Z.Y. Liu, et al, *Analytical Chemistry*, **1994**, 66, 3068.

[114] J.B. Phillips, et al, *J. High Res. Chromatogr.* **1999**, 22, 3.

[115] P.J. Marriott and R.M. Kinghorn, *Analytical Chemistry*, **1997**, 69, 2582.

[116] E.B. Ledford and C.Billesbach *J. High Res. Chromatogr.* **2000**, 23, 202.

[117] L.M. Blumberg, *Journal of Chromatography A*, **2003**, 985, 29.

Chapter 2

Static Coated, High Performance Silicon/Glass Micro-Fabricated Columns for Gas Chromatography*

Introduction

Several laboratories are working on the development of microfabricated columns for gas chromatography[1,2,3,4,5,6,7,8]. These columns are attractive because of their small size, low thermal mass allowing rapid temperature programming with relatively low power, and parallel manufacturing, which should result in low production costs. These attributes make these devices attractive for a number of applications involving on-site monitoring of environmental samples.

Most microfabricated column designs have used silicon microelectromechanical system (MEMS) technologies for column fabrication. Gas-phase reactive ion etching produces high-quality rectangular channels in silicon wafer substrates[4,6,9-13]. After etching, the open channels are sealed with Pyrex glass anodically bonded to the silicon surface. Back etching of the silicon substrate is used to remove excess substrate to further reduce thermal mass[10]. The high thermal conductivity of silicon allows for relatively uniform heating using spot heaters patterned on the back surface of the substrate[10-12].

Published : Reidy, S,. et al. Analytical Chemistry, **2006, 78(8) 2623.*

Several methods have been used for the deposition of a stationary phase on the silicon MEMS column walls. Most work has been done with nonpolar stationary phases suchs as dimethyl polysiloxane (PDMS)[14-16]. The use of moderately polar trifluoropropyl methyl polysiloxane also has been reported[14,15]. Vapor deposition prior to sealing the channel has been used[17], but this restricts the upper temperature limit for further wafer processing to the upper temperature limit of the stationary phase. After the channel is sealed, stationary-phase application is usually performed by liquid coating means.

Static coating and dynamic coating are the two most frequent used methods for the production of wall-coated open-tubular fused silica columns[18]. With dynamic coating, a plug of stationary phase in a suitable solvent is pushed through the column by the flow of a nonreactive gas. Stationary-phase film thickness can be controlled by means of the plug velocity and the stationary-phase concentration in the solvent. After the plug is expelled from the end of the column, the excess solvent is evaporated by continued as flow leaving behind a film of stationary phase on the wall of the fused-silica tube. There are numerous variations on this general approach[18].

For static coating, the entire column is filled with the stationary phase, one end of the column is sealed, and a vacuum is applied to the open end. A front representing the liquid-vapor transition point propagates through the column away from the low-pressure end. The coating is complete once the solvent is completely pumped away. Static coating is preferred over dynamic coating for two reasons. First, all of the stationary phase initially introduced is deposited on the column wall; thus, the calculation of average film thickness is straightforward, using the surface area of the column, the concentration of stationary phase. Second, the stationary-phase coating may be more

uniform than with dynamic coating due to the lack of axial motion of the stationary phase during deposition.

Glass on silicon columns produced as part of the Engineering Research Center for Wireless Integrated Micro Systems (WIMS) at the University of Michigan have previously used dynamic coating for stationary-phase application. The columns are formed as 150-μm wide by 240-μm deep channels etched in 1-mm thick by 4-inch diameter silicon wafers. Columns with lengths of 0.25 m, 0.5 m, 1.0 m and 3.0 m have been fabricated. Dynamic coating of PDMS has yielded columns with typically 2000-2500 theoretical plates per meter.

Initial attempts at static coating of the silicon on glass columns failed due to bubble formation at the point where the round fused silica connecting lines jointed with the rectangular silicon channel. This occurred even after thorough degassing of the solvent[18]. This may be the result of cavitation in the liquid when the vacuum is applied. Recent work has solved these problems, and this chapter describes the coating and evaluation of silicon on glass columns with PDMS stationary phase applied by using static coating methods. Coatings in the 0.1-0.2 μm thickness range are explored. Applications are emphasized where on-site, high-speed separations would be useful.

Experimental

Apparatus. Most experiments were conducted using the oven of a Varian 3500 conventional GC to ensure accurate temperature control. Commercial split/splitless inlets for an HP 6890 GC and flame ionization detectors (FID) from a Varian 3500 GC were used for all experiments. The Varian FID was used because it was easier to connect to

alternative electrometer/amplifiers designed in house for faster data logging. Data were logged with a sampling rate of 100 Hz. Some experiments were conducted at room temperature without a GC oven. For these experiments, a stand-alone HP 6890 inlet and Varian FID were used.

Column Production and Coating. Column design and properties have been described in detail[9-12]. Briefly, the columns were produced in standard 4-in. silicon wafers by deep reactive ion etching using a modified Bosch process[9-12]. The rectangular-cross-section channels, 150-μm wide by 240-μm deep, are etched as a double square spiral to accommodate a square chip format while utilizing chip surface area. Ports, 350-μm wide by 250-μm deep, were etched at opposite corners of each column, to accommodate fused silica connection lines. After etching, the open surface of the wafer was sealed by anodically bonding a Pyrex® glass wafer to the top surface of the silicon wafer. Fabrication conditions have been described[9-12]. After sealing, the wafers were diced into the individual columns. Columns of four different lengths were fabricated. Critical dimensions are summarized in Table 2.1.

Table 2 1. Column properties for the different column lengths.

Column Length	Chip Dimension	Volume	Surface Area	# of Turns
25 cm	1.1 cm x 1.1 cm	0.009 cm^3	1.95 cm^2	70
50 cm	1.5 cm x 1.5 cm	0.018 cm^3	3.9 cm^2	102
100 cm	1.9 cm x 1.9 cm	0.036 cm^3	7.8 cm^2	142
300 cm	3.2 cm x 3.2 cm	0.108 cm^3	23.4 cm^2	230

Parallel processing is one of the potential advantages of micro-fabricated columns. For the 3.0-m long columns, four were simultaneously etched on a single wafer. For the shorter columns, all three sizes were fabricated on a single wafer (nine 0.25 m, ten 0.50 m and six 1.0 m). After dicing, 245-μm o.d., 100-μm i.d. deactivated fused silica tubing

(Polymicro Technologies, Pheonix, AZ) was connected to the etched ports by means of an epoxy seal (Hysol Epoxy Patch 1C, Rocky Hill, CT). Figure 2.1 shows a photograph of the completed columns illustrating the four column lengths. A coin is shown for size comparison.

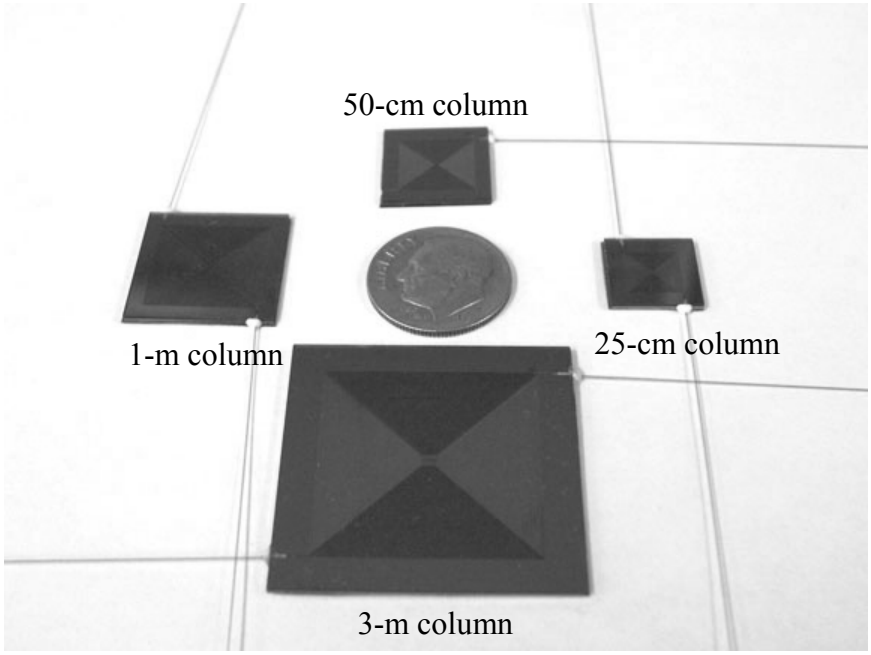

Figure 2.1. Photograph of silicon on glass micro-fabricated columns.

Previous work with 3.0-m long columns of similar design used a dynamic coating procedure, and these columns typically generated 2000-2500 theoretical plates per meter[14-16]. Coating thickness was estimated at 1-2 μm based on fit to theoretical data. Static coating allows for more accurate estimation of film thickness and generates thinner, more uniform films[18]. Figure 2.2 shows the apparatus used for static coating of these microfabricated columns.

Typically, coating solutions were prepared to give coating thickness in the range 0.1-0.2 μm. About 0.008 g of non-polar dimethyl polysiloxane (OV-1, Ohio Valley, Specialty Chemical, Marietta, OH) was dissolved in 2.0 ml of a 1:1 (vol./vol.) mixture of

n-pentane and dichloromethane. The mixture was agitated for 30 min to ensure complete dissolution. After the columns were leak tested, they were filled completely with coating solution by using house nitrogen at a pressure of 24 psig at the solvent reservoir, which was connected to the column inlet by means of a segment of 250-µm i.d. deactivated fused silica tubing.

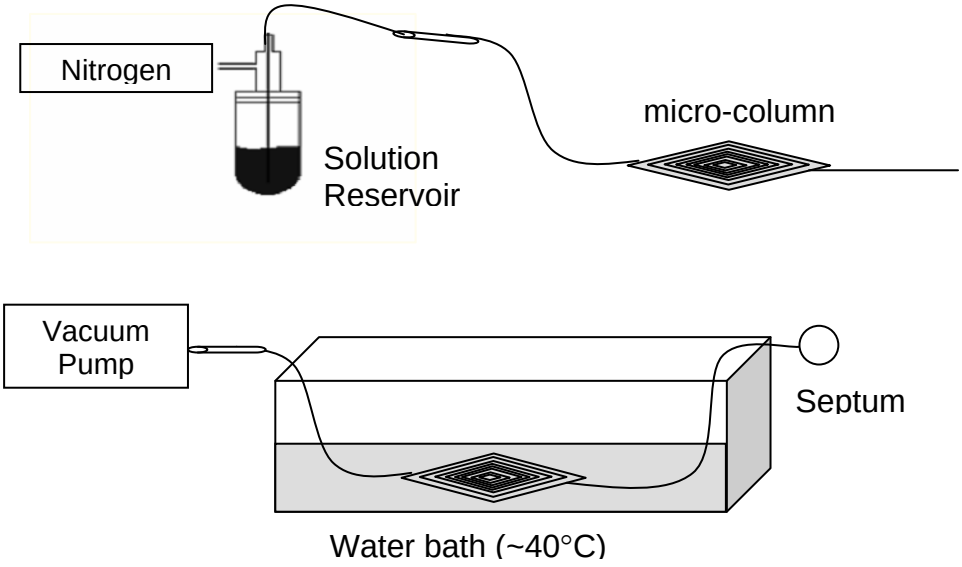

Figure 2.2. System used for static coating of silicon MEMS columns. Top shows filling configuration, and bottom shows solvent removal configuration.

After filling, the open end of the fused silica connecting line was sealed by forcing it into a conventional GC septum. The column was then placed in a 40°C water bath for one minute, the house nitrogen turned off and the reservoir disconnected. The open end was then connected to a vacuum pump (Model UN 85.3 KTI, Newberger, Inc., Trenton, NJ) by means of a segment of 530-µm i.d. deactivated fused silica tubing. The solvent was evaporated at a pressure of about 3.25 psia until the column appeared empty (about 15 min. for a 1.0-m long column). The column remained under vacuum in the water bath for an additional 2 hours to ensure complete evaporation of the solvent.

Preliminary studies with static coated silicon MEMS columns showed that even modest heating (80-100°C) resulted in loss or degradation of the stationary phase. To stabilize the stationary phase for temperature programmed applications, *in situ* cross linking was used. Prior to coating, a thermally activated cross-linking agent[18] (dicumyl peroxide, 1% by weight nominal, Aldrich, Milwaukee, WI) was added to the liquid polymer phase. After coating, the column was heated to 180°C at 5°C/min and held at 180°C for four hours under nitrogen flow.

Materials and Procedures. Test mixtures were prepared using reagent-grade chemicals (Aldrich, Milwaukee, WI). Table 2.2 lists the compounds and their boiling points used for column evaluation.

Table 2.2. List of compounds for 15 component chromatograms.

#	Compound	B.P. (°C)	#	Compound	B.P. (°C)
1	pentane	36.1	9	1-chloropentane	107
2	dichloromethane	39.8	10	toluene	110.6
3	2-butanone	79.6	11	2-fluorotoluene	113
4	ethylacetate	77.1	12	cycloheptane	118.4
5	1,1,1 trichloroethane	74.1	13	octane	126
6	benzene	80.1	14	butylacetate	126.1
7	2-pentanone	103.3	15	chlorobenzene	130
8	heptane	98.4			

House air is used as carrier gas after purification for removal of water vapor and traces of organic compounds. Data acquisition from the FID is provided with a 16-bit A/D board (Model DAS 1602-16, Computer Boards, Inc. Middleboro, MA) interfaced to a PC (Dell Dimension 8400). Interface control is provided by LabTech Notebook software (Version 10.1, Laboratory Technologies, Corp., Andover, MA). Column efficiency and flow calculations are made with Microsoft Excel spreadsheets.

Chromatograms were processed with Grams/32 software (Galactic Industries, Salem, NH).

Results and Dicusssion

Column Efficiency. Previous studies with columns of the same design as described here and with a non-polar dimethyl polysiloxane stationary phase used dynamic coating and typically produced 2000-2500 theoretical plates per meter[14-16]. With dynamic coating, the film thickness could not be directly determined, but was assumed to be relatively thick (1-2 μm) based on the viscosity of the coating solution[14]. These relatively thick stationary-phase films are useful for increasing retention of very volatile target compounds, but under these conditions, resistance to mass transfer in the stationary phase makes a large contribution to overall peak variance. In addition, because the film thickness is unknown, it is difficult to quantitatively model the kinetic performance of the column.

The much thinner films and easily calculated film thickness provided by static coating offers the possibility of using a kinetic model to describe column efficiency. Several kinetic models that predict the dispersion of chromatographic bands in square and rectangular channels have been described. When Golay presented his classic kinetic model for the efficiency of wall-coated open-tubular columns, he also provided a theory for square columns[19]. He later extended the model for the case of rectangular columns[20] by developing a complex expression for gas flow through a rectangular column. Giddings et al.[21] developed a similar model for rectangular cross-section columns, which they called open parallel plate columns, but their expression for non-equilibrium effects in the moving phase considered only binary diffusion normal to the parallel plates.

Recently, Spangler[22,23] developed a kinetic model that addresses the efficiency of both rectangular and square-cross-section channels. It considers binary diffusion in all directions for the calculation of non-equilibrium band broadening in the moving phase and thus takes into account the aspect ratio of the rectangular channel. A complex expression for average carrier-gas velocity is derived and greatly simplified for the case of high-aspect ratio (>5) rectangular channels. This expression was compared with literature values of gas velocity with excellent results[23].

The work reported here is for a micro-GC column using silicon-based technologies, and Si-chip size is an important consideration for a highly miniaturized, very-low-power instrument. High-aspect-ratio columns have been made in silicon wafers by the use of a relatively shallow etch (less than 50 μm) and a channel width of several tenths of millimeters[23-24]. For the present system, deep-reactive-ion etching was used to produce a deeper, narrower channel to make better use of the chip surface area.

High-aspect-ratio columns were not used for this study, and both the Golay and Spangler models[20] for rectangular-cross-section columns were chosen as starting points for the evaluation of the static coated columns. Equation 2.1 gives the kinetic-model expression for rectangular-cross-section open-tubular columns according to Golay[20].

$$H = 2\frac{f_1 f_2 D_g}{u} + \frac{1+9k+\frac{51}{2}k^2}{105\left(1+k\right)^2}\frac{f_1 w^2}{f_2 D_g}u + \frac{2k{d_f}^2\left(w+h\right)^2}{3\left(1+k\right)^2 h^2 D_s}u \qquad (2.1)$$

where H is the height equivalent to a theoretical plate, u is the average carrier gas velocity, k is the solute retention factor, d_f is the stationary phase film thickness, D_g and D_s are the solute diffusion coefficients in the carrier gas (air) and the stationary phase, respectively, and w and h are width and height of the rectangular channel, respectively.

In this equation, D_g is specified at the column outlet pressure, and f_1 and f_2 are Golay-Giddings and Martin-James gas compression corrections, respectively.

The first term on the right side of equation 2.1 describes band dispersion from longitudinal diffusion. The second term describes band dispersion from non-equilibrium effects in the gas phase, and the last term describes dispersion from non-equilibrium effects in the stationary phase. If w is at least 1000 times larger than d_f, the third term may be negligible for non-polar silicone gum phases. Thus, for thin stationary-phase films, the critical parameter that impacts column efficiency is w^2/D_g. This term is proportional to the time required for solute molecules to diffuse from the center of the column to the column wall.

The average carrier gas velocity u for rectangular columns is obtained from equation 2.2.

$$u = \frac{w^2 p_o \left(P^2 - 1\right)}{24 \eta L} f_2 \qquad (2.2)$$

where p_o is the outlet pressure, P is the inlet-to-outlet pressure ratio, η is the carrier gas viscosity at the column temperature and L is the column length.

Spangler presented a revised version of the Golay equation 2.3 to describe band dispersion in rectangular-cross-section channels[23].

$$H = 2\frac{f_1 f_2 D_g}{u} + \frac{0.9 + 2k + 35k^2}{96(k+1)^2}\frac{f_1 w^2}{f_2 D_g}u + \frac{2kd_f}{3(k+1)^2 D_s}u \qquad (2.3)$$

Spangler's theory found the terms describing dispersion from longitudinal diffusion and non-equilibrium effects in the stationary phase to be identical to Golay's theory for round-cross-section columns. The average linear carrier gas velocity equation and the dispersion term from non-equilibrium effects in the gas phase were revised. The

coefficients in the second term were revised[23] from Golay[19]. Another notable difference is the omittance of an aspect ratio contribution by Spangler in the third term of the equation, which under high aspect ratios also drops from Golay's equation.

The average carrier gas velocity derived by Spangler[22] for rectangular-cross-section columns is obtained from equation 2.4,

$$u = \frac{h^2 w^2 p_o (P^2 - 1)}{24 \eta L (h^2 + w^2)} f_1 \qquad (2.4)$$

where column dimensions play a larger role for low aspect ratios, and converges with Golay's derivation for linear carrier gas velocities at high aspect ratios.

Plots 1 and 2 in Figure 2.3 show height equivalent to a theoretical plate versus average carrier gas velocity from equation 2.1 (Golay model) and from equation 2.3 (Spangler model) for the conditions used in this study. The values of D_g and D_s were chosen as 0.093 cm^2/s[25] and 6.4 x 10^{-6} cm^2/s[26], respectively. A k value of 2.5 and a viscosity of air (carrier gas) at 40°C of 1.9 x 10^{-4} poise[27] were used in the calculations. The column length was assumed to be 3.0 m with channel width and depth of 150 μm and 240 μm, respectively. From Plot 1, the minimum plate height is about 0.016 cm at an optimum carrier gas velocity of about 22 cm/s, while for Plot 2, the minimum plate height is about 0.019 cm at an optimal carrier gas velocity of about 19 cm/s. Plot 3 in Figure 2.3 shows experimental data of plate height versus average carrier gas velocity obtained for n-octane at 40°C using the 3.0-m long micro-fabricated column. The retention factor was 2.5 at this temperature. The minimum plate height is 0.025 cm and the optimum carrier gas velocity is 14 cm/s.

Note that the loss in column efficiency at the higher gas velocities is much more rapid and more non-linear than predicted by equations 2.1 and 2.3. This is characteristic

of flow dependent instrumental dead time and is not surprising considering the relatively short column used in this study. In order to evaluate this, the extra-column band broadening term from equation 2.5[28] was added to equations 2.1 and 2.3.

$$H_{ec} = \frac{\Delta t^2}{L(k+1)^2} u^2 \qquad (2.5)$$

where H_{ec} is the height equivalent to a theoretical plate considering only extra-column band broadening, and Δt is the total instrumental dead time, which accounts for any dead time contributions from the inlet, connection lines, and the detector. Note that this source of band broadening increases as the square of the carrier gas velocity and thus can become very significant on the right-hand flanks of the Golay and Spangler plots.

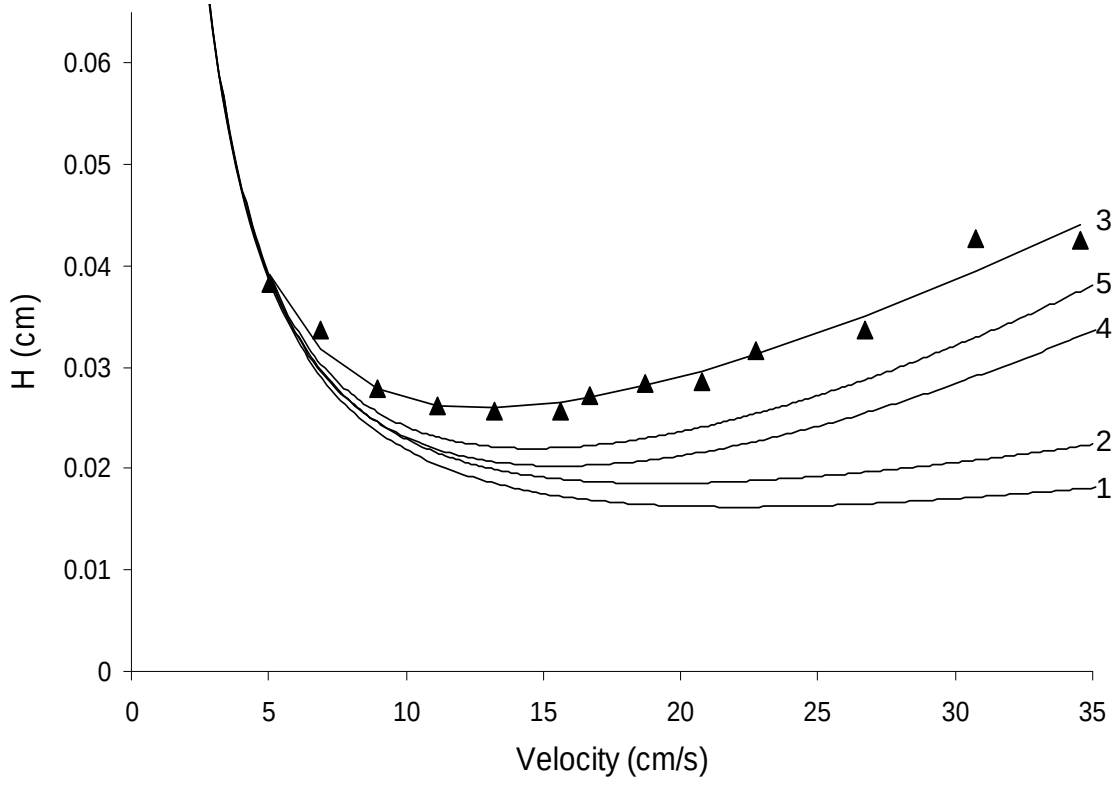

Figure 2.3. Plots of height equivalent to a theoretical plate versus average carrier gas (air) velocity for a 3-m long static-coated column. 1, plot from equation 2.1; 2, plot from equation 2.3; 3, plot for experimental data using n-octane at 40°C; 4 and 5, plots 1 and 2 corrected for extra-column band broadening using experimental data and equation 2.4 respectively.

The coefficient of u^2 in equation (5) was determined by fitting the experimental data in Plot 3 of Figure 2.3 to the general form of the Golay equation given in equation 2.6.

$$H = \frac{B}{u} + Cu + Du^2 \qquad 2.6$$

The line shown in Plot 3 of Figure 2.3 is the fit to equation 2.6. From the coefficient *D* and the known values of the column length and solute retention factor, the total instrumental dead time was found to be about 0.21 s for octane. Most of this can be attributed to the split inlet, the connecting lines, and the electrometer used to monitor the FID signal.

When this extra-column band broadening term is added to equations 2.1 and 2.3, Plots 4 and 5 in Figure 2.3 are obtained for the Golay and Spangler theory, respectively. The shapes of the plots and the plate height values are significantly closer to those of the experimental data in Plot 3. The Spangler model proves to be a better fit to the experimental data, and thus further consideration will only be given to this model. The minimum plate height from Plot 5 is 0.022 cm, and the optimum carrier gas velocity is 15 cm/s.

From Plot 3 in Figure 2.3, the 3.0-m long column used in this study generates about 12,500 theoretical plates at the optimum carrier gas velocity. This is nearly 4,200 plates per meter and is substantially greater than the 2,000-2,500 plates per meter typically generated with the dynamically coated columns previously described[14-16]. However, according to Plot 5 in Figure 2.3, this column should be able to generate nearly 4,700 plates per meter when used with air carrier gas at the optimum operating velocity and with the experimental platform used in this study.

In Figure 2.4 (a) Plot 5 from Figure 2.3 is resolved into its components based on the coefficients of the model described in equation (3) along with the extra-column band broadening term (D) from equation (6). Plot 5 from Figure 2.3 is also reproduced for reference (H_5). In Figure 2.4 (b), Plot 3 from Figure 2.3 is resolved into its components based on the coefficients B, C and D from equation (6). Plot 3 from Figure 2.3 is also reproduced for reference (H_3).

Plots labeled *D,* for extra-column band broadening, in the two sets are identical since in both cases, they are from fits to the experimental data of plate height versus average carrier gas velocity. Plots labeled *B,* for longitudinal diffusion, are quite similar for the two sets of plots suggesting that the value of gas-phase binary diffusion coefficient used in the calculations (0.093 cm^2/s) is reasonably accurate. For Plots *C* from non-equilibrium effects, both the gas-phase contribution C_g and the stationary-phase contribution C_s obtained from equation (3) are shown in Figure 2.4 (a). The sum of these is also shown in the figure. In Figure 2.4 (b) only the sum can be obtained from equation (6) using the fit to the experimental data.

Two things should be noted regarding the *C* terms. First, from Figure 2.4 (a), the C_s contribution is very small, typically contributing about 2.5% to the sum. This is the result of the thin stationary-phase films obtained from static coating. Second, the *C*-term sum is substantially larger in Figure 2.4 (b), and this is the main source of difference between the overall values of *H* for the model modified by the extra-column band broadening (Plot 5 in Figure 2.3) and the fit to the experimental data (Plot 3 in Figure 2.3). It is not expected that pooling or sagging of the stationary phase in the 90° turns or down the column walls contributes significantly to band dispersion as a result of

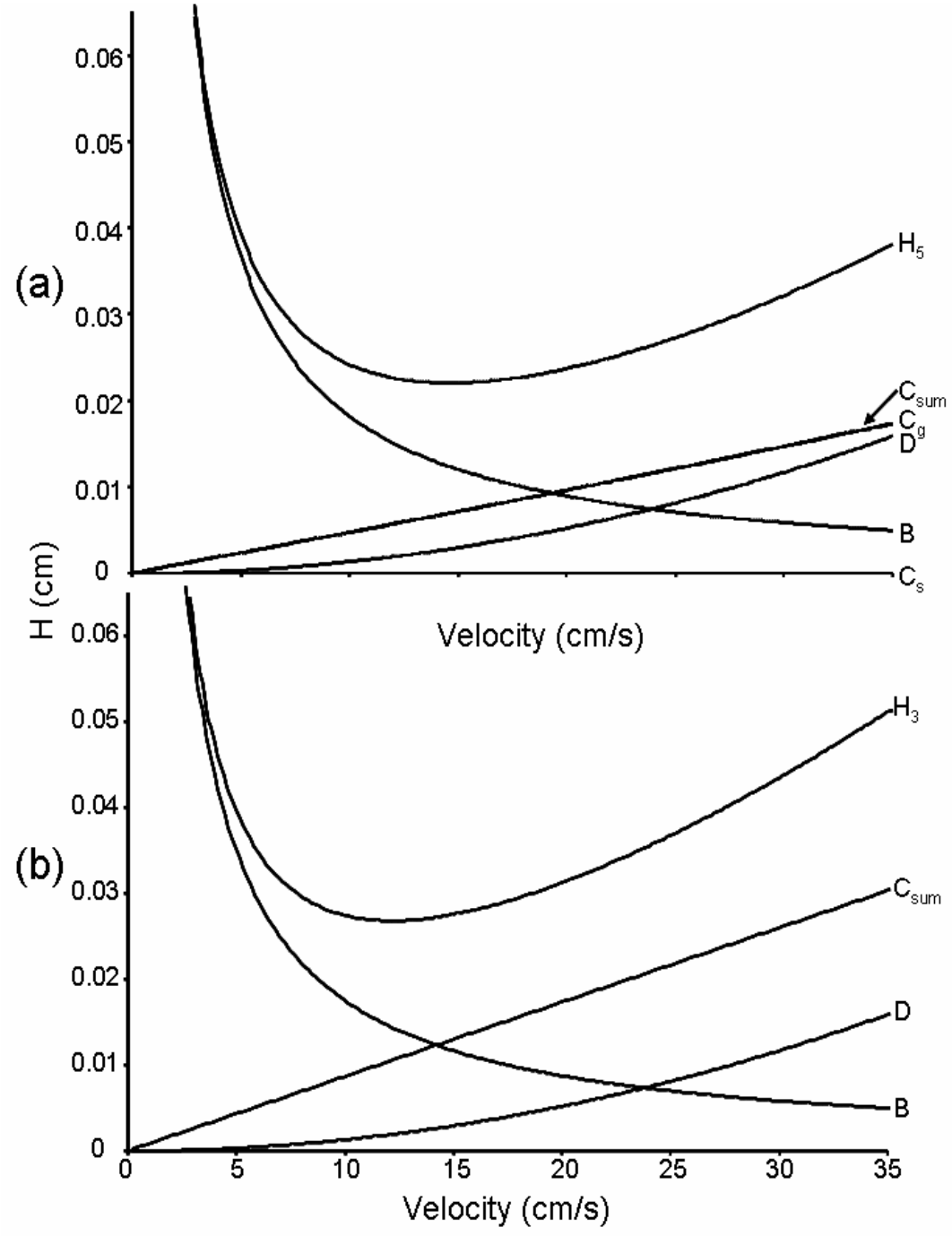

Figure 2.4. Plots of height equivalent to a theoretical plate versus average carrier gas (air) velocity for a 3-m long static-coated column showing Plot 5 (a) and Plot 3 (b) from Figure 2.3 resolved into the individual band-broadening sources. *B*, longitudinal diffusion; C_g, gas-phase non-equilibrium effects; C_s, stationary-phase non-equilibrium effects; *D*, extra-column band broadening. In (a), the sum of C_g and C_s is shown. In (b) only the sum is shown.

static coating. Even significant errors in the estimation of the stationary-phase diffusion coefficient or the channel dimensions are unlikely to change C_s enough to account for the difference in the sums. Thus it is probable that the value of the C_g term accounts for the poorer efficiency of the micro-fabricated column relative to the predictions of the model.

These data suggest either a significant error in the channel width value used in computing the C_g term or an additional source of gas-phase band broadening not accounted for in equation (3). The columns used in this study make many sharp turns. For the 3-m long column, a total of 230 right-angle turns are made, half left turns and half right turns. Studies with micro-column liquid-phase separations[29-31] have shown that the so-called race-track effect can cause significant dispersion in the moving phase. The point is that solute molecules on the outside of a turn travel further during the turn than molecules on the inside. Because of diffusion across the channel, having the same number of right and left turns does not completely cancel this added dispersion. Modeling of this source of band broadening for liquid-phase separations shows that like the C_g term, dispersion increases with increasing moving phase velocity and decreases with increasing moving-phase binary diffusion coefficient. This could explain the larger C term observed in the results from the experimental data relative to the value predicted from equation (3). Further work is in progress to clarify these points for micro-fabricated GC columns.

Test Chromatograms. Figure 2.5 shows chromatograms from a 15-component multi-functional test mixture using a 0.5-m (a), a 1.0-m (b) and a 3.0-m long (c) static-coated micro-fabricated column. Properties of the columns are listed in Table 2.1. Peak numbers correspond to component numbers in Table 2.2 under Isothermal

Chromatograms. The chromatograms were obtained at room temperature (24°C) using a stand-alone split/splitless inlet and a stand-alone FID. The injection size was 0.1 μL, and the split ratio was 400:1. All columns were operated at their optimal flow rate (15-20 cm/s). With all three columns, peak shapes are excellent with no signs of tailing or other artifacts. Since the stationary-phase film thickness is only about 0.15 μm, the lack of tailing suggests that the untreated silicon surface is not highly active for these components, and for many applications may be directly coated without the need for prior deactivation.

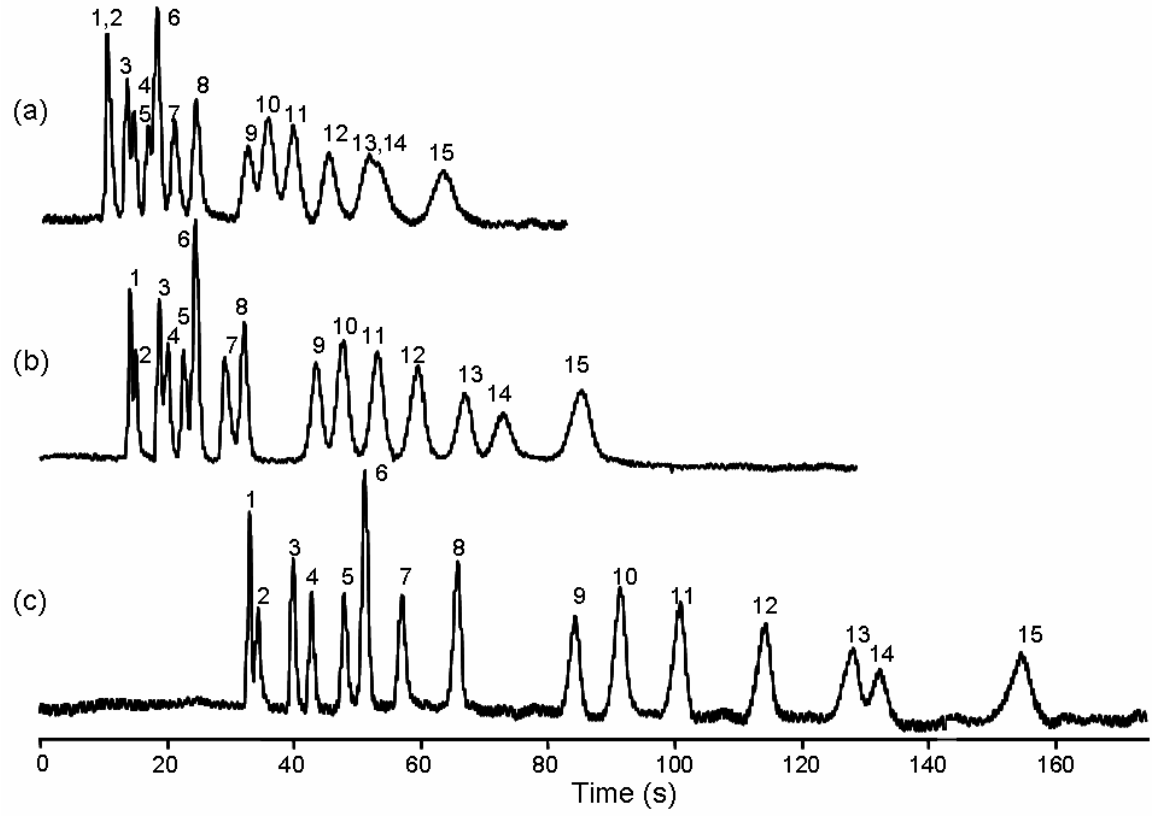

Figure 2.5. Test chromatograms of a 15-component mixture separated isothermally at 30°C using a 0.5-m (a), 1.0-m (b) and 3.0-m long static-coated columns. Peak numbers correspond to compound numbers in Table 2.2.

Temperature-Programmed Operation. Previous studies with fused silica capillary columns using air as the carrier gas showed that commercial columns with cross-linked dimethyl polysilxane could be heated to 210°C for extended periods of time without degradation of the stationary phase[32,33]. Rapid degradation occurred at a temperature of 230°C. The thermal stability of silicon MEMS columns with air carrier gas at elevated temperatures has not been studied. To reduce the risk of column degradation, temperature programmed studies were limited to a maximum temperature of 180°C.

Figure 2.6 shows temperature-programmed chromatograms of a n-C_5 to n-C_{12} normal alkane mixture using a 3.0-m long column (a) and a 0.25-m long column (b). Both columns were static coated and cross-linked. The starting temperature was 30°C and the programming rates were 30°C/min (A), 20°C/min (B) and 10°C/min (C) for the 3.0-m long column and 50°C/min (A), 30°C/min (B), 10°C/min (C) for the 0.25-m long column. The 3-m and 0.25-m long columns were operated at 14 cm/s and 18 cm/s respectively. Note that with temperature programming, higher boiling point compounds benefit from on-column focusing, and the effects of extra-column band broadening from the split inlet are reduced. This is particularly useful with the relatively short columns used in this study. No peak tailing or other artifacts are observed. With the shorter column and the 50°C/min programming rate, n-C_{12} is eluted in about 120 s with a peak capacity of about 28 peaks.

Figure 2.7 shows plots of cumulative peak capacity n_c versus retention time obtained from the chromatograms shown in Figure 2.6. The cumulative peak capacity n_c (resolution = 1.18) for the retention range n-C_x to n-C_y is obtained by summing the

Trenzahl numbers (*TZ*) according to equations 2.6 and 2.7 and adding the reference peaks[34-37].

$$TZ = \frac{t_{R(n+1)} - t_{R(n)}}{w_{1/2(n)} + w_{1/2(n+1)}} - 1 \qquad (2.6)$$

$$n_c = \sum_{n=x}^{n=y} (TZ + 1) \qquad (2.7)$$

Where $t_{R(n)}$ and $t_{R(n+1)}$ are the retention times of two adjacent normal alkanes, and $w_{1/2(n)}$ and $w_{1/2(n+1)}$ are the corresponding full widths at half peak height. For example, with the 0.25-m long column and a programming rate of 50°C/min, n-C_{10} is eluted in about 70 s with a total peak capacity of 18 peaks. Note that with the 3.0-m long column and a 10°C/min programming rate the entire chromatogram has a peak capacity of about 105 peaks.

Previous work with temperature-programmed GC has shown that if the temperature change of the column is no more than about 15 °C during a time interval equal to the column holdup time, then the loss of peak capacity relative to lower programming rates is minimal[38]. For the 0.25-m long column used in this study, the holdup time is about 2 s. This suggests that much higher programming rates than the 50°C/min used here can be used with corresponding reductions in analysis time.

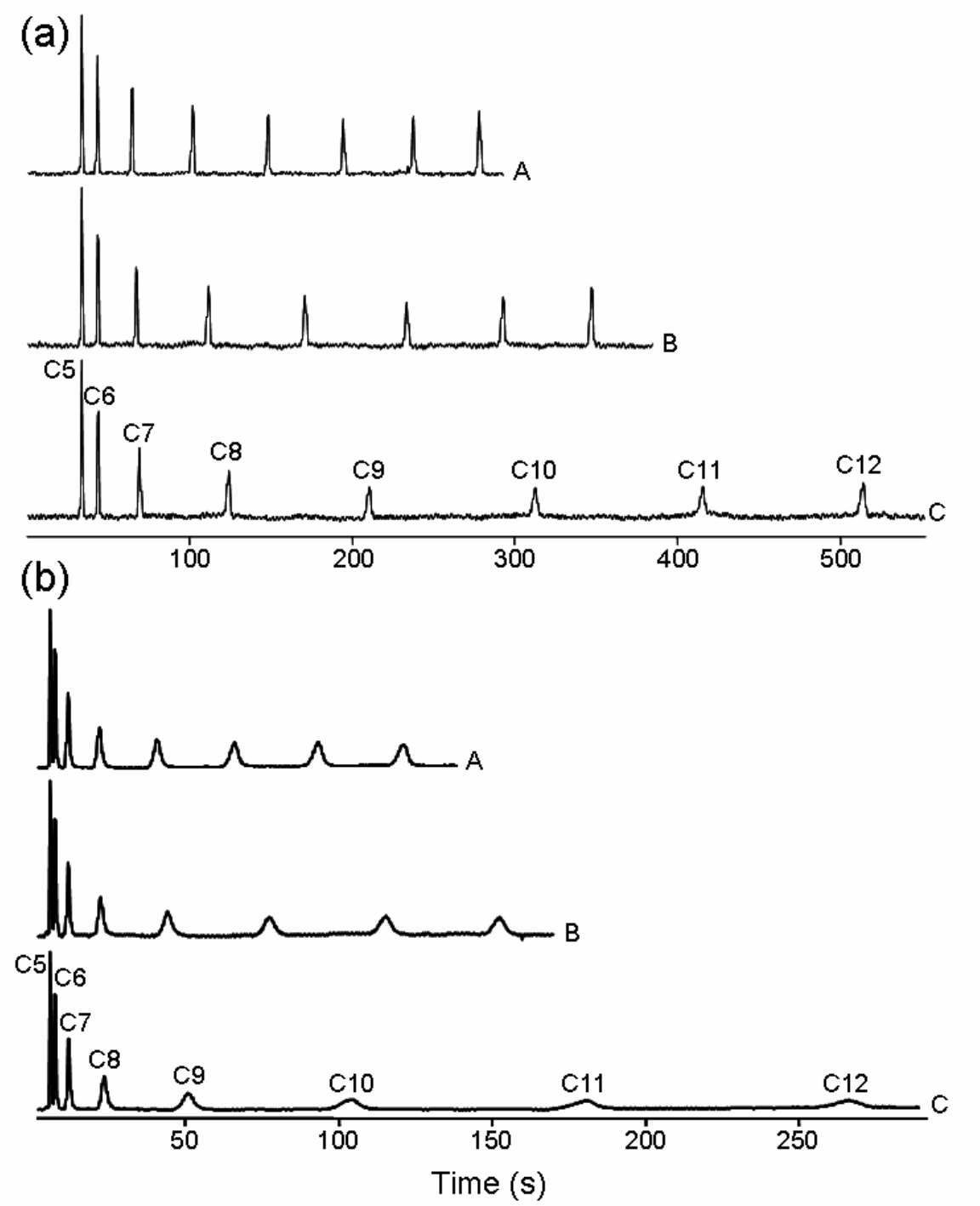

Figure 2.6. Temperature-programmed chromatograms of an n-C_5 to n-C_{12} mixture of normal alkanes using a 3.0-m long column (a) and a 0.25-m long column (b). For (a), programming rates were 30 ^{o}C/min (A), 20 ^{o}C/min (B) and 10 ^{o}C/min (C). For (b), the programming rates were 50 ^{o}C/min (A), 30 ^{o}C/min (B) and 10 ^{o}C/min (C). In all cases, the starting temperature was 30^{o}C and the final temperature was 180^{o}C.

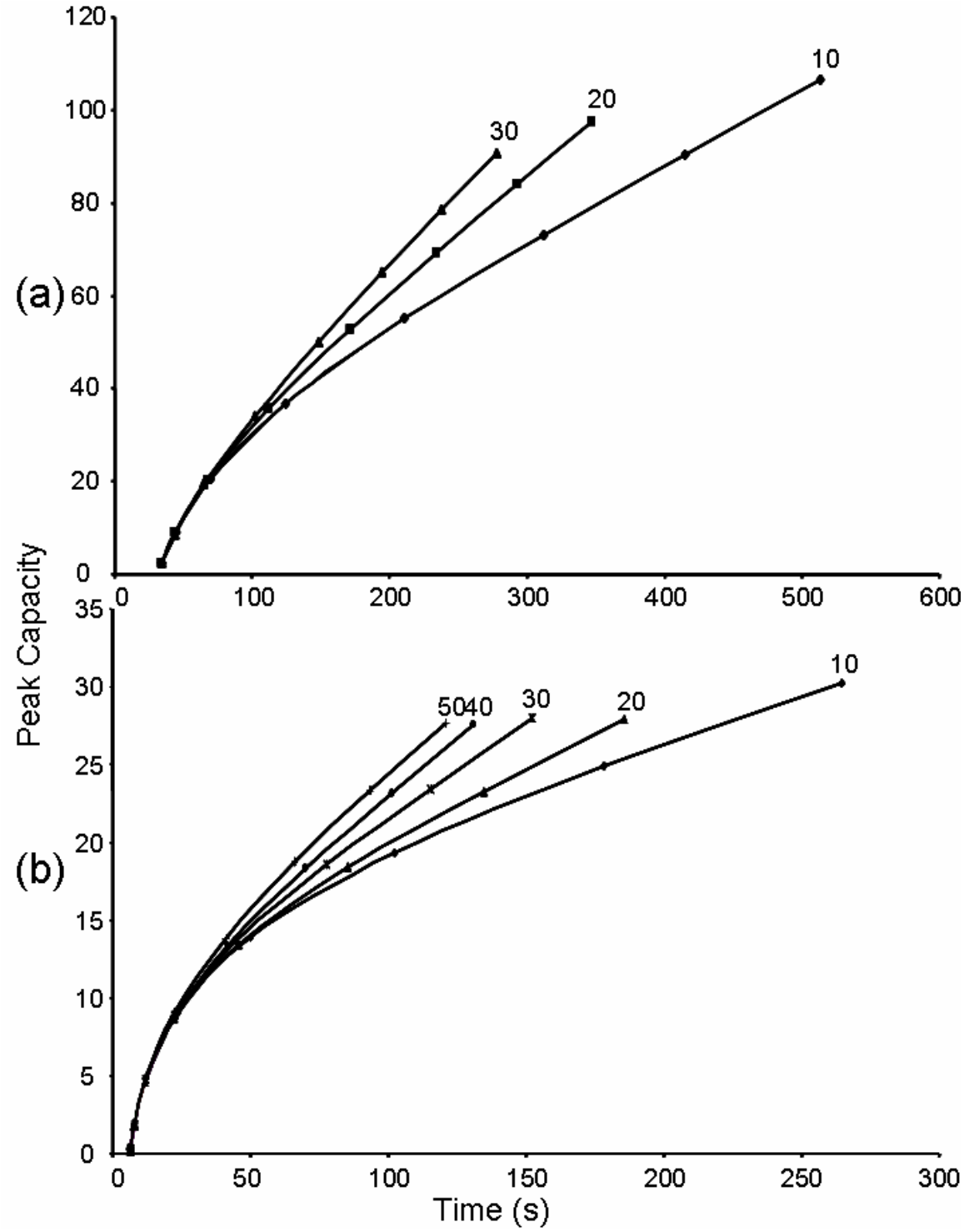

Figure 2.7 Plots of cumulative peak capacity nc versus retention time for the temperature-programmed separation of a n-C_5 to n-C_{12} normal alkane mixture using a 3.0-m (a) and a 0.25-m (b) long static-coated column. Numbers next to plots give temperature-programming rates in ^{o}C/min. In all cases, the starting temperature was 30^{o}C and the final temperature was 180 ^{o}C.

However, 50°C/min is about the highest rate that can be achieved with the commercial GC used in this study. This clearly shows the limitations of conventional convective ovens for high-speed GC with short micro-fabricated columns.

Figure 2.8 shows temperature-programmed chromatograms of an air-phase petroleum hydrocarbon mixture (a) using a 3.0-m long column and a mixture of chemical warfare agent markers (b) using a 0.25-m long column. Mixture (a) is available commercially and is used to monitor waste-site remediation. For this mixture, the starting temperature was 30°C and after a 2.0-min isothermal hold, the column was heated at 30°C/min to 180 °C with an average carrier gas velocity of ~14 cm/s. The inset above and to the left shows the early portion of the chromatogram on an expanded time scale. The peak shapes are excellent. Two co-elutions are observed. Note that the two xylene isomers (peaks 12 and 13) are difficult to separate with any column. Note that under isothermal conditions the separation of components 19 and 20 can be improved. For chromatogram (b), the programming rate was 30°C/min. with a starting temperature of 40°C with an average carrier gas velocity of ~12 cm/s. The chromatogram is complete in less than 1 min. Note that the very polar DMMP is severely tailed on the micro-fabricated column. This is potentially due to active sites on the column. Tailing is seen with many polar compounds though DMMP is most severe. Peak numbers correspond to compounds listed in Table 2.3, Applications Chromatograms (a) and (b), respectively.

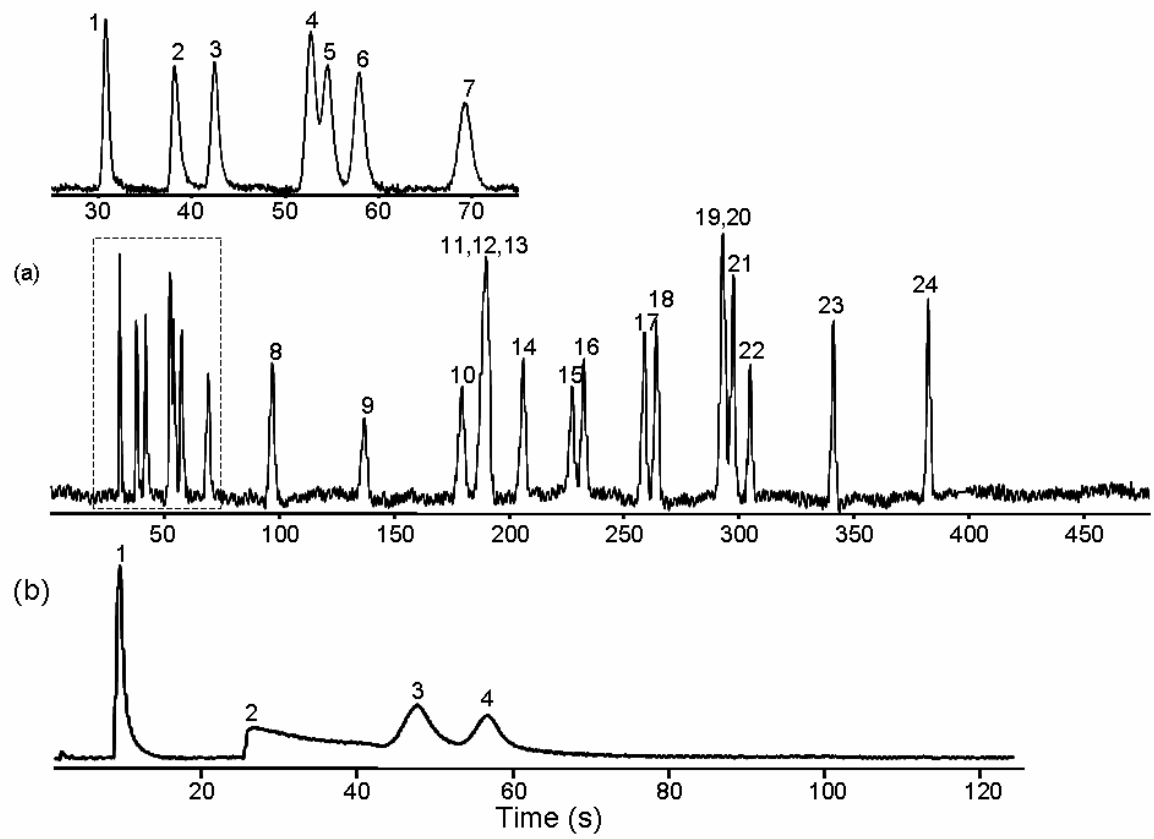

Figure 2.8. Temperature-programmed chromatograms of an air-phase petroleum hydrocarbon mixture (a) using a 3.0-m long column and a mixture chemical warfare and explosive agent markers (b) using a 0.25-m long column. Chromatogram (a) had an initial hold at 30°C for 2 min and then ramped to 180°C at 30°C/min. Chromatogram (b) was ramped at 30°C/min from 40-180°C.

Table 2. 3. Component list for applications chromatograms and their boiling points (in °C)

(a)

1	Isopentane	30	13	p-xylene	138.3
2	Methyl tert-butyl ether	55.2	14	o-xylene	144
3	Hexane	69	15	Nonane	150.8
4	Benzene	80.1	16	Isopropylbenzene	151
5	Cyclohexane	80.7	17	1-methyl-3ethyl-benzene	158
6	2,3-dimethylpentane	90	18	Mesitylene	165
7	Heptane	98.4	19	Decane	174.1
8	Toluene	110.6	20	1,2,3-trimethylbenzene	175
9	Octane	126	21	p-isopropyltoluene	177
10	Ethylbenzene	136.2	22	Butylcyclohexane	181
11	2,3-dimethylheptane	141	23	Undecane	195.9
12	m-xylene	139	24	Dodecane	216.3

(b)

1	Cyclohexanone	155	3	2-nitrotoluene	220
2	DMMP	181	4	Methylsalicylate	224

Conclusions

Static coated, thin film silicon MEMS columns with *in situ* cross-linking have been prepared that can generate over 4000 theoretical plates per meter. This compares favorably with commercial fused silica wall-coated open-tubular columns. The cavitation problems experienced with earlier attempts at static coating appear to be solved, and column coating is relatively straightforward and rapid. It appears that the surface activity of the native etched silicon surface is sufficiently low that it can be wetted by a thin film of PDMS, and thus for many potential applications, no surface deactivation is necessary prior to coating. A 3.0-m long column generates about 12,500 theoretical plates under isothermal conditions with air as the carrier gas and a peak capacity of over 100 peaks for temperature programmed separation at 10^{o}C/min of an n-C_5 to n-C_{12} alkane mixture.

With *in situ* cross-linking, these columns appear thermally stable to at least 180^{o}C using air carrier gas. The use of air is particularly attractive for on-site applications and for remote sensing where the need for on-board carrier gas supplies is a significant limitation. However, the optimum carrier gas velocities in air are significantly lower than with more diffusive gases such as hydrogen and helium. This results in longer separation times at a specified resolution. In addition, the upper temperature limit with air is significantly lower than with hydrogen or helium.

Column efficiency studies suggest that there is additional gas-phase band broadening occurring with these silicon MEMS columns beyond that usually associated with longitudinal diffusion and non-equilibrium effects. This may be attributed to the large number of turns in the gas flow path associated with the column geometry (race-

track effect). For the 3.0-m long column evaluated in this study, this geometric dispersion appears comparable in magnitude to non-equilibrium effects in the gas phase. Further work is needed in this area.

References

[1] Lorenselli, L.; Benvenuto, A.; Adami, A.; Guarnieri, V.; Margesin, B.; MUlloni, V.; Vincenzi, D. *Biosensors and Bioelectronics*, **2005**, 20, 1968-1976.

[2] Abhinav Bhushan, Dawit Yemane, Praveen Pasupuleti, Edward B. Overton, Jost Goettert, and Michael C. Murphy, "Fabrication and Testing of High Aspect Ratio Metal Micro-Gas Chromatograph Columns", Proc. of the ASME IMECE 2004, 2004 ASME International Mechanical Engineering Congress & Expo, Anaheim, CA, November 13-19, **2004**.

[3] A. Bhushan, V. Challa, J. McKeon, D. Yemane, E. B. Overton, M. C. Murphy, J.Goettert, "Application of Scanning Acoustic Microscopy in Characterizing Metal Micro Gas Chromatograph Columns", TMS Letters, 1 (7) **2004**, 145-146.

[4] Manginell, R. P.; Okandan, M.; Bauer, J. M.; Manley, R.G.; Trudell, D.; Kottenstette, R. J.; Lewis, P. R.; Adkins, D.; Heller, E. J.; Stewart, H.; Shul, R. J. "Advancements in the monolithically integrated MicrochemLab (TM)", Micro Total Anlysis Systems 2004 - *μTAS '04*, Vol. 2 (297) (**2005**), 61-63.

[5] Overton, E. B.; Carney, K. R.; Roques, N.; Dharmasena, H. P. *Field Anal. Chem. Technol.* **2001**, *5* (1-2), 97.

[6] Yu, C. M.; Lucas, M.; Koo, C.; Stratton, P.; DeLima, T.; Behymer, E. *Micro*-Electro-Mechanical Systems (MEMS) **1998**; DSC Vol. 66, 481.

[7] Noh, H.; Hesketh, P. J.; Frye-Mason, G. C. *J. Microelectromech. Syst.* **2002**, *11* (6), 718.

[8] Kolesar, E. D.; Reston, R. R. IEEE Trans. Compon., Packag., Manuf. Technol. **1998**, 21 (4), 324.

[9] Potkay, J. A.; Driscoll, J. A.; Agah, M.; Sacks, R. D.; Wise, K. D. *Proc. 16th Annual IEE Conference on Micro-Electro-Mechanical Systems (MEMS),* Kyoto, Japan, January 19-22, **2003**;. 395.

[10] Agah, M.; Potkay, J.; Elstro, A.; Lambertus, G.; Sacks, R.; Wise, K. "A high-performance temperature-programmed gas chromatography column," *North American Solid-State Sensors, Actuators, and Microsystems Workshop*, Hilton Head Island, SC, June 6-10, **2004**, 302-305.

[11] Agah, M.; Potkay, J. A.; Driscoll, J. A.; Sacks, R. D.; Kaviany, M.; Wise, K. D. "Thermal Behavior of High-Performance Temperature-Programmed Microfabricated Gas Chromatography Columns," *Technical Digest of the 12th International Conference on Solid-State Sensors, Actuators and Microsystems*, Boston, Massachusetts, June 8-12, **2003**, 1339-1342.

[12]Agah, M.; Potkay, J. A.; Lambertus, G. R.; Sacks, R. D.; Wise, K. D. "High-performance Temperature-Programmed Microfabricated Gas Chromatography Columns," *IEEE J. Microelectromech. Systems, 14* (5), **2005**, .1039-1050.

[13] Zellers, E. T.; Steinecker, W. H.; Lambertus, G. R.; Agah, M.; Lu, C.-J.; Chan, H. K. L.; Potkay, J. A.; Oborny, M. C.; Nichols, J. M.; Astle, A.; Kim, H. S.; Rowe, M. P.; Kim, J.; Da Silva, L. W.; Zheng, J.; Whiting, J. J.; Sacks, R. D.; Pang, S. W.; Kaviany, M.; Bergstrom, P. L.; Matzger, A. J.; Kurdak, Ç.; Bernal, L. P.; Najafi, K.; Wise, K. D., "A versatile MEMS gas chromatograph for environmental vapor mixture analysis," (Invited) *Proceedings Solid-State Sensor, Actuator, and Microsystems Workshop*, Hilton Head Island, SC, June 6-10, **2004**, 61-66.

[14] Lambertus, G. R.; Elstro, A.; Sensenig, K.; Potkay, J.; Agah, M.; Scheuering, S.; Wise, K. D.; Dorman, F.; Sacks, R. *Anal. Chem*. **2004**, *76*, 2629.

[15] Lambertus, G. R.; Sacks, R. *Anal. Chem*. **2005,** *77,* 2078.

[16] Lambertus, G. R.; Fix, C. S.; Reidy, S. M.; Miller, R.; Wheeler, D.; Nazarov, E.; Sacks, R. D. *Anal. Chem*. **2005**, *77*, 7563.

[17] Lehmann, U.; Krusemark, O.; Müller, A.; Vogel, A.; Binz, P.; Krippner, P.; Schmidt, C. J.; "Micro machined analytical gas chromatograph with a plasma polymerized stationary phase", proceedings *Sensor,* **2001**, vol. 2, 487-492.

[18] Grob, K. *Making and Manipulating Capillary Columns for Gas Chromatography*; Dr. Alfred Huthig Verlag: Heidelberg, **1986**.

[19] Golay, M. J. E. *In gas Chromatography* **1958** (East Lansing Symposium); Coates, V. J.; Noebels, H. J.; Fagerson, I. S., *Eds.; Academic Press: New York,* **1958**, 1-13.

[20] Golay, M. J. E. *J Chromatogr*. **1981**, 216, 1.

[21] Giddings, J. C.; Chang, J. P.; Myers, M. N.; Davis, J. M.; Caldwell, K. D. *J Chromatogr.* **1983**, 255, 359.

[22] Spangler, G. E. *Technical Proceedingsof the Third International Conference on Modeling and Simulation of Microsystems,* San Diego, CA, March 2000, 562-565.

[23] Spangler, G. E. *J. Microcolumn Separations*, **2001**, 13 (7), 285.

[24] Kolesar, E. S.; Reston, R. R. *Surf. Coat. Technol*. **1994**, 68/69, 679.

[25] Fuller, E. N.; Schettler, P. D.; Giddings, J. C. *Industrial and Engineering Chemistry*, **1966**, 58 (5), 19.

[26] Kong, J.M.; Hawkes, S. *J. Journal of Chromatographic Science*, **1976**, 14 (6), 279-287.

[27] Weast, R., Ed. *CRC,* 49th ed.; The Chemical Rubber Co., **1968**.

[28] Gaspar, G.; Annino, R. Vidal-Madjar, G.; Guiochon, G. *Anal. Chem.* **1978**, 50, 1512

[29] Fu, L-M.; Yang, R-J; Lee, G-B. *Electrophoresis*, **2002**, 23, 602-612.

[30] Molho, J. I.; Herr, A. E.; Mosier, B. P.; Santiago, J. G.; Kenny, T. W. *Anal. Chem*. **2001**, 73, 1350-1360.

[31] Culbertson, C. T.; Jacobson, S. C.; Ramsey, J. M. *Anal. Chem*. **1998**, 70, 3781-3789.

[32] Grall, A. J.; Sacks, R. D. *Anal. Chem*. **1999**, *71*, 5199.

[33] Grall, A. J.; Zellers, E. T.; Sacks, R. D. *Environ. Sci. Technol.* **2001**, *35*, 163.

[34] Hurrell, R. A.; Perry, S. G. *Nature* **1962**, *196*, 571.

[35] Grob, K., Jr.; Grob, K. *J. Chromatogr*. **1981**, *207*, 291.

[36] Ettre, L. A. *Chromatographie* **1975**, *80*, 291.

[37] Kaiser, R. *Chromatographie in der Gasphase*, 2nd ed.; Bibliografisches Institut: Mannheim, Germany. 1966; Vol. 2.

[38] Grall, A.; Leonard, C.; Sacks, R. *Anal. Chem*. **2000,** *72*, 591.

Chapter 3

Temperature Programmed Gas Chromatograph using Silicon Microfabricated Columns with Integrated Heaters and Temperature Sensors*

Introduction

Micro-fabricated columns for gas chromatography (GC) are under development in several laboratories[1-8]. These columns are particularly attractive for on-site applications due to their very small size and very low power requirements for column heating. Several studies have shown the utility of silicon etched columns for GC[4,7,9-13]. With deep reactive ion etching, columns as long as 3.0 m are fabricated on standard 4-in silicon wafers[12-15]. Both dynamic coating[16], where a plug of coating solution is pushed through the column, and static coating[17], where the entire column is filled with coating solution and the solvent pumped away, are used to introduce stationary phase onto the walls of the rectangular silicon channels. Static coating is preferred since thinner, more uniform stationary-phase films can be applied, and film thickness is more easily determined[18].

Columns are fabricated using a modified Bosch process for deep reactive ion etching[12-15]. The rectangular cross-section channels are shaped as a double square spiral to accommodate a square chip format while obtaining maximum use of chip surface area.

Published : Reidy, S. et al. Analytical Chemistry, **2007, 79(7), 2911.*

The channels are sealed by anodically bonding a thin Pyrex wafer onto the open surface of the channel. Columns with channel lengths of 0.25 m, 0.50 m, 1.0 m, and 3.0 m have been described. Recently a 0.1-0.2 μm thick poly(dimethylsiloxanes) (PDMS) film, statically coated on a 3-m long by 150 μm wide by 240 μm deep channel, etched in silicon substrates, generated more than 12,000 theoretical plates when using air as the carrier gas[17]. The number of theoretical plates was calculated by dividing the column length by the minimum plate height, as found experimentally by plotting plate height versus carrier gas velocity, a Golay plot, under isothermal conditions (23°C).

Columns using both non-polar PDMS and moderately polar poly(3,3,3-trifluoropropylmethylsiloxanes) have been described[16,19]. Tunable selectivity[20-25] has been achieved with a tandem ensemble of silicon micro-fabricated columns using these two stationary phases[19]. These columns also have been used with a micro-fabricated differential ion mobility spectrometer for detection. The result is high-peak-capacity two-dimensional separations[26].

For the GC separation of wide-boiling-point range mixtures, temperature programming is essential. Most previous work with silicon micro-fabricated columns used conventional convection ovens for heating to ensure uniform heating with accurate temperature control[16,26]. For on-site applications, alternative heating techniques, which operate with much lower power and are much smaller and lighter weight, are required[27-29]. In addition, for fast separations using relatively short columns, convection ovens can not be heated fast enough while maintaining linear temperature ramps.

Columns fabricated at Sandia National laboratories use thin film resistance heaters patterned in the etched silicon channels[7,30] to achieve this.

This study describes the use of resistance heaters and resistance-temperature detectors (RTD) patterned on the back side of silicon chip columns[13,15]. Because of the high thermal conductivity of silicon, localized heaters can be used to achieve reasonably uniform temperatures across the silicon chip[14]. A versatile temperature controller using a proportional-integral microcontroller also is described. The device can generate linear programming ramps of several hundred ^{o}C/min. Test chromatograms are presented using etched silicon micro-fabricated columns with lengths of 0.25 m and 3.0 m with programming rates as high as 1000^{o}C/min.

Experimental

Apparatus. The GC instrument is constructed entirely from stand-alone components. A split/splitless inlet system from an HP 6890 is used for all experiments. This inlet generated injection plug widths of 250 ms or less. Detection is accomplished with a Varian FID from a Varian 3500 GC. The Varian FID is used because it is easier to connect to alternative electrometer/amplifiers designed in house for faster data logging. Data are logged with a sampling rate of 100 Hz. All connections are made with 100-μm i.d. deactivated fused silica tubing. Connecting lines are heated to approximately 150^{o}C (±5°C) using Kapton flexible heater strips (Omega, Stamford, CT) wrapped around machined aluminum blocks. Connecting line temperature is controlled by varying the voltage applied from a Variac power supply as measured by a J-type thermocouple (Omega, SA1-J).

Column Design. Column fabrication and stationary-phase coating have been described in detail[12-15]. Channels are etched in standard 4-in silicon wafers. Nearly rectangular cross-section channels are formed by deep reactive-ion etching. Nominal channel dimensions are 150-µm wide by 240-µm deep. For 3-m long channels, four columns are fabricated on each wafer and diced into 3.2 cm x 3.2 cm chips after sealing the open channel surface with a 4-in Pyrex glass wafer. Column lengths of 1.0 m, 0.5 m and 0.25 m, are etched on a single chip, sealed and diced. For all columns, ports to accommodate 100-µm i.d., 245-µm o.d. fused silica connected lines (Polymicro Technologies, Pheonix, AZ) are etched into the wafers prior to sealing. Connected lines are epoxied (Loctite, Hysol 1C, Rocky Hill, CT) into the ports forming gas-tight seals. The upper temperature limit of this epoxy is approximately 150°C when held continuously at elevated temperatures.

Prior to dicing, resistance thermometers and RTD sensors are patterned on the back (substrate) side of each column[13-15]. This is accomplished by evaporating a 250Å thick film of Ti followed by a 500Å thick layer of Pt. Each heater has a nominal resistance of 280 ohms. For the 0.5-m, 1.0-m and 3-m long columns, heaters are positioned at the center of each edge of each chip to obtain more uniform heating over the chip surface. For the 0.25-m long column, only two heaters are patterned at the center of opposite edges. Pressure sensors also are fabricated near each end of the channel, but they are not used in the present study. The completed chips are epoxied (Loctite) to phenolic substrates and wire-bonded to solder terminals. A photograph of the back side of a mounted chip showing detailed micrographs of the heaters and sensors is shown in Figure 3.1.

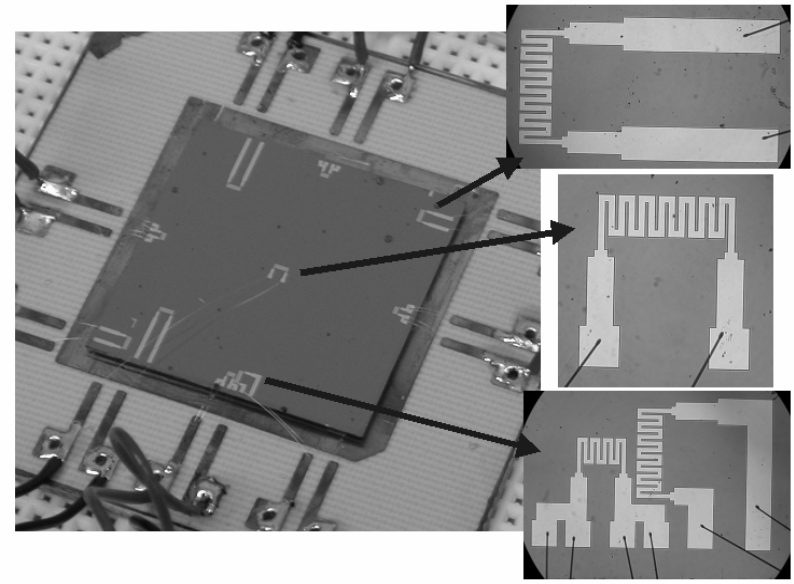

Figure 3.1. Photograph of 3.0-m long column chip mounted on a substrate and wire bonded to solder terminals. Insets show photomicrographs of integrated heaters and RTD sensors.

Temperature Controller. Initial studies with a simple on/off temperature control relay showed excessive temperature oscillations, and the proportional integral-derivative (PID) controller shown in Figure 3.2 was constructed. A micro-controller (Parralax, BS2p-24, Rocklin, CA) generates a pulse-width modulated signal that controls a relay that supplies current to the four heating units. The heaters are operated in parallel giving a total resistance of about 75 ohms. The drawing shows three heaters and an RTD. The forth heater, not shown, is located near the RTD. The room-temperature resistance of the RTD is about 650 ohms. The RTD is used as a feedback resistor in an oscillator circuit based on a high-input-impedance operational amplifier. The frequency of the square-wave output from the oscillator varies with the surface temperature of the silicon column chip. This square wave is used as the input to the controller which measures the width of the pulse. The pulse width is measured in units (counts) of 0.75 μs. The counts-to-temperature correlation is calibrated with an IR thermometer (Fluke 61, Everett, WA).

The column is calibrated by inputting a known count into the microcontroller and holding the column at that count value for 100 s. During this time the temperature of the column is measured five times. At the end of the 100 s, the temperature count value is increased by 500 counts and the column temperature is measured again. The average of the temperature values are plotted against the average of the corresponding count values. The columns are calibrated for the temperature range in which they are being operated. For every linear temperature ramp, the corresponding count rate and total number of counts for the final set-point temperature are input to the controller via a PC. Multiple ramps with different rates and isothermal intervals can be programmed into the device. The output of the controller controls the duty cycle of a 2.0 Hz square wave which is applied to the heater power relay. The duty cycle can be as high as 100%.

The photograph on the right side of Figure 3.2 shows the modular design of the controller and the column support substrate. A 0.25-m long column chip is shown wire-bonded to the left-hand phenolic board. The controller and associated circuitry is on the right-hand board. The boards are connected with a cable so that the controller can be used with different columns. An additional cable is used to connect the controller board to power supplies and a PC. The columns are heated using a regulated DC power supply. (Elenco Precision, XP-603, Wheeling, IL)

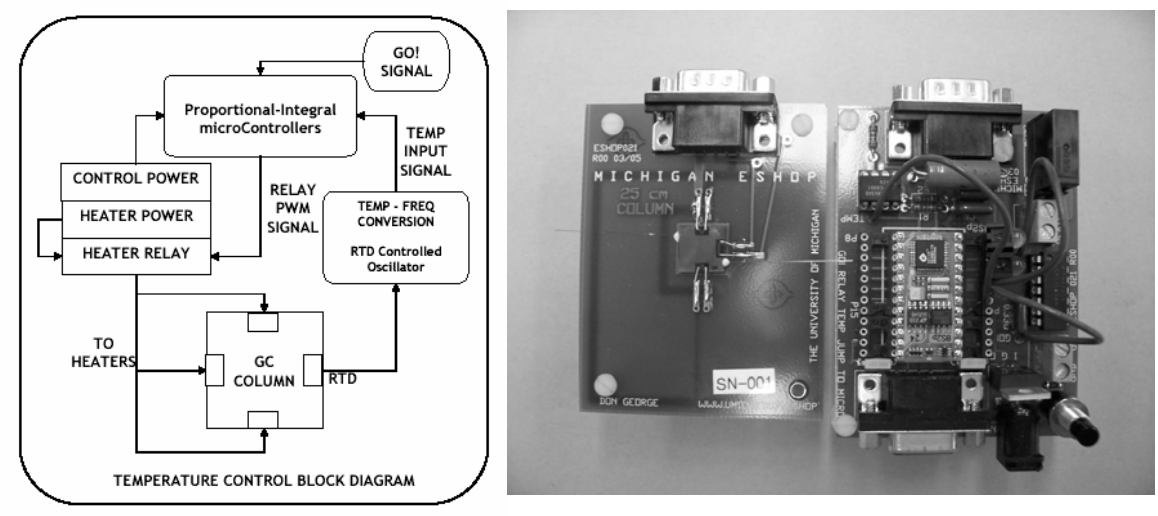

Figure 3.2. Left, diagram of the proportional integral controller used for heating the silicon MEMS columns; right, photographs of the 0.25-m long column wire-bonded to solder terminals on a phenolic support and the control board used for column heating.

Materials and Procedures. Air was used as carrier gas after filtering to remove water vapor and hydrocarbons. Head pressure was controlled using an electronic pressure controller (Model 640, MKS, Andover, MA). All data were logged at 100 Hz with an electrometer built in house and a 16-bit A/D board (Model DAS 1602-16, Computer Boards, Inc. Middleboro, MA) interfaced with a PC (Gateway GP6-350, Irvine, CA) . The RTD was calibrated with an IR thermometer. Test mixtures were injected with a split ratio of 300:1. Injection volume was 0.1μL. Interface control was provided by LabTech Notebook software (Version 10.1, Laboratory Technologies, Corp., Andover, MA). Chromatograms were processed with Grams/32 software (Galactic Industries, Salem, NH). Test mixtures were prepared using reagent-grade chemicals (Aldrich, Milwaukee, WI).

Results and Discussion

Temperature Uniformity. Initial attempts at heating the columns without thermal insulation showed that linear ramps could be obtained but only at temperatures below about 100°C and only with relatively low heating rates. The Pyrex glass plate used to seal the channel is a good thermal insulator but the silicon substrate is a good thermal conductor. The chips are mounted on the phenolic boards with the silicon surface facing up to facilitate wire bonding and connection to the controller and power supply. The worst case occurs for the 3.0-m long column, which uses a 3.2 x 3.2 cm chip. This is a relatively large surface area and heat loss is extensive especially at higher temperatures. Figure 3.3 shows thermal images of a 3.0-m long un-insulated micro-fabricated column mounted on a printed circuit board and wire bonded to solder terminals.

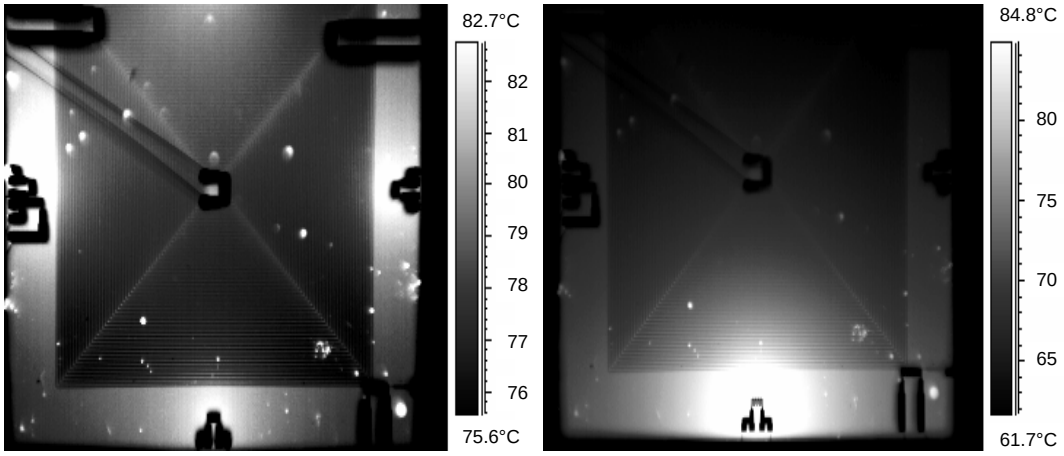

Figure 3.3. Thermal images of 3-m long columns with only one heater operating (right) and with all four heaters operating (left). Temperatures are shown on the gray scales to the right of each image. The two gray scales are not the same.

The right panel shows the case where only one of the four heaters is operating, and the left panel shows the case where all four heaters are operating. Temperature is shown on the gray-scale to the right of each panel. Note that the two scales are not the same. When only one heater is used, the temperature variation across the column chip is more than 10°C. When all four heaters are used, the temperature variation is less than

$2^{o}C$[14]. Because of smaller distances between the heaters, smaller temperature variations across the chips are observed for the shorter columns. However, for heating with linear ramps above 100°C, the chips were insulated with 1-cm thick fiber-glass padding having one surface clad with aluminum foil. The phenolic board containing the column was placed on a segment of this insulation, and an additional segment was placed loosely over the column so that it could be easily removed without disturbing the delicate wire bonds.

Temperature Programming with the 3-m Column. Figure 3.4 shows temperature time profiles for the 3.0-m long column. All temperature programs end with isothermal intervals at 150°C. Numbers next to plots show temperature programming rates in °C/min. Plots (a) show simple heating ramps. Plots (b) show more complex temperature programs consisting of linear ramps and isothermal intervals. Plots labeled (c) show four similar ramps superimposed. The plots are smooth with minimal oscillations. In most cases, excellent linearity is observed. In (a), some curvature is observed for the highest ramp rate especially for temperatures above 120°C. In plots (b), temperature changes at transition points at the beginning and end of each control segment are very abrupt suggesting very good temperature control. The temperature ramp for each control segment appears very linear for ramp rates at least as high as 125°C/min. At the end of each temperature-programmed run, the power-control relay is opened and the column cools to ambient temperature or to a new set-point temperature which takes several minutes. With the aid of a fan the column cooling time is decreased by a factor of five.

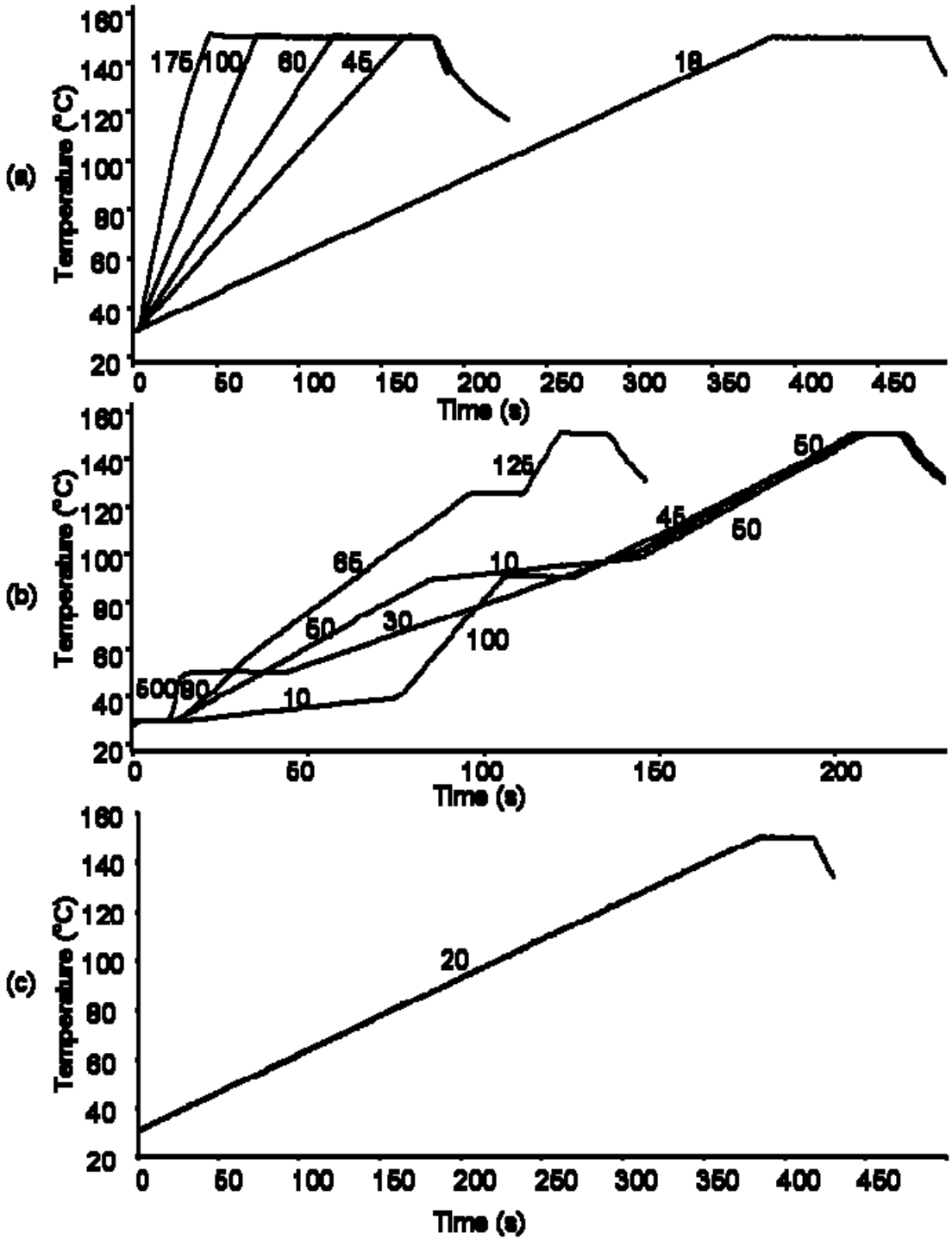

Figure 3.4. Temperature versus time plots for the 3-m long column using the proportional integral controller showing simple temperature ramps (a), complex ramps with isothermal intervals (b) and the superimposition of five similar ramps (c). Numbers on plots give the ramp rates in ^{o}C/min.

Figure 3.5 shows chromatograms obtained from an n-C_5 to n-C_{15} alkane mixture using the 3.0-m long micro-fabricated column with temperature programming rates of 20°C/min (a), 40°C/min (b) and 60°C/min (c). In all cases, the starting temperature was 30°C. The peak shapes are excellent with no indication of artifacts. For the 60°C/min case, n-C_{15} elutes in less then 2 min. For the 20°C/min. case, retention time reproducibility for four replicate injections ranges from about ±1.6% for the smallest retention times to about ±0.25% for the longest retention times.

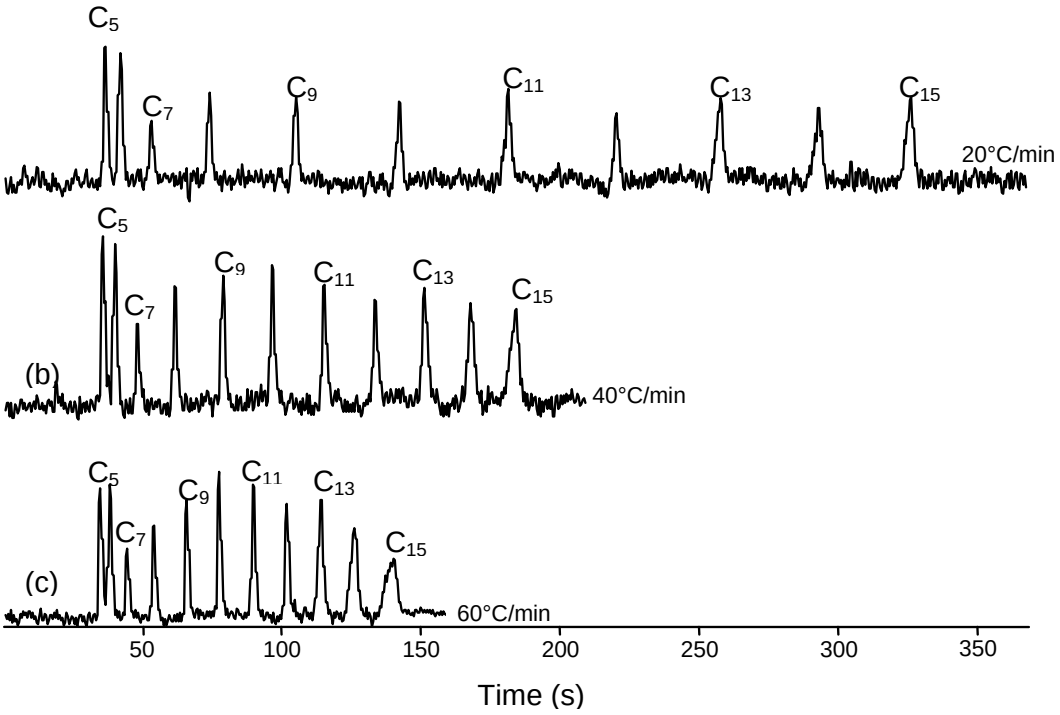

Figure 3.5. Chromatograms of an n-C_5 to n-C_{15} mixture using the 3-m long column temperature programmed at 20 °C/min. (a), 40 °C/min. (b), and 60 °C/min (c).

The columns described here are for use in a completely micro-fabricated, autonomous GC instrument for global environmental monitoring. A target goal is the use of a tunable, series-coupled ensemble of 3.0-m long non-polar and polar columns that can separate a mixture of 30-50 volatile and semi-volatile organic compounds in under 10

min. Figure 3.6 shows the separation of a 30-component multi-functional test mixture using the 3.0-m long column temperature programmed at 20°C/min. from a starting temperature of 30°C. Peak numbers correspond to component numbers in Table 3.1. The last component elutes is about 250 s. This is the most complex mixture reported to be separated with a silicon MEMS column and clearly illustrates the potential for these columns in a variety of environmental applications.

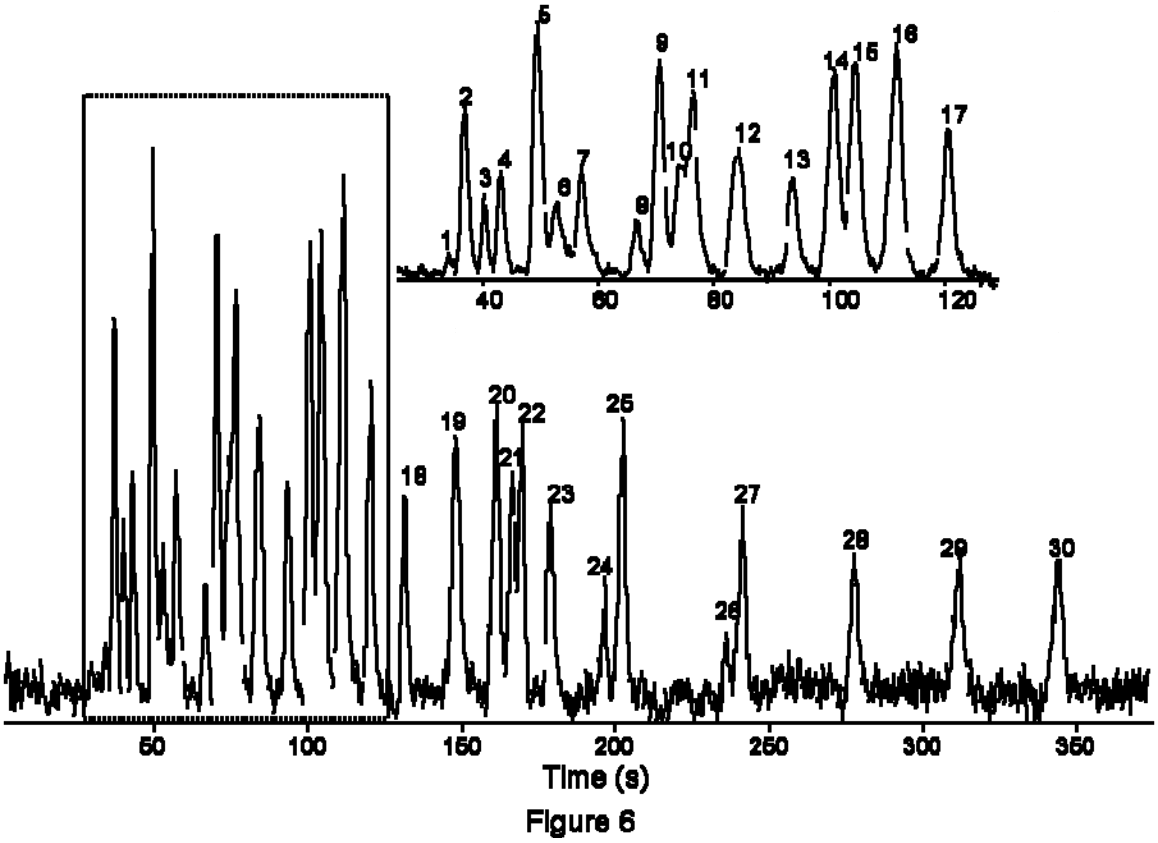

Figure 3.6. Chromatogram of a 30-component mixture obtained with the 3-m long column temperature programmed at 20 °C/min. Peak numbers correspond to compound numbers in Table 3.1.

Temperature Programming with the 0.25-m Column. The shorter column requires less power for heating and obtains better temperature control at higher temperatures than the 3.0-m long column. However, it heats very fast (>1500°C/min) and is more prone to show oscillations in temperature during heating due to the relatively low sampling rate of

Table 3.1. Component list for 30-component separation.

#	Compound	Boiling points (°C)	#	Compound	Boiling Point (°C)
1	Ethanal	20.1	16	Styrene	145.2
2	Pentane	36.1	17	Nonane	150.8
3	2-butanone	79.6	18	A-pinene	155
4	Hexane	69	19	3-octanone	168
5	Benzene	80.1	20	Decane	174.1
6	2-pentanone	100-110	21	Limonene	176
7	Heptane	98.4	22	1,2 dichlorobenzene	180.5
8	Chloropentane	107	23	Acetophenone	201.7
9	2-hexanone	127	24	Nonyl aldehyde	195
10	Toluene	110	25	Undecane	195.9
11	2-fluorotoluene	113	26	Decanal	207-209
12	Octane	126	27	Dodecane	216.3
13	Chlorobenzene	130	28	Tridecane	235.4
14	Ethylbenzene	136.2	29	Tetradecane	253.7
15	P-xylene	138.3	30	Pentadecane	270.6

the micro-controller. Figure 3.7 shows temperature versus time plots for the 0.25-m long column. All temperature programs end with isothermal intervals at 200^{o}C. This is near the upper temperature limit of the stationary phase when using air as carrier gas. Numbers next to plots show temperature programming rates in ^{o}C/min. Plots (a) show simple heating ramps. Plots (b) show more complex temperature programs consisting of linear ramps and isothermal intervals. Plots labeled (c) show four similar ramps superimposed.

Good temperature linearity is observed for ramp rates up to 350^{o}C/min., but significant temperature oscillations are observed. In (a), some curvature is observed for the highest ramp rate especially for temperatures above 150^{o}C. For temperatures below about 150^{o}C, linear ramps as fast as 1000^{o}C/min can be obtained. Again, transitions at the beginning and end of each linear segment are sharp indicating good temperature control.

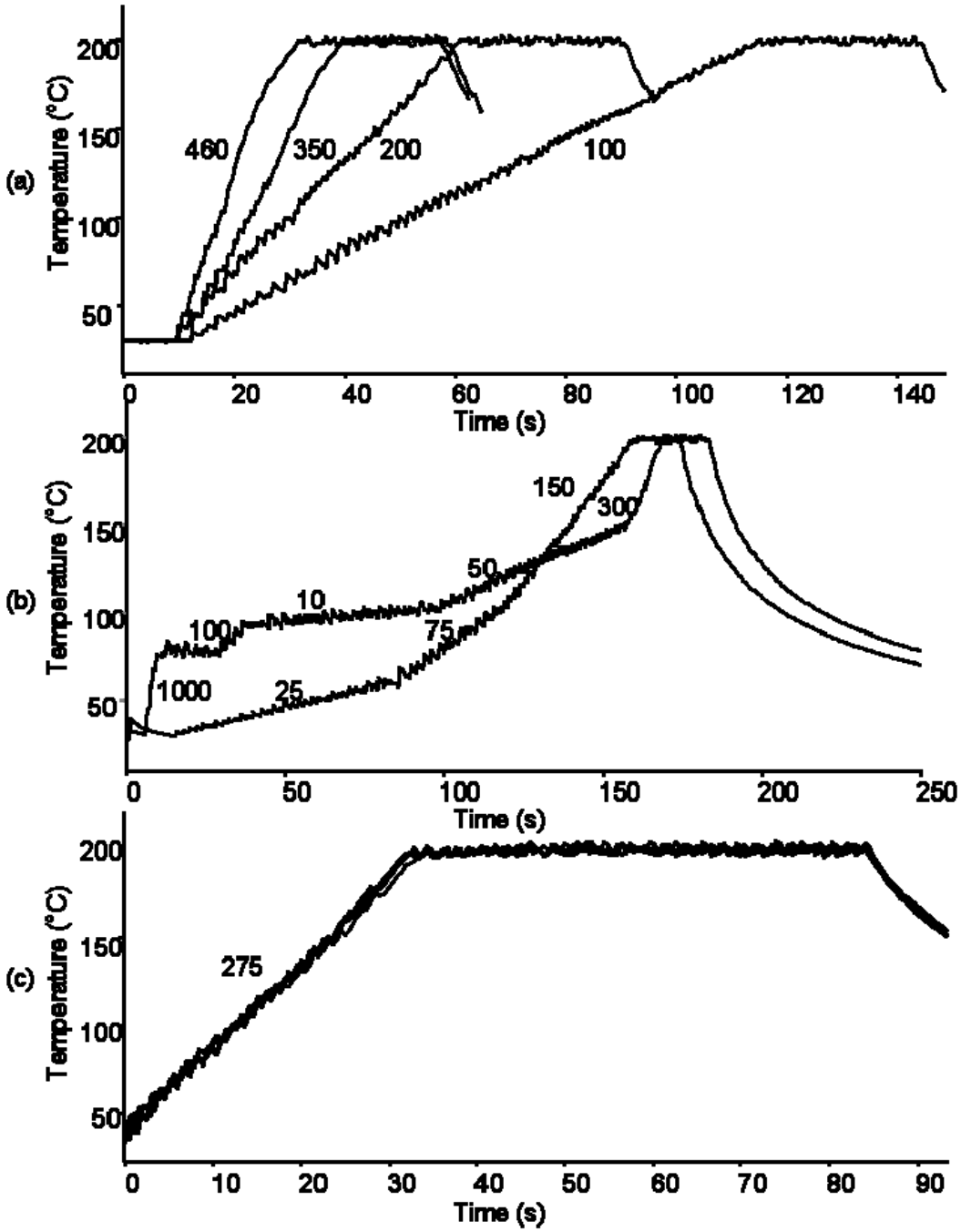

Figure 7

Figure 3.7 Temperature versus time plots for the 0.25-m long column using the proportional integral controller showing simple temperature ramps (a), complex ramps with isothermal intervals (b) and the superimposition of five similar ramps (c). Numbers on plots give the ramp rates in ^{o}C/min.

Figure 3.8 shows chromatograms of an n-C_5 to n-C_{15} mixture separated on the 0.25-m long column with temperature programming rates of 100°C/min. (a), 300°C/min (b) and 1000°C/min. (c). Peak shapes are excellent with not sign of tailing or other artifacts. With a programming rate of 1000°C/min, n-C_{15} elutes in 12 s.

In order to evaluate retention time reproducibility of the very fast separations obtained with fast temperature programming of the 0.25-m long column, five replicate injections were made of an n-C_6 to n-C_{12} alkane mixture. The temperature of the column returned to a baseline controlled temperature of 30°C before the next injection was made. There was approximately two minutes between injections. A programming rate of 275°C/min was used with a starting temperature of 30°C. Mean retention time ranges from 5.14 s for n-C_6 to 18.95 s for n-C_{12}. Corresponding relative standard deviations ranged from 1.7% for n-C_6 to 0.17% for n-C_{12}. These values are very good considering the very small retention time values.

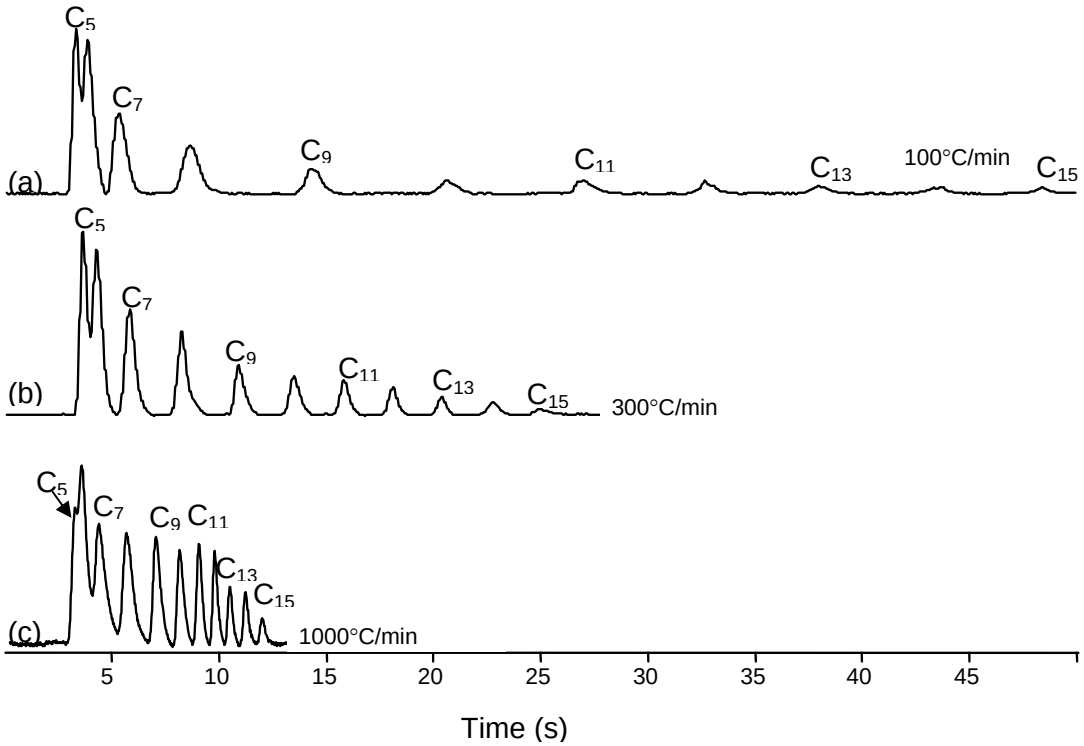

Figure 3.8 Chromatograms of an n-C_5 to n-C_{15} mixture using the 0.25-m long column temperature programmed at 100 ^{o}C/min. (a), 300 ^{o}C/min. (b) and 1000 ^{o}C/min (c).

Conclusions

Silicon MEMS columns with integrated heaters and RTD sensors show great promise for the development of miniature and micro-fabricated instruments for on-site monitoring of organic compounds. These columns can be heated with far less power and at much higher speeds than can be achieved with conventional convention ovens. The high conductivity of silicon allows for the use of spot heaters, which are easy to fabricate, while providing relatively uniform temperature across of column chip. With simple means of thermal insulation, columns can be efficiently heated to at least 200^{o}C, which is near the upper limit using air as carrier gas. Additional studies with hydrogen or helium at higher temperatures are needed to evaluate the use of these columns at high temperatures in order to extend the boiling point range to semi-volatile compounds.

The temperature controller described in this report is well suited for use with the silicon MEMS columns. The controller can be used to generate simple temperature ramps or more complex heating profiles with multiple ramps and isothermal intervals. The modular design of the controller and the columns allows for different columns to be operated from the same controller and power supply. A significant limitation of the current micro-controller design is the low data sampling rate, which results in oscillations in the heating profiles for the shorter columns. These columns heat very rapidly, and thermal overshoot appears to be occurring. Work is in progress to correct this limitation.

With the 3.0-m long column, 12,000 theoretical plates are produced and a 30-component multi-functional test mixture was separated is less than 5 min with a programming rate of 20°C/min. However, two co-elutions did occur. With a programming rate of 60°C/min, an n-C_5 to n-C_{15} mixture was completely eluted in less than 2 min. With the 0.25-m long column, linear temperature programming to 200°C with rates greater than 300°C/min is easily achieved. With the maximum programming rate of 1000°C/min, a n-C_5 to n-C_{15} mixture is completely eluted in 12 s. Retention time reproducibility is very good with both column lengths, ranging from about 1.5% for the low boiling point compounds to about 0.2% for the higher boiling point compounds.

To be useful for highly miniaturized and micro-fabricated GC instruments, the silicon MEMS columns need to be supported by alternative inlet devices and detectors. Work is in progress to interface these columns to micro-scale and micro-fabricated sorption-based preconcnetrators for large volume air sampling and to micro-fabricated sensor arrays and differential ion mobility spectrometers for selective detection with low recourse requirements.

References

[1] Lorenselli, L.; Benvenuto, A.; Adami, A.; Guarnieri, V.; Margesin, B.; MUlloni, V.; Vincenzi, D. *Biosensors and Bioelectronics*, **2005**, 20, 1968-1976.

[2] Abhinav Bhushan, Dawit Yemane, Praveen Pasupuleti, Edward B. Overton, Jost Goettert, and Michael C. Murphy, "Fabrication and Testing of High Aspect Ratio Metal Micro-Gas Chromatograph Columns", Proc. of the ASME IMECE 2004, 2004 ASME International Mechanical Engineering Congress & Expo, Anaheim, CA, November 13-19, **2004**.

[3] A. Bhushan, V. Challa, J. McKeon, D. Yemane, E. B. Overton, M. C. Murphy, J.Goettert, "Application of Scanning Acoustic Microscopy in Characterizing Metal Micro Gas Chromatograph Columns", TMS Letters, 1 (7) **2004**, 145-146.

[4] Manginell, R. P.; Okandan, M.; Bauer, J. M.; Manley, R.G.; Trudell, D.; Kottenstette, R. J.; Lewis, P. R.; Adkins, D.; Heller, E. J.; Stewart, H.; Shul, R. J. "Advancements in the monolithically integrated MicrochemLab (TM)", Micro Total Anlysis Systems 2004 - *μTAS '04*, Vol. 2 (297) (**2005**), 61-63.

[5] Overton, E. B.; Carney, K. R.; Roques, N.; Dharmasena, H. P. *Field Anal. Chem. Technol.* **2001**, *5* (1-2), 97.

[6] Yu, C. M.; Lucas, M.; Koo, C.; Stratton, P.; DeLima, T.; Behymer, E. *Micro-Electro-Mechanical Systems (MEMS)* **1998**; DSC Vol. 66, 481.

[7] Noh, H.; Hesketh, P. J.; Frye-Mason, G. C. *J. Microelectromech. Syst.* **2002**, *11* (6), 718.

[8] Kolesar, E. D.; Reston, R. R. *IEEE Trans. Compon., Packag., Manuf. Technol.* **1998**, *21* (4), 324.

[9] Matzke, C. M.; Kottenstette, S. A.; Casalnuovo, G. C.; Frye-Mason, G.; Hudson, M. L.; Sasaki, D. Y.; Manginell, R. P.; Wong, C. C. *Proc. 1998 SPIE Conf. Micromach. Microfabricat. Process Technol. IV*; p 262.

[10] Frye-Mason, G.; Kottenstette, R. J.; Lewis, P. R.; Heller, E. J.; Manginell, R. P.; Adkins, D. R.; Dullock, D.; Martinez, D.; Sasaki, D.; Mowry, C.; Matzke, C.; Anderson, L. *Proceedings of Micro Total Analysis Systems 2000*; Kluwer Academic Publishers: Dordrecht, The Netherlands, 2000; p 229.

[11] Zellers, E. T.; Steinecker, W. H.; Lambertus, G. R.; Agah, M.; Lu, C.-J.; Chan,

H. K. L.; Potkay, J. A.; Oborny, M. C.; Nichols, J. M.; Astle, A.; Kim, H. S.; Rowe, M. P.; Kim, J.; Da Silva, L. W.; Zheng, J.; Whiting, J. J.; Sacks, R. D.; Pang, S. W.; Kaviany, M.; Bergstrom, P. L.; Matzger, A. J.; Kurdak, Cü .; Bernal, L. P.; Najafi, K.; Wise, K. D., A versatile MEMS gas chromatograph for environmental vapor mixture analysis. *Proceedings Solid-State Sensor, Actuator, and Microsystems Workshop*, Hilton Head Island, SC, June 6-10, 2004; p 61-66.

[12] Potkay, J. A.; Driscoll, J. A.; Agah, M.; Sacks, R. D.; Wise, K. D. *Proc. 16th Ann. IEE Conf. Micro-Electro-Mech. Syst.* (MEMS), Kyoto, Japan, January 19-22, 2003; p 395.

[13] Agah, M.; Potkay, J.; Elstro, A.; Lambertus, G.; Sacks, R.; Wise, K. A high performance temperature-programmed gas chromatography column. *North American Solid-State Sensors, Actuators, and Microsystems Workshop*, Hilton Head Island, SC, June 6-10, 2004; p 302-305.

[14] Agah, M.; Potkay, J. A.; Driscoll, J.A.; Sacks, R.D.; Kaviany, M.; Wise, K.D. "Thermal Behavior of High-Performance Temperature-Programmed Microfabricated Gas Chromatography Columns," *Technical Digest of the 12th International Conference of Solid-State Sensors, Actuators and Microsystems,* Boston, MA, June 8-12, **2003**, 1339-1342

[15] Agah, M.; Potkay, J. A.; Lambertus, G. R.; Sacks, R. D.; Wise, K. D. "High-performance Temperature-Programmed Microfabricated Gas Chromatography Columns," *IEEE J. Microelectromech. Systems, 14* (5), **2005**, .1039-1050.

[16] Lambertus, G. R.; Elstro, A.; Sensenig, K.; Potkay, J.; Agah, M.; Scheuering, S.; Wise, K. D.; Dorman, F.; Sacks, R. *Anal. Chem.* **2004**, *76*, 2629.

[17] Reidy, S.; Lambertus, G.; Reece, J.; Sacks, R.D. *Anal. Chem.* **2006**, *78, (8),* 2623.

[18] Grob, K. *Making and Manipulating Capillary Columns for Gas Chromatography*; Dr. Alfred Huthig Verlag: Heidelberg, **1986**.

[19] Lambertus, G.R.; Sacks, R.D.; *Anal. Chem.*, **2005**, *77*, 2078

[20] Veriotti, T.; Sacks, R. *Anal. Chem*. **2001**, *73*, 3045.

[21] Veriotti, T.; Sacks, R. *Anal. Chem*. **2001**, *73*, 4395.

[22] Veriotti, T.; McGuigan, M.; Sacks, R. *Anal. Chem*. **2001**, *73*, 279.

[23] Whiting, J.; Sacks, R. *Anal. Chem*. **2003**, *75*, 2215.

[24] Grall, A. J.; Zellers, E. T.; Sacks, R. D. *Environ, Sci. Technol.* **2001**, *35*,163.

[25] Lu, C.-J.; Whiting, J. J.; Sacks, R. D.; Zellers, E. T. *Anal. Chem*. **2003**, *75*, 1400.

[26] Lambertus, G. R.; Fix, C. S.; Reidy, S. M.; Miller, R.; Wheeler, D.; Nazarov, E.; Sacks, R. D. *Anal. Chem*. **2005**, *77*, 7563.

[27] Ciucanu, I.; Chiriac, A. *J. Sep. Sci.* **2002**, *25* (7), 247.

[28] Segal, A.; Gorecki, T.; Mussche, P.; Lips. J.; Pawliszyn, J. *J. Chromatogr., A* **2000**, *873* (1), 13.

[29] Whalley, L. K.; Lewis, A. C.; McQuaid, J. B. *J. Environ. Monit.* **2004**, *6* (3), 234.

[30] Noh, H.; Hesketh, P.; Frye-Mason, G.; *IEEE MEMS,* **2002,** 73.

Chapter 4

Separation Enhancement by Thermal Tuning using Silicon Microfabricated Columns with Integrated Heaters and Temperature Sensors

Introduction

High speed separations typically use higher flow rates or shorter columns[1-10] to achieve the separation in a shorter time frame. Field portable GC systems are designed often with the intention of obtaining sensitive information quickly. Therefore, high speed separations would be necessary. One of the major disadvantages of this is the reduction in peak capacity[11,12] when operating at higher flow rates or with shorter columns. One way to optimize available peak capacity is with a dual column ensemble with differing stationary phases[13-32].

When separating mixtures using such an ensemble there are components pairs that are separated by the first column and remain separated on the second column. There are some component pairs that are not separated on the first column but are on the second column, and lastly there are some component pairs that are separated on the first column but co-elute from the column ensemble because of different selectivities of the two columns. For these components, enhanced separation often is possible by varying the

temperature programming ramps on the two columns. These are the component pairs that are of interest in this work.

Previous separation enhancement techniques have used a valve had been placed at the junction point of the two columns[27-31]. Components would be separated by adjusting the pressure at the junction point. Others have used temperature pulses to reduce the k-value on the second column[32]. Both of these techniques have some limitations when integrating them into field portable instrumentation. Both have mechanical parts that can be of high maintenance which means that alternative approaches are necessary.

A new tuning technique of series-coupled column ensembles has been developed. This technique uses two micro-fabricated columns with on-board heaters and temperature sensors that are capable of independent temperature programming. Since k-value is temperature dependent, by varying the temperature on one column independent of the other, retention time can be varied. With typical GC systems this can not be achieved because both columns are housed in the same GC oven, therefore independent heating of the columns is unobtainable. The at-column heating capabilities of the micro-columns allows for the two columns to be programmed independent of each other.

A number of models have been used for predicting retention times for temperature programmed separations using gas chromatography[25,33-35]. Typically these models use thermodynamic data for the target compounds and result in equations for the prediction of solute retention times. These equations, however, are often complex and application of these models to pressure or temperature tuned separations has not yet been reported.

In this chapter, a model has been developed to the prediction of a solute band elution time for isothermal applications using pressure-tunable and programmable dual

column ensembles[25]. This model is useful for determining the effects of changing junction point pressure on ensemble retention times and peak elution order. The model is based on dividing the column ensemble into 1.0-cm segments and calculating solute band migration rate through each segment. The ensemble retention time is then found by the sum of these times over the entire column length.

Later, this model was modified to also include the effects of temperature on the overall system[36]. Using empirical retention factor values over a range of temperatures and carrier gas acceleration along the column axis target component retention times can be predicted.

Clean air is used as a carrier gas for all separations to more closely simulate the conditions that will be used in the μGC.

Experimental

Apparatus. All experiments were performed using a free standing HP 6890 split/splitess inlet and Varian 3500 flame ionization detector with a high speed electrometer built in-house. A dual column ensemble consisting of 0.5 m lengths of micro-fabricated columns (150 μm wide by 240 μm deep) was used for the separation columns. The first column was a nonpolar, poly(dimethyl)siloxanes (PDMS), and the second column was a polar poly(trifluoropropylmethyl)siloxanes. Both columns were coated in house using a previously described static coating method.

Independent temperature control was achieved using heaters and temperature sensors patterned on the backside of the columns as controlled by a stamp plot μcontroller (as described in detail in Chapter 3). Columns were fabricated using a

modified BOSCH process for deep reactive ion etching. Heated connection lines were obtained using resistively heated NiChrom wire. Connection line temperature was maintained at 150°C. The electrometer was interfaced to a PC (Gateway, GP6-350, Sioux Falls, ND) with a 16-bit A/D board (ISA-PCI 1602-16, Computer Boards, Inc., Mansfield, MA)

Band Trajectory Modeling. As an optimization tool for determining the appropriate temperature programming ramp for thermal tuning, a spreadsheet model modified from original work by Dr. Megan McGuigan[36] is used to predict the band trajectory for targeted components in a mixture. The model has been modified to best model flow through the rectangular channels of the microfabricated columns. Previous modeling work has been published by Dr. McGuigan and described in detail[36]. This model uses column dimensions, inlet and outlet pressures, carrier gas viscosities, Van't Hoff data, and retention factor versus temperature to calculate the retention time along the column ensemble.

In the model, the column ensemble is divided into 1.0-cm-long intervals where the time required for a solute band to migrate through each interval is calculated. These times are added over the total length of the column ensemble and retention time is determined. Retention factors are measured over a range of set column temperatures on both columns in the ensemble. Van't Hoff plots (ln k versus $1/T$) are generated for all components in the mixture, and the resulting slope and intercept values are used as inputs into the model. The spreadsheet model is used to plot solute band position along the column versus time. It is used to predict when co-elutions will occur and what temperature programming ramp should be applied to separate co-eluting compounds.

The two columns in the ensemble are treated independently. The exit velocity u_o for each column is found from equation 4.1.

$$U_o = \frac{h^2 w^2 p_o \left(P^2 - 1\right)}{24\eta L\left(h^2 + w^2\right)} \tag{4.1}$$

Where w the width of the channel, h the depth of the channel, p_o the outlet pressure, P the inlet-to-outlet pressure ratio, η the temperature dependent carrier-gas viscosity, and L the column length. For the first column in the ensemble, the inlet pressure is the GC inlet pressure p_i, and the outlet pressure is the column junction point pressure p_j For the second column, the inlet pressure is the junction point pressure and outlet pressure is atmospheric.. The inlet-to-outlet pressure ratio is found from equation 4.2.

$$P = \frac{p_i}{p_o} \tag{4.2}$$

Carrier gas viscosity values were found from interpolation between literature values at various temperatures.

For each column, the ratio of the local carrier-gas velocity u_z at any coordinate z along the column to the exit gas velocity is given by equation 4.3,

$$U_z = \frac{U_o}{\sqrt{P^2 - z/L\left(P^2 - 1\right)}} \tag{4.3}$$

The time increment Δt_g required for the carrier-gas to move an incremental distance Δz along the column is given by equation 4.4,

$$\Delta t_g = \frac{\Delta z}{u_z} \tag{4.4}$$

The time increment Δt_s required for a solute band to move an incremental distance Δz along the column is given by equation 4.5,

$$\Delta t_s = \frac{\Delta z}{u_z}(k_T + 1) \tag{4.5}$$

where k_T is the temperature dependent retention factor for the solute. The total time, t_x, required for a solute band to reach coordinate x along the column is given by equation 4.6,

$$t_z = \sum_0^z \frac{\Delta z}{u_z}(k_T + 1) \tag{4.6}$$

Materials and Procedures. Compressed air is used, after purification with filters for water vapor and hydrocarbons, at a flow rate of 15 cm/s. Head pressure is controlled using an electronic pressure controller (Model 640, MKS, Andover, MA). Temperatures were controlled using proportional-integral μcontroller (StampPlot). Each column is connected electrically to a printed circuit board which interfaced with a proportional integral controller. All data were logged at 100 Hz with an electrometer built in-house and a 16-bit A/D board (Model DAS1602-16, Computer Boards Inc, Middleboro, MA) interfaced with a PC (Gateway GP6-350, Irvine, CA). All chemicals used in test mixtures were reagent grade or better. Test mixtures are injected with a split ratio of 300:1. Injection volume was 0.1μL. Interface control is provided by LabTech Notebook Software (Version 10.1, Laboratory Technologies Corp., Andover, MA). Chromatograms are processed with GRAMS/32 software (Galactic Industries, Salem, NH). Table 1 lists the compounds and boiling points. The injector and detector temperature is 300°C.

Results and Discussion

Model Testing. Initial testing of the model was performed on isothermal chromatograms. Testing was done to see if accurate elution order prediction could be

obtained. Five compounds were injected onto a single nonpolar 3-m column. The inlet pressure of the column was input into the model and band trajectory plots were obtained, Figure 4.1, for each of the five compounds using previously obtained k-value information.

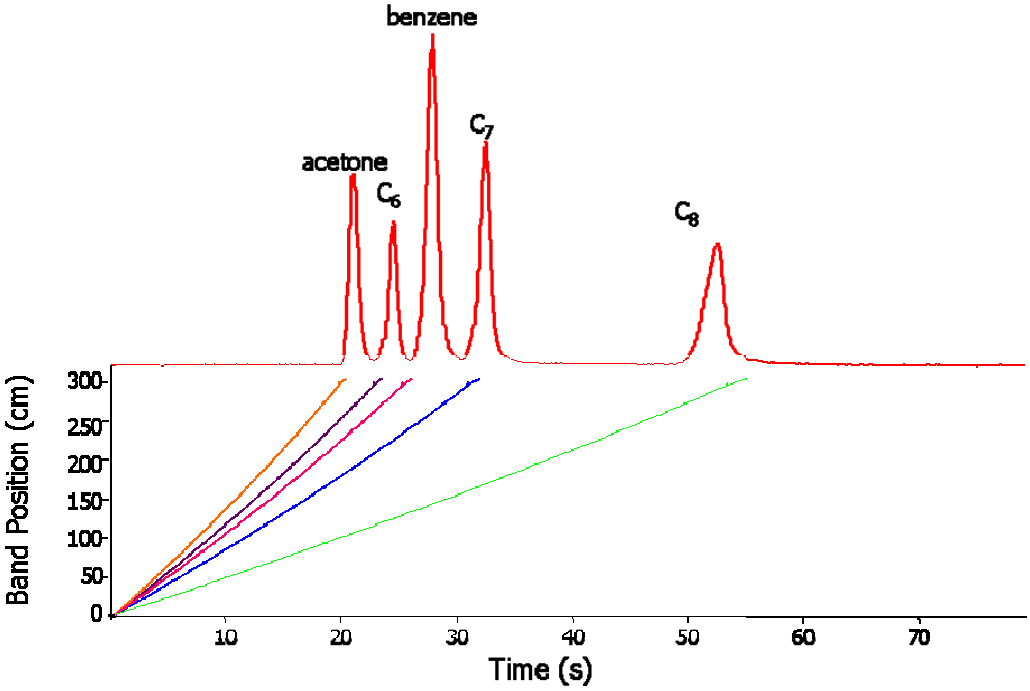

Figure 4.1. A band trajectory plot and chromatogram of a 5-compound isothermal separation on a single three-meter-nonpolar microfabricated column.

Accurate prediction of all five compounds was obtained. There are some slight (<10%) errors in retention time prediction. These errors can be attributed to the fact that there is a change in the flow dynamics due to the round capillary connection lines. These errors are small and still predict elution order correctly.

Next, the model was tested under temperature programmed conditions. The same 3-m column was connected to the micro-controller and temperature programmed at 60°C/min. A 10-component mixture was injected onto the column. Van't Hoff information (k-value as function of temperature), as well as column head pressure, were used as inputs into the model. The resulting band positions as a function of time were

plotted, Figure 4.2, and resulting elution order and retention time prediction were compared to the resulting chromatogram

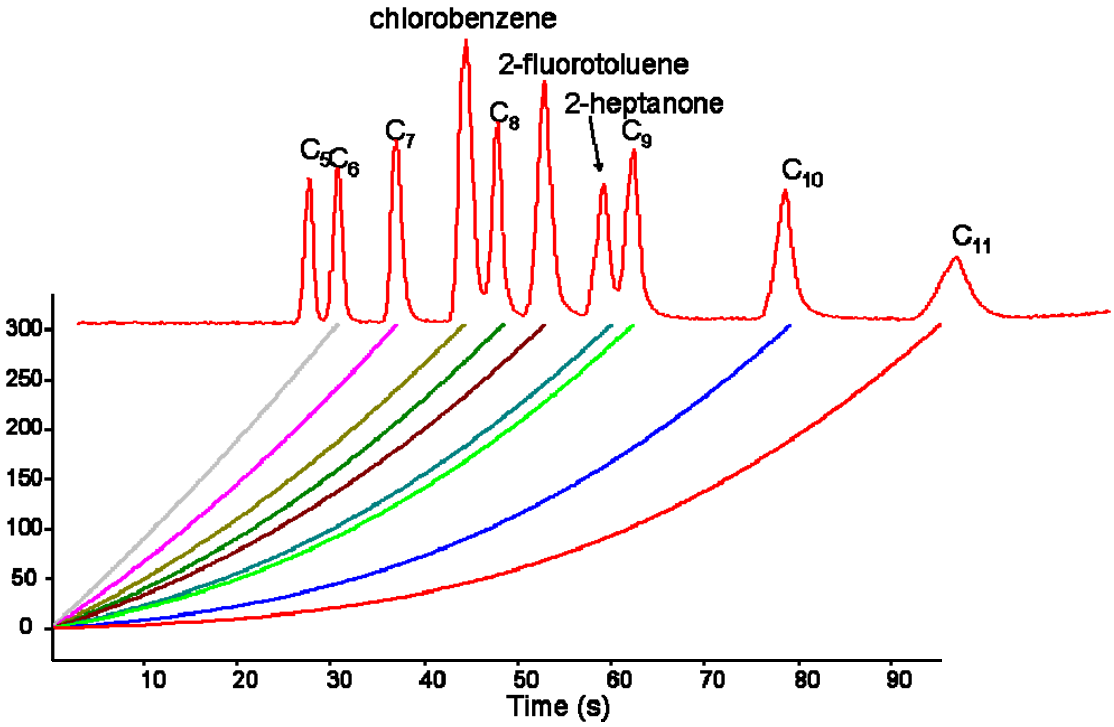

Figure 4.2. A temperature programmed separation of a 10-compound mixture. The column was temperature programmed at 60°C/min. An accompanying band trajectory plot for 9 of the 10 compounds shows good correlation between predicted retention times and actual retention times.

Due to the low volatility of pentane (C_5), Van't Hoff data could not be obtained and therefore a band trajectory under temperature programmed conditions could not be obtained. However, accurate prediction of elution order of the remaining 9 compounds and fairly good prediction of retention time was achieved. Therefore it was determined that the model could be used for thermal tuning studies.

Thermal Tuning Operation. Two 50-cm columns were connected in series and each column was connected to its own micro-controller (Figure 4.3). Using a free-standing split/splitless inlet (I) from an Agilent 6890 and air as a carrier gas (CG), sample was introduced onto the microfabricated columns. Both columns were 50-cm in length

and were coated in-house using a static coating method. The two columns were connected in series where the first column (C_1) was a nonpolar PDMS and the second column (C_2) was a moderately polar poly(trifluoropropylmethyl)siloxanes. Bands eluting from the column ensemble were detected using a flame ionization detector (D).

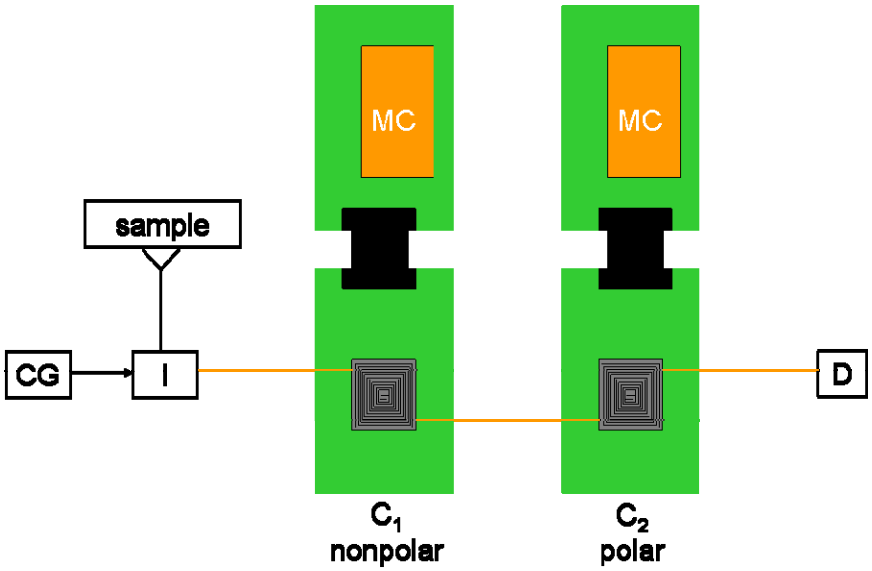

Figure 4.3. Instrument schematic of thermal tuning system. Sample is injected into a split/splitless inlet (I), and introduced onto the first column (C_1) a 50-cm-nonpolar column, which is temperature programmed using a micro-controller (MC). After separation on the first column, components are separated on the second column (C_2), a 50-cm-polar column and are detected by a flame ionization detector (D).

Each column was independently temperature programmed using a commercially available micro-controller (MC). Micro-controller operation has been previously described in detail in Chapter 3. To review the micro-controller (Parralax, BS2p-24, Rocklin, CA) generates a pulse-width modulated signal that controls a relay that supplies current to the four heating units. The RTD is used as a feedback resistor in an oscillator circuit based on a high-input-impedance operational amplifier. The frequency of the square-wave output from the oscillator varies with the surface temperature of the silicon column chip. This square wave is used as the input to the controller which measures the

width of the pulse. The columns are calibrated and the calibration curve information is input into the micro-controller via a PC.

Initial testing of the setup was done with a two compound co-elution as shown in Figure 4.4. Dodecane (C_{12}) and acetophenone were chosen since they are well separated on the first column when both columns are temperature programmed at the same rate but co-elute from the column ensemble.

Both column temperatures were held at 30°C for 30s, then the temperature was ramped from 30-100°C at 100°C/min and then held at 100°C for 60s. With both columns programmed at the same rate it mimics what the separation would be if the columns were housed in a traditional GC oven, where the two columns would have to be temperature programmed at the same rate.

The solid line in the middle of the y-axis indicates the junction point between the two columns. Due to the differences in retention on the two columns, there is a drastic change in slope of the band trajectory plot. To fluidically connect to the micro-fabricated columns, uncoated fused silica is epoxied into the inlet and outlet ports of the columns prior to coating. This length of fused silica is minimized but some connection line remains. Due to this the junction point position does not fall at 50 cm, but rather 60.5 cm, due to the 10.5 cm of coated capillary connection line. There is a complete co-elution between the two compounds from the column ensemble but there is a very good separation at the junction point.

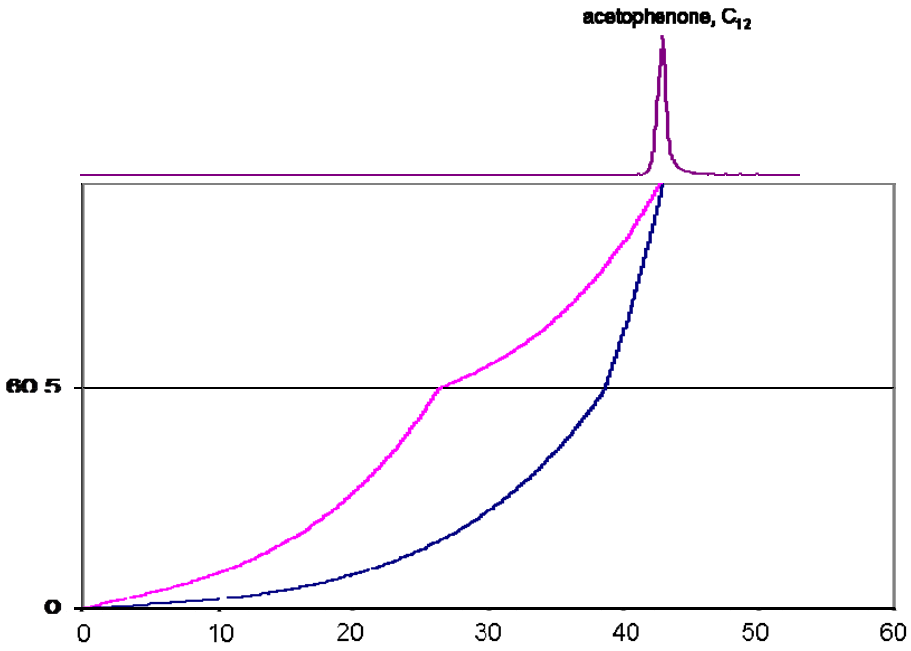

Figure 4.4. Band trajectory plot, band position versus time, of a two-component co-elution. Both columns were temperature programmed at the same rate.

Figure 4.5 shows that by varying the temperature programming ramp on the first column independent of the second column's temperature programming ramp the separation of the two compounds can be enhanced. Since the retention of a compound on a column is dependent on column temperature, by optimizing the temperature programming ramp the separation of the two compounds can be altered and in this case the two compounds are baseline separated. Since there is a very good separation of the two compounds at the junction point of the two columns but the two compounds co-elute from the ensemble, increasing the separation on the first column will allow for the two compounds to be separated from the column ensemble. This was done by changing the temperature programming ramp on the first column. It was temperature programmed at 100°C/min from 30-70°C and then held isothermally at 70°C for 60 s, and then at 100°C/min from 70-100°C and the second column was temperature programmed from

30-100°C at 100°C/min. The same initial and final temperature holds as in the first case remained.

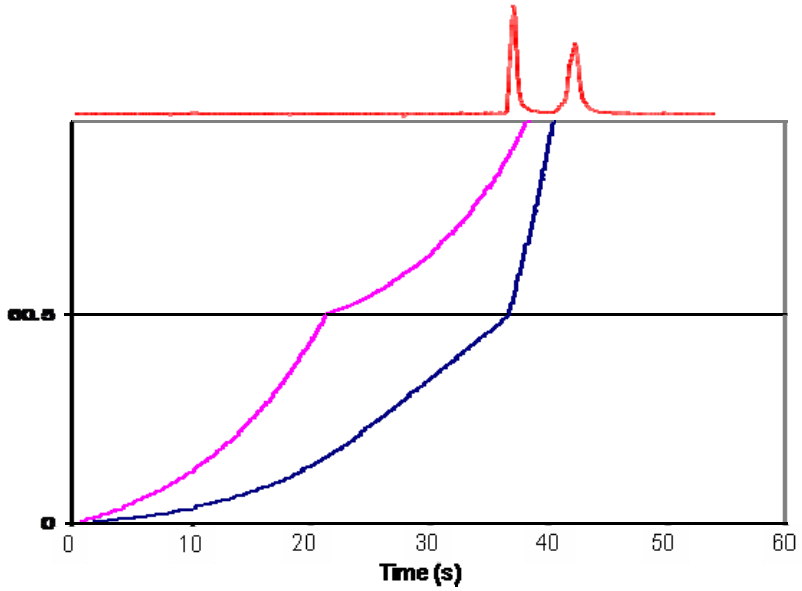

Figure 4.5. Thermally tuned separation of C_{12} and acetophenone. The first column was temperature programmed from 30-70°C at 100°C/min and held at 70°C for 60s and then from 70-100°C at 100°C/min. The second column was temperature programmed from 30-100°C at 100°C/min.

This was done by changing the temperature programming ramp on the first column. It was temperature programmed at 100°C/min from 30-70°C and then held isothermally at 70°C for 60 s, and then at 100°C/min from 70-100°C and the second column was temperature programmed from 30-100°C at 100°C/min. The same initial and final temperature holds as in the first case remained.

At 70°C, the first compound, acetophenone, has eluted from the first column, and is being separated by the second column. The band velocity of the second compound has slowed down, allowing the first compound to move further along the column before the second compound is introduced onto the second column.

Multicomponent Mixture. Since varying the temperature programming ramp on the column affects the overall separation, not just the two target compounds, more

complex mixtures were analyzed and thermal tuning conditions were applied. Initially an attempt was made to separate a 14-component mixture on each of the individual columns (Figure 4.6). A list of the 14-components and the boiling points can be found in Table 4.1.

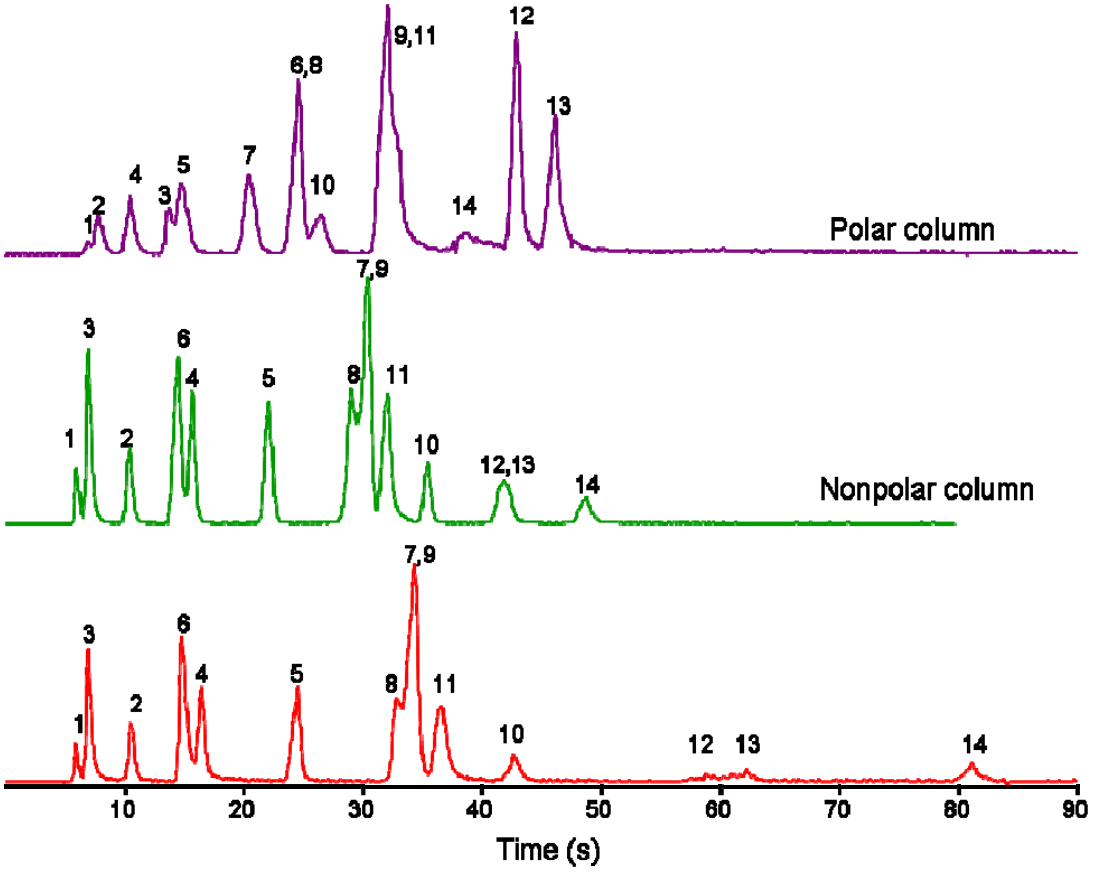

Figure 4.6. A 14-component multifunctional mixture on a single (a) polar and (b and c) nonpolar column. (a and b) Separation temperature programmed at 100°C/min from 30-100°C with multiple co-elutions on both columns. (c) Separation on nonpolar column temperature programmed from 30-100°C with an isothermal hold at 70°C for 60s.

Table 4. 1 Components from 14-component mixtures and their boiling points (in °C)

1	dichloromethane	39.8°C	8	Limonene	176°C
2	heptane	98.4°C	9	dichlorobenzene	180°C
3	2-butanone	80°C	10	Undecane	196°C
4	octane	125.5°C	11	Acetophenone	202°C
5	nonane	151°C	12	Dodecane	216°C
6	2-hexanone	128°C	13	Decanal	207°C
7	decane	174.1°C	14	Tridecane	234°C

Plot (a) is the 14-component mixture separated on the polar column, when temperature programmed from 30-100°C at 100°C/min, there are multiple co-elutions that occur (3,5:6,8:9,11). Plot (b) is the separation on the nonpolar column temperature programmed at the same rate as the polar column. Again there are multiple co-elutions that occur (4,6:7,8,9:12,13). The last separation is when the nonpolar column is temperature programmed from 30-70°C at 100°C/min, held at 70°C for 60s, then from 70-100°C at 100°C/min. Peaks 12 and 13 are now separated, however, there is still a 3-component co-elution with peaks 7,8 and 9. Since there are no co-elution sets that occur on both columns, this mixture can be separated using thermal tuning.

In Figure 4.7, the two columns were connected in series. When both columns are temperature programmed at (a) the same rate (100°C/min) there are three new co-elutions that occur. Since these compounds are separated on the first column, by varying the temperature programming ramp on the first column, the three co-elutions can be separated.

By holding the column isothermally at (b) 70°C for 60s in the middle of the temperature programming ramp all 14 components now are nearly baseline separated.

The peak shape on component 14 is not as sharp as the others due to the fact that this peak eluted during the isothermal hold at the end of the temperature programming ramp. Initially a conservative upper temperature limit was applied. If temperature programmed to a higher temperature a better peak shape would be obtained.

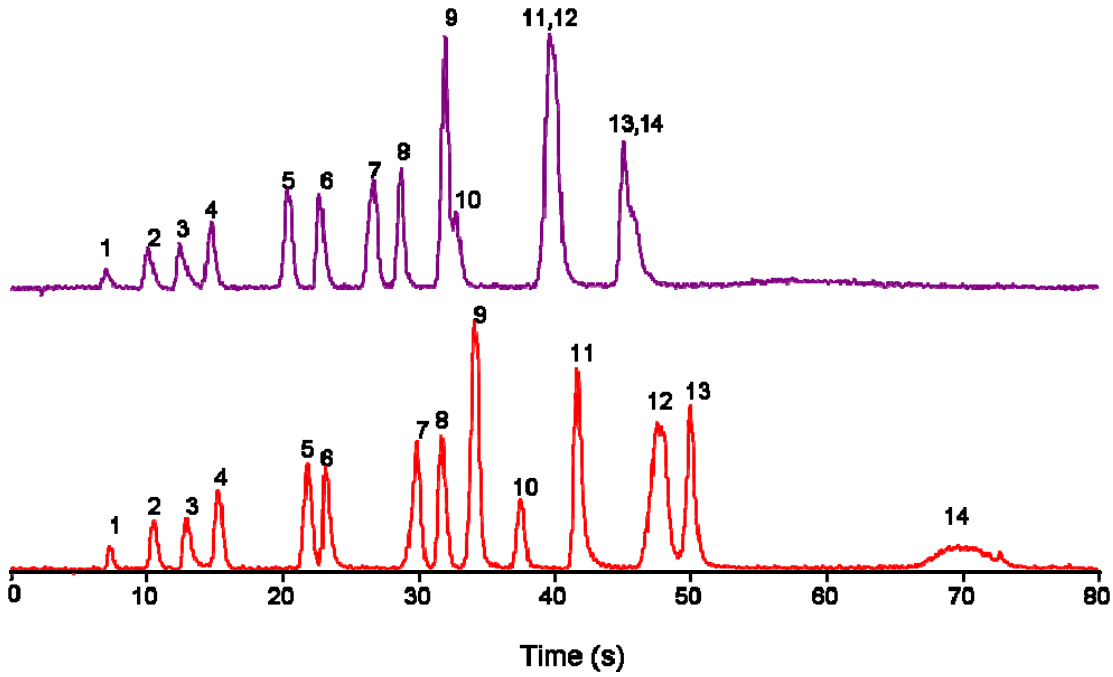

Figure 4.7. Temperature programmed separation of 14-component mixture (a) when both columns temperature programmed at the same rate and (b) when there is a 60s isothermal hold at 70°C.

Conclusions.

Thermal tuning proves to be a very useful separation enhancement technique and completely achievable with micro-fabricated columns. One of the major limitations of high-speed separations is the decrease in peak capacity due to the higher flow rates. Thermal tuning is one way to overcome this decrease in peak capacity. By being able to selectively move peaks from crowded regions of chromatograms to open areas. By having columns with differing stationary phases, components that co-elute from the

column ensemble can be tuned apart by varying the temperature programming ramp on one column independent of the second.

The on-board heaters and temperature sensors patterned on the back-side of the micro-fabricated columns allows for independent temperature programming. This allows for accurate control of the temperature and is necessary for thermal tuning. The band trajectory model proves useful to determine if co-elutions are going to occur and what temperature programming ramp is necessary to separate them. There are some limitations to this model and this separation enhancement technique. This technique and model are best used for targeted analysis or quality control, since some information about co-eluting pairs is necessary.

Also, more accurate retention time prediction is necessary. For this a "more accurate" flow equation is required. This would not only need to account for the differences in flow profile when going from round capillary to rectangular channels but also the right angle turns that occur in the micro-fabricated columns.

Accurate elution order prediction is also necessary for thermal tuning to be successful. This modeling allows for the determination of the necessary temperature programming ramps without the need for trial and error. More work needs to be done on the reduction of error in retention time prediction.

References

1. R. Sacks, H. Smith and M. Nowak, *Anal. Chem.* **70** (1998), p. 29A.
2. L.S. Ettre, *LC GC N. Am.* **22** (2004), p. 452.
3. C.A. Cramers, G. Janssen, M.M. van Deursen and P.A. Leclercq, *J. Chromatogr. A* **856** (1999), p. 315.
4. M.L. Lee, F.J. Yang and K.D. Bartle, Open Tubular Column Gas Chromatography, Wiley, New York (1984).
5. W. Jennings, Analytical Gas Chromatography, Academic Press, Inc., Orlando (1987).
6. N.H. Snow, *J. Liquid Chromatogr. Relat. Technol.* **27** (2004), p. 1317.
7. Gaspar, G.; Annino, R.; Vidal-Madjar, C.; Guichon, G. *Anal. Chem.* **1978**, *50*, 1512.
8. Tijssen, R.; van den Hoed, N.; van Kreveld, M. *Anal. Chem.* **1987**, *59*, 1007.
9. Gaspar, G.; Arpino, P.; Guichon, G. *J. Chromatogr. Sci.* **1977**, *15*, 256
10. Klemp, M.; Sacks, R. *J. Chromatogr. Sci.* **1991**, *29*, 243.
11. Peters, M. Klemp, L. Puig, C. Rankin and R. Sacks, *Analyst* **116** (1991), 1313
12. C.A. Cramers, G. Janssen, M.M. van Deursen and P.A. Leclercq, *J. Chromatogr. A* **856** (1999), 315.
13. Hinshaw, J.; Ettre, L. *Chromatographia* **1986**, *21*, 561
14. Sacks, R.; Akard, M. *J. Environ. Sci. and Tech.* **1994**, *28*, 428A.
15. Repka, D.; Krupcik, J.; Benicka, E.; Leclercq, P.; Rijks, J. *J. Chromatogr.* **1989**, *463*, 243.
16. Kaiser, R.; Leming, L.; Blomberg, L.; Rieder, R. *J. High Resolut. Chromatogr.Chromatogr. Commun.* **1985**, *8*, 92.
17. Toth, T.; Garay, F. In *Proceedings of the Eight International Symposium on Capillary Chromatography*; Sandra, P., Ed.; Huethig: Hiedelberg, 1987; p585.
18. Sandra, P.; David, F.; Proot, M.; Diricks, G.; Verstappe, M.; Verzele, M. *J.High Resolut. Chromatogr. Chromatogr. Commun.* **1985**, *8*, 782.
19. Purnell, J.; Williams, P. *J. Chromatogr.* **1985**, *325*, 1
20. Deans, D.; Scott, I. *Anal. Chem.* **1973**, *45*, 1137.
21. Purnell, J.; Watten, M. *Anal. Chem.* **1991**, *63*, 1261.

22. Matasova, E.; Kovacicova, E.; Garaj, J.; Kraus, G. *Chromatographia* **1989**,*27*, 494.
23. Smith, H.; Sacks, R. *Anal. Chem.* **1997**, *69*, 5159.
24. Smith, H.; Sacks, R. *Anal. Chem.* **1998**, *70*, 4960.
25. Leonard, C and R. Sacks, *Anal. Chem.* **1999**, 71, 5501
26. Lambertus, G.R. and Sacks R.D. *Anal. Chem.* 2005, 77, 2078
27. Grall, A. J.; Zellers, E. T.; Sacks, R. D. *Environ, Sci. Technol.* **2001**, *35*,163.
28. Lu, C.-J.; Whiting, J. J.; Sacks, R. D.; Zellers, E. T. *Anal. Chem*. **2003**, *75*,1400.
29. Veriotti, T.; Sacks, R. *Anal. Chem*. **2001**, *73*, 3045.
30. Veriotti, T.; Sacks, R. *Anal. Chem*. **2001**, *73*, 4395.
31. Veriotti, T.; McGuigan, M.; Sacks, R. *Anal. Chem*. **2001**, *73*, 279.
32. Whiting, J.; Sacks, R. *Anal. Chem*. **2003**, *75*, 2215
33. Dose, E. *Anal. Chem.* **1987**, *59*, 2414
34. Dolan, J.; Snyder, R.; Bautz, D. *J. Chromatogr*. **1991**, *541*, 21
35. Snow, N.; McNair, H. *J. Chromatogr. Sci.* **1992**, *30*, 271
36. McGugian, M. and R. Sacks *Anal. Chem.* **2001**, 73, 3112

Chapter 5
Evaluation and Optimization of Micro-Fabricated Testbed System

Introduction

A number of reports have appeared over the past 15 years on micromachined gas chromatographs[1-6] equipped with a separation column, a preconcentrator injector, and detector. Most of these instruments are designed for targeted analysis. The Engineering Research Center (ERC) for Wireless Integrated MicroSystems (WIMS) at the University of Michigan has been developing a small low power micro-fabricated gas chromatograph (μGC) for the analysis of complex mixtures[7-10]. The final system will have autonomous operation, being battery operated, which will be remotely charged, use wireless communication, and use ambient air as a carrier gas. The system will operate under vacuum outlet conditions, having programmable selectivity and sensor array detection.

Figure 5.1 shows the fluidic layout of the analytical subsystem. Each analysis is performed in two discrete steps. These two steps are referred to as the sampling step and the analysis step. The sampling step consists of air samples drawn through the inlet particle filter, past the calibration vapor source and through the multi-stage adsorbent preconcentrator. The analysis stage starts with a reversal of flow direction and rapid desorption of the preconcentrator. The analytes are introduced onto a dual column

system which can be pressure-or temperature-tuned. After the analytes are separated on the analytical column the vapors pass across an array of chemiresistors coated with thin film of different gold thiolate monolayer protected nanoparticles whose responses vary with the nature of the interactions between the analyte vapors and the ligands on the nanoparticle.

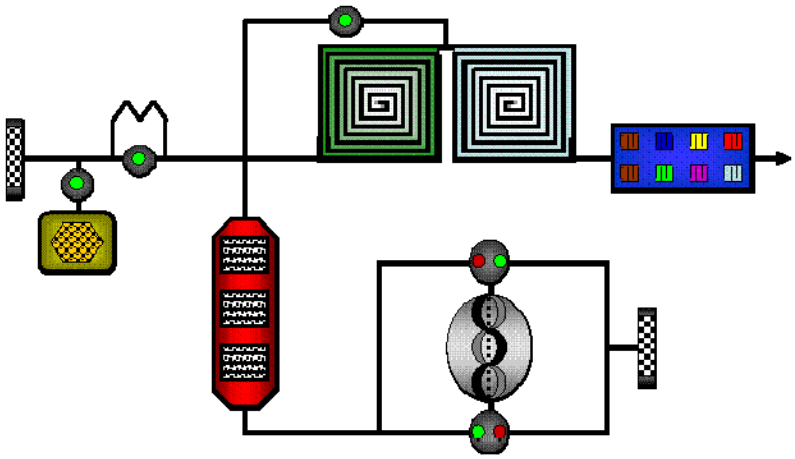

Figure 5.1. Block diagram of μGC layout with all component parts. Operation is described below.

There are certain criteria that each component must fulfill as overall system requirements. The performance goals of the WIMS μGC is for the separation of 30-50 components in less than a ten minute cycle time, with analytes spanning a range of four orders of magnitude in vapor pressure. The analytes of interest are a subset of the EPA "189 Air Toxins", with a wide range of chemical structures, as well as a wide range of volatilities. The preconcentrator inlet[11-13] should be capable of sampling volumes up to 0.5 L (10 min sampling at 50 mL/min), with a sample mass of 5-20 ng per analyte. There should be a preconcentration factor of 10^4 fold. Not only should the columns[14,15] be able to separate the 30-50 components with a 3-7 minute analysis time, but they should also be

capable of temperature[15,16,17]- and pressure-programmed separations[18,19]. The sensor array detector[20-24] should have detection limits in the 1-10 part per billion (ppb) range per analyte. The detector should aide in the identification and quantification of each analyte by giving an accurate retention time, sensor response pattern and magnitude of each analyte.

Microsystem Overview. The overall system will contain a microporous silicon memebrane as an inlet particle filter[25]. The filter is 3.5 mm in diameter and 120 μm thick and consists of tortuous pores which allow for the high capture efficiency of submicron particles at low pressures. After the filter is the calibration source[26,27]. The source is a 2-layer structure whose base contains a deep porous silicon reservoir for retaining the volatile liquid calibrant and a silicon cap with a deep reactive-ion-etched diffusion channel and exit port. These two components are in the final system but were not on the system tested here.

The final system will have a three stage microfabricated preconcentrator inlet and is designed to capture organic vapors from a large sample volume. The inlet desorbs them as a small plug onto the separation column. For this system, short channels fabricated in the same manner as the separation columns were used. This fabrication process has been described in detail[14, 15] in previous chapters. The channels are filled post-fabrication with two different adsorbents.

The two separate separation columns are columns coated with different stationary phases. The first column is a three-meter-long statically-coated[29] nonpolar (polydimethylsiloxane) column and at optimal velocity yielded over 12,000 plates (4000 plates/m). The second column is a three-meter-long dynamically[30]-coated polar

(trifluoropropylmethylsiloxane) column and at optimal velocity yielded approximately 7500 plates (2500 plates/m). Both coating procedures have been described in detail in Chapter 2.

The detectors used on this system are integrated chemiresistor arrays. These arrays use solvent-cast monolayer-protected nanoparticles (MPN) as interface layers and detect eluting vapors by monitoring changes in resistance due to vapor sorption. Response patterns are generated from the different interactions that occur from the differences in the MPN. The current μGC prototype contains a glass/Si electrical and fluidic integration substrate, a preconcentrator, and two series-coupled microcolumns with independent temperature programming capabilities as well as junction-point pressure control.

At the beginning of this work, many of the performance goals had been achieved on the component level but testing on the system level had not yet been done. Integration of the individual components to the fluidic substrate was completed and performance data of the system was obtained after the integration of each individual component. Previous testbed systems have either used a single stage micro-fabricated preconcentrator or a meso-scale preconcentrator and a single column configuration. Many improvements have been made to the individual components since previous reports of the WIMS μGC[31,32].

Experimental Section

Apparatus. Figure 5.1 above shows the schematic of the system being tested. For injections prior to the integration of the preconcentrator, a split/splitless inlet was used. It

was connected to the fluidic substrate through nonports on the fluidic substrate. The split/splitless inlet and flame ionization detector (FID) are from the Agilent 6890 (Santa Clara, CA) and are connected to the system by uncoated fused silica capillary. All connection lines where 100μm i.d.

Materials and Procedures. Both columns were integrated on a Si/Glass fluidic substrate fabricated using DRIE. Performance analysis was completed by connecting the testbed system to a conventional split/splitless inlet and the FID of an Agilent 6890. Connection lines were minimized and heated to reduce extra column band broadening. Following the analysis of the columns with the fluidic substrate, the sensor array was integrated into the system. Again performance was evaluated using a Golay plot (flow rate vs. height equivalent to a theoretical plate). This was achieved by connecting the tailpipe of the sensor array to a commercial FID. Full width at half height data was collected from both the sensor array and the FID. Optimal flow rate was determined and the preconcentrator was integrated. Separations were then optained with all components integrated and the flow adjusted to optimal flow rate. All compounds were reagent grade or better.

Results and Discussion

Column and Fluidic Substrate. The system (Gen 0.6) consists of a preconcentrator inlet, dual column configuration and sensor array detection (Figure 5.2). There is a stop-flow valve at the junction point of the two columns. There are two other valves on the system. One valve is to close off the calibration source and the second is used to operate the split flow valve on the inlet. There are channels etched into the

fluidic substrate which connect the column injection to the columns and the columns to the detector. There is also a fluidic channel that connects the junction point of the two columns to the inlet of the first column.

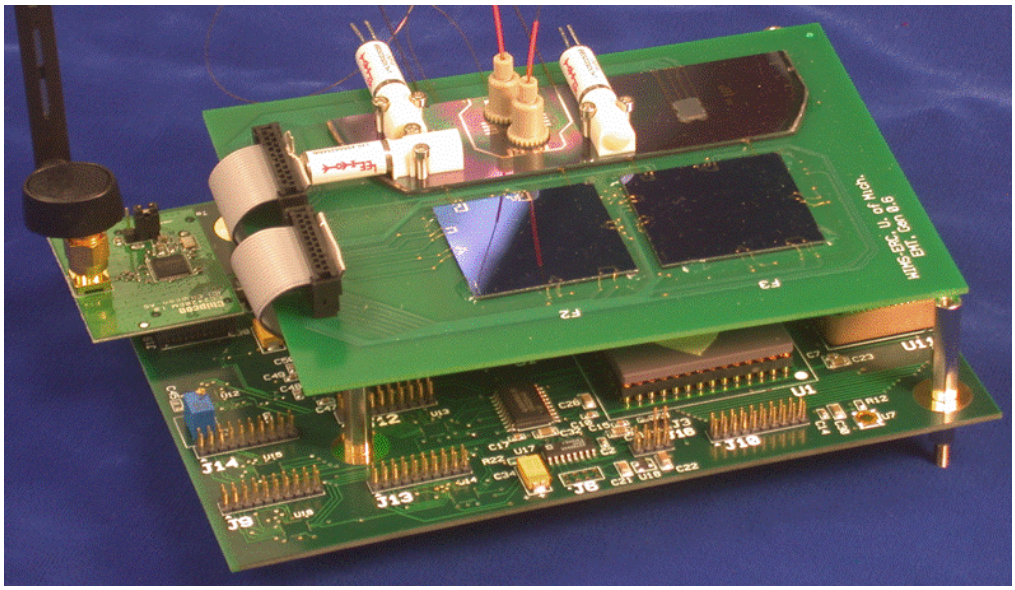

Figure5.2. Photograph of Gen 0.6 system with all of the components that have been evaluated.

A sample is captured under vacuum across the preconcentrator using a mini-vacuum. Flow is then reversed and the μPCF is rapidly heated. The components are desorbed and introduced onto the column. Analytes are then detected on the four channels of the sensor array. Since the four sensor arrays are coated with a different functional group ligands on the nanoparticle, there are different peak intensities that result from increased or decreased swelling of the nanoparticle films. This difference in intensity on each array yields a response pattern, and this pattern can be used in the identification of analytes.

All component parts were analyzed on an individual basis and then integrated piece by piece onto the fluidic substrate. Both columns were integrated onto the substrate

first. A Golay plot was obtained of the column ensemble and fluidic substrate. Figure 5.3 illustrates the column ensemble performance. Optimal flow rate, the flow rate that yields the lowest plate height, i.e. the best column performance, was found to be approximately 16 cm/s. This gives a total number of plates of 9800 at this flow rate. This number of plates is greater than the highest number of plates on the polar column but lower than the highest number of plates on the nonpolar column. This is due to differences in stationary phase film thicknesses, since column dimensions, column length and column temperature are the same. With the thicker stationary phase, there is a greater influence of that column on the overall separation. In this case, the polar column is the column with the thicker stationary phase. Even with the poorer performance of this column, the system still yields the largest number of plates of any completely micro-fabricated system.

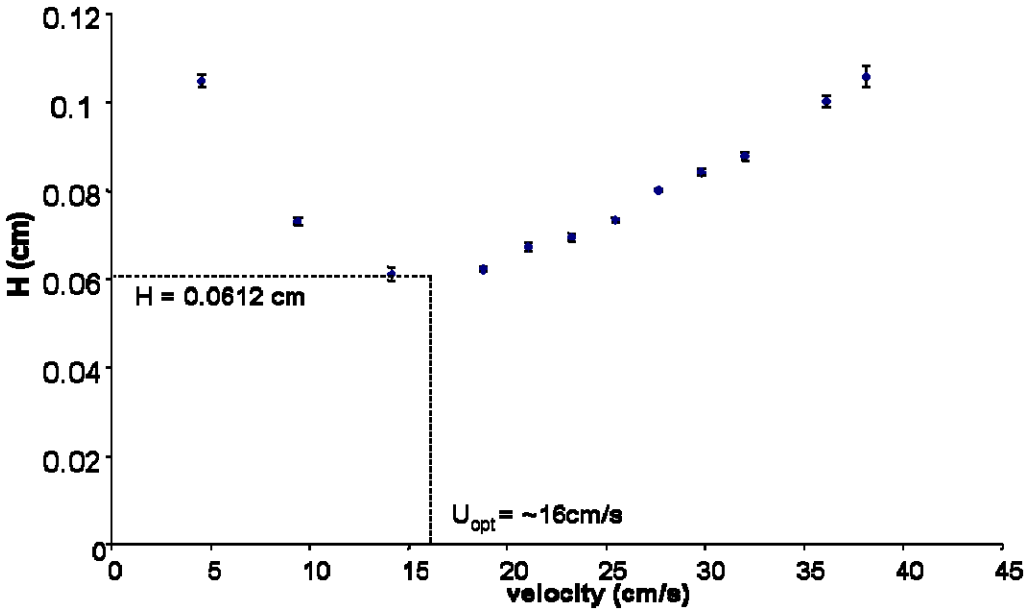

Figure5.3. Golay plot Gen 0.6 system with a nonpolar column, polar column and fluidic substrate. Optimal velocity was found to be approximately 16 cm/s yielding a minimum plate height of 0.0612 cm. This plate height gives a maximum number of 9800 plates on the system.

Initial separations were performed to evaluate column performance at optimal velocity of approximately 16 cm/s. Figure 5.4 shows three different separations of mixtures. Figure 5.4 (a) is a temperature programmed separation of normal alkanes C_7-C_{13}; (b) is another separation of normal alkanes C_7-C_{13}, this time with heated connection lines; and (c) a temperature programmed separation. There is a range of functional groups and overall peak shape is good, indicating minimal activity on the column.

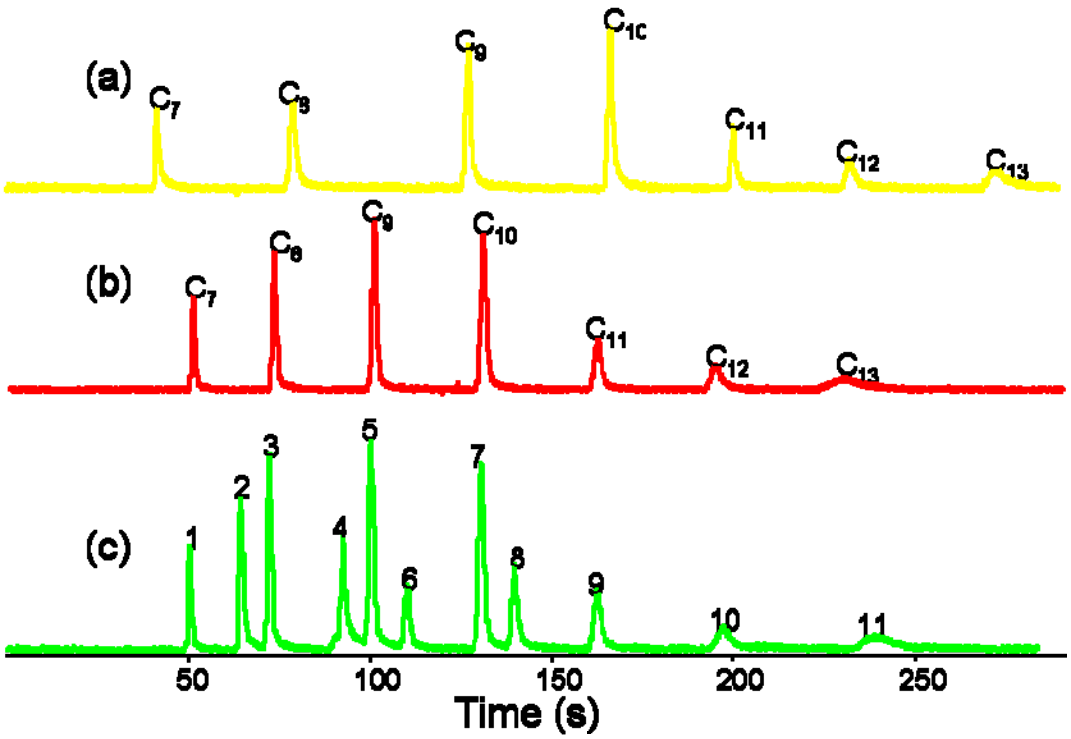

Figure5.4. Three separations illustrating column performance with the fluidic substrate. Detection is obtained using a commercial FID. All separations are temperature programmed,;separations (b&c) are temperature programmed at the same rate.

Table 5.1. Components from 11 component separation and their boiling points (in °C)

1	heptane	98.4	7	decane	174.1
2	toluene	110.6	8	limonene	176
3	octane	125.5	9	undecane	196
4	ρ-xylene	138	10	dodecane	216
5	nonane	151	11	tridecane	234
6	α-pinene	156			

Due to some electrical connection problems on the second column, the columns had two different temperature programming ramps. The first column was held at 30°C for 30 s, ramped from 30°C to 100°C at a rate of 30°C/min and held at 100°C for another 30 s. The second column was held at 50°C for the entire separation. When the substrate heaters were turned on, the substrate temperature was maintained at 70°C. A list of components from chromatogram c, in Figure 5.4, can be found in Table 5.1.

Preconcentrator Inlet. After evaluation of the columns, a two-stage preconcentrator inlet was added to the system. Flow was adjusted so that the optimal flow rate through the columns was achieved. Ideally, a high flow rate through the preconcentrator with rapid heating will lead to a narrow injection plug. However, under splitless conditions this can result in a higher flow rate through the column. The system was tested under both split and splitless operation. Peak width and flow rate were measured. Under split conditions, with a split ratio of approximately 20:1, flow rate was much less than the optimal velocity and this resulted in much poorer performance even with the benefit of the narrower injection plug.

When splitless flow was used, optimal flow rate was achieved. This is due to the pressure restrictions inherent in the system. Initial chromatograms were obtained using a homologous series. A 20 component mixture (Figure 5.5) was separated using the μPCF, dual column configuration and commercial FID. A list of the 20 components and boiling points can be found in Table 5.2.

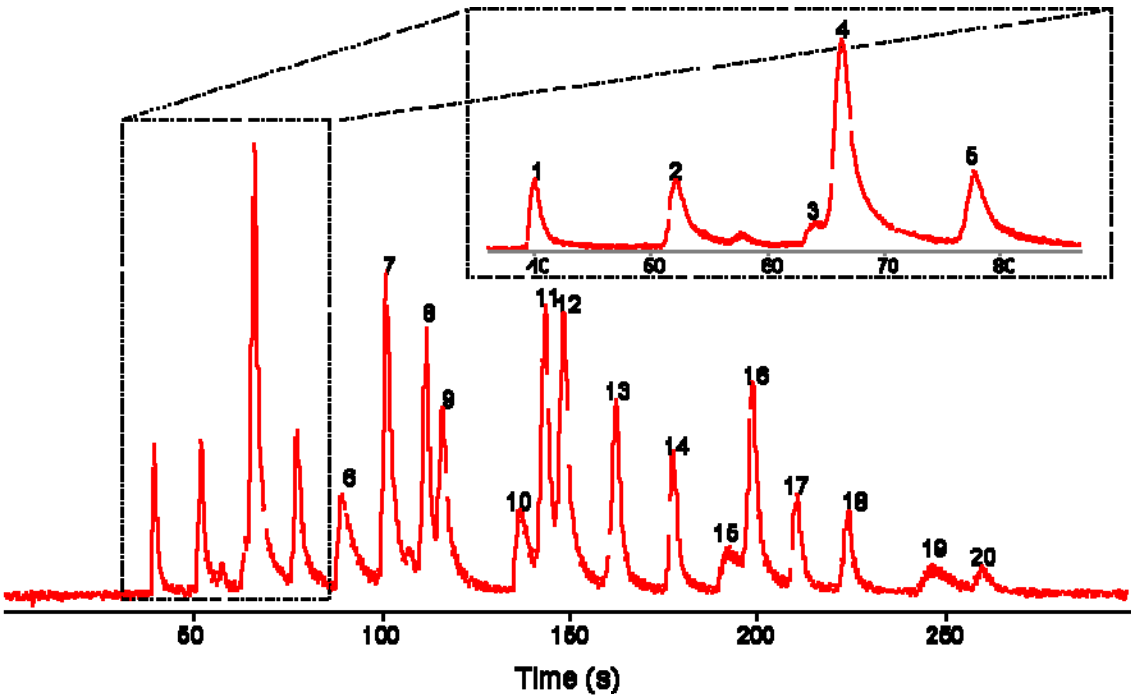

Figure 5.5. A 20-component mixture using a µPCF injector, dual columns and fluidic substrate. Detection was obtained using a commercial FID.

*Table 5.2.*Components from the 20 component mixture and their boiling points (in °C)

1	pentane	36.1	11	ethylbenzene	136
2	hexane	69	12	ρ-xylene	138
3	ethylacetate	77.1	13	nonane	151
4	benzene	80.1	14	α-pinene	156
5	heptane	98.4	15	2-heptanone	149
6	2-pentanone	101	16	β-pinene	164
7	toluene	110.6	17	decane	174.1
8	cycloheptane	118.4	18	d-limonene	176
9	octane	125.5	19	3-octanone	167
10	butylacetate	126	20	undecane	196

To separate a wider range of boiling point components, the columns were temperature programmed. The first column was held at 27°C for 60s, ramped at 11°C/min to 60°C, and held at 60°C for another 60s. The second column had some problems with the electrical connection at higher temperatures. Therefore, the column was ramped to 43°C, at a rate of 15°C/min, after being held at 27°C for 45s. The substrate was also heated, to 70°C, to reduce band broadening on the system.

Sensor Array Detector. After evaluation of the columns with the fluidic substrate, the chemiresistor sensor array was added. A similar evaluation procedure was performed. A Golay plot was again obtained for the columns with the fluidic substrate; however, peak width was obtained from both the sensor array as well as the FID that has been connected in series to the tail pipe of the sensor.

Due to the fact that analytes adsorb onto the surface of the sensor array, it is expected that peak widths will be wider than when the sensor array is not present. Also, the sensor array has a finite response time so as the flow rate increases there is actually a decrease in peak intensity. The Golay plot, with the sensor array and FID connected in series (Figure 5.6) shows that there is band broadening that occurs in the sensor array due to the fact that plate height is much higher when octane is detected by the FID after the sensor array.

System performance with the sensor array shows that there is some degradation in efficiency and this is due to the response time of the sensor. By decreasing the volume and electrode size of the sensor array the response time should increase and extra column band broadening would decrease making overall system performance better.

Octane was injected to obtain Golay plot information, since octane response best to the C_8 sensor, only that sensor was monitored and peak width values recorded. Optimal velocity with the sensor array was found to be approximately 22 cm/s and yields almost 10,000 plates.

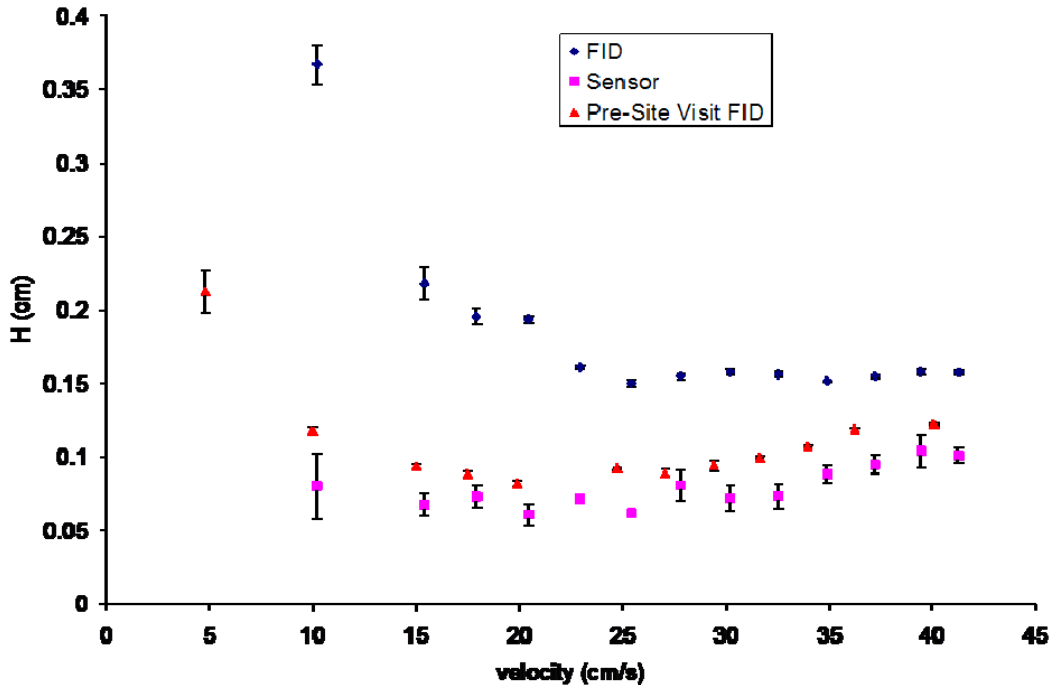

Figure 5.6. Golay plots of dual column system with fluidic substrate and chemiresistor sensor array. The bottom square plot shows the results from just the sensor array. The top diamond plot is from the FID as connected to the tail pipe of the sensor array. Due to the finite response time of the sensor array, there is some band broadening that occurs. The middle plot, is the original Golay plot.

The two FID plots differ greatly from each other. The middle (triangle) plot is the original Golay plot from the FID, prior to the sensor array being integrated. The top plot (diamond) is the Golay plot from the FID after it has passed over the sensor array. Due to the fact that there is a finite response time on the sensor array, the peaks are broadened. The difference between the middle plot and the top plot, is the contribution of band broadening from the sensor array. The bottom (square) plot, is the Golay plot from the sensor array. The sensor array has a better response at slower flow rates since analytes have more time to diffuse into the sensor film. At higher flow rates, there is less band broadening and, in turn, a narrower peak, and better system performance.

Lastly, a ten component mixture was sampled (Figure 5.7) using μPCF and injected onto the column. The mixture was separated under isothermal conditions at 25°C. Detection was obtained with the four sensor array and the FID attached to the tail pipe of the sensor array.

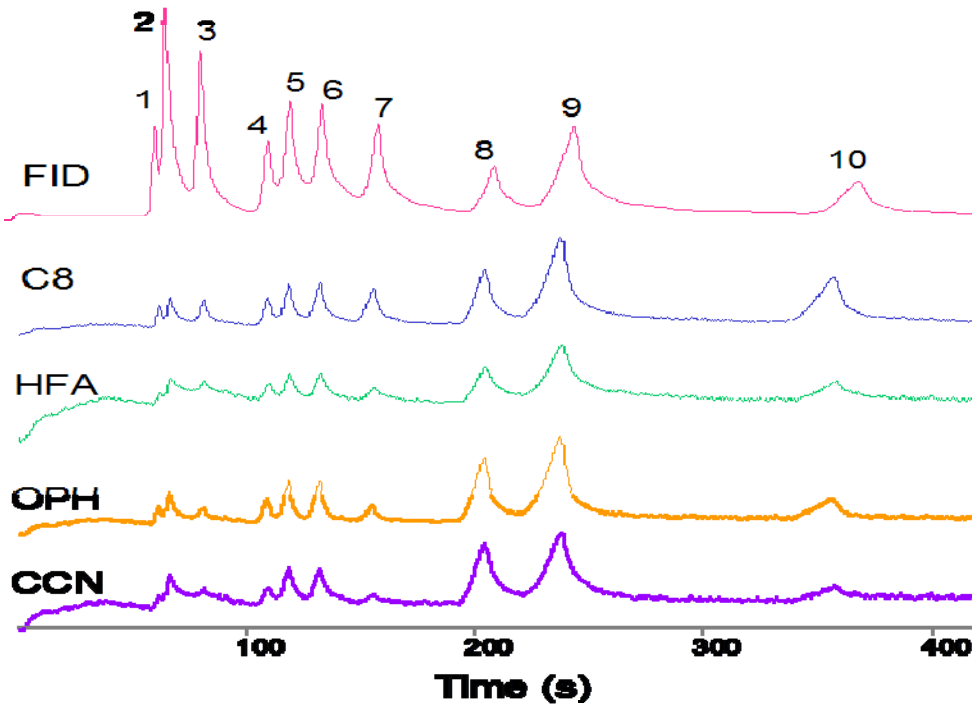

Figure 5.7. Chromatograms of ten component mixture separated under isothermal conditions. The top plot is the chromatogram from the FID as connected to the tail pipe of the sensor array. The bottom four chromatograms are from the different channels of the sensor array.

Table 5.3 lists the ten components and their boiling points. The top plot is the FID trace. There is a slight shift in retention times due to the response time of the sensor array and the additional connection line length. The bottom four traces are the four sensor arrays, each coated with different nanoparticles. All compounds are easily identifiable. Due to differences in functionality on the sensor array, each compound yields a different response on the four channels. For example, peak 7 is barely seen on

the CCN sensor, but has a much greater response on the C_8 sensor. Using these response patterns compounds that co-elute can be differentiated.

Table 5. 3 Components from the 10 component mixture and their boiling points (in °C)

1	methylchloroform	74.1	6	chlorobenzene	131
2	benzene	80.1	7	octane	125.5
3	heptane	98.4	8	2-fluorotoluene	113
4	cyclopentane	49	9	1-chlorohexane	133
5	toluene	110.6	10	nonane	151

Temperature programming utilizing the onboard heaters and temperature sensors has also been performed. Using the micro-controller described in Chapter 3, temperature programming on both columns was achieved. The system has separated a large range of compounds with different functionalities and vapor pressures spanning four orders of magnitude.

Conclusions

The Gen 0.6 system employs all of the component parts for the final WIMS μGC system, a microfabricated preconcentrator, dual column system, and a sensor array. These separations are the first separations on a completely microfabricated system with a dual column configuration. The initial separations show excellent overall peak shapes when using the FID. There is also good system performance, yielding 9800 plates with 6-m column. This performance is currently limited due to the polar column performance. There is great potential for more complex separations. Some additional system optimization needs to be done to be able to achieve the full range of vapor pressures desired. Also, work has been on-going to improve column performance for both the

nonpolar and polar columns. Passivation of the fluidic substrate will also improve overall system performance.

There is some additional optimization of the temperature programming that needs to be done when connected to the system. Once that improvement has been made, a wider range of vapor pressures may be separated. Determining column and system performance is important for knowing what the limitations are for given separations. Also, these limitations can dictate system redesigns for overall improvements.

References.

1. S.C. Terry, et al.,*IEEE Trans. Electron Dev.* **1979***, 26,* 1880.
2. A. de Mello, *Lab on a Chip*, **2002**, 2, 48N.
3. P. R. Lewis, et al., *IEEE SensorsJ*., **2006**, 6, 784.
4. http://www.arpa.mil/MTO/Programs/mga/index.html
5. http://www.sls-micro-technology.de/
6. M. Stadermann, *Anal.Chem.,***2006,** 78, 5639.
7. www.wimserc.org
8. K.D. Wise, et al., *Tech.Digest Sensors Expo*, **2001,** 175-182.
9. E. T. Zellers, et al. *IEEE International Conference on Solid-State Sensors and Actuators (Transducers),* **2007,** 1491-1496.
10. H. Kim, W. et al. *IEEE International Conference on Solid-State Sensors and Actuators (Transducers)*, **2007,** 1505-1508.
11. W.C. Tian, et al., *JMEMS* 12, 264, 2003;
12. W.C. Tian, et al., *JMEMS*, 14, 498, 2005.
13. H. K. Chan, et al. *IEEE International Conference on Solid-State Sensors and Actuators (Transducers)*, Seoul, Korea, 2, pp. 2091-2094, June 2005.
14. J. A. Potkay, J. A. Driscoll, M. Agah, R. D. Sacks, and K. D. Wise, *IEEE International Conference on Micro Electro Mechanical Systems (MEMS)*, 2003, 395-398.
15. M. Agah, et al., *JMEMS,* **2005**, 14*,* 1039.
16. M. Agah, J. A. Potkay, J. A. Driscoll, M. Kaviany, R. D. Sacks, and K. D. Wise, *IEEE International Conference on Solid-State Sensors and Actuators (Transducers)*, **2003**, 1339-1342.
17. S. Reidy, et al., *Analytical Chemistry*, **2007,** 79, 2911-2917.
18. J. A. Potkay, et al., *Proc*. *Solid-State Sens., Act. & Microsys.Workshop*, **2006**, 144–147.
19. G. R**.** Lambertus and R. D. Sacks, *Anal. Chem.,* **2005**, 77, 2078.
20. W.H. Steinecker, et al., *Proc. 12th Int. Conf. Solid-State Sens., Actuat. & Microsys. -- Transducers '03,* **2003**, 1343-1346.
21. W. H. Steinecker, et al., *Anal. Chem*, **2007**, 79, 4977.

22. Q Zhong, et al.,*J.Environ. Monit.,* 9,5, **2007**, 440

23. M. P. Rowe, et al., *Anal. Chem*.,**2007**, 79, 1164.

24. W. H. Steinecker, M. P. Rowe, H. Xu, Q. Zhong, C. Jin, L. Farina, C. Kurdak, and E. T. Zellers, *Eurosensors XIX*, **2005**, I1-I6.

25. J. Zheng, et al., *Physica Status Solidi A,* **2005**, 202(8), 1662–1667.

26. M.C. Oborny, et al., *Proc.* µ*TAS '03*, **2003**, 1243-1246.

27. J. Z. Wallner, K. S. Hunt, H. Obanionwu, M. Oborny, P. L. Bergstrom, and K. D. Wise, *Physica Status Solidi a*, **2007,** 204 (5), 1449-1453.

29. Reidy, S, Lambertus, G, Reece, J and Sacks, R., *Anal. Chem*, **2006**, 78**(**8**),** 2623.

30. Lambertus, G, Elstro A, Sensenig K, et al. *Anal. Chem.,* **2004**, 76 (9), 2629**.**

31. C. -J. Lu, W. H. Steinecker, W. -C. Tian, M. Agah, J. A. Potkay, M. C. Oborny, J. Nichols, H. K. Chan, J. A. Driscoll, R. D. Sacks, S. W. Pang, K. D. Wise, and E. T. Zellers, *Lab On A Chip*, **2005** 5, 1123.

32. C. -J. Lu, S. W. Pang, K. D. Wise, R. D. Sacks, M. C. Oborny, M. Agah, A. Guyon, W. H. Steinecker, W. -C. Tian, and E. T. Zellers, *International Conference on Miniaturized Chemical and Biochemical Analysis Systems (µTAS)*, **2003**, 411-415.

Chapter 6
Microfabricated GCxGC Development

Introduction

Since its invention over a decade ago, the novel technique of comprehensive two-dimensional gas chromatography (GCxGC)[1] has been developed to separated and analyze complex samples such as, petroleum[2-24], flavors[25-35], environmental[36-55] and even human breath samples[56,57]. The technique of GCxGC employs two coupled columns of different selectivity and subjects the entire sample to a two-dimensional separation. Effluent from the primary column is modulated to produce sharp chemical pulses, which are rapidly separated on the second column. A separation plane is produced by the two orthogonal retention time axes for the columns[58]. Usually, the first column contains a non-polar stationary phase and the second column a polar stationary phase. This combination allows components to be independently separated, first according to their volatility and then according to their polarity[59]. In comparison to conventional single-column gas chromatography, GCxGC has a much higher peak capacity because the available peak capacity is the product of the peak capacity of both dimensions. Other advantages of GCxGC include enhanced detectibility due to analyte refocusing, true background around

resolved peaks, and more reliable identification due to two retention times and well ordered bands of compound groups[60].

Modulator Devices. The most important instrumental component in GCxGC is the modulator. Modulation is necessary for transfer of the sample from the primary column to the second column. The modulator continuously traps, focuses and re-mobilizes components eluting from the primary column. The modulator thus acts as a continuous injector for the secondary column. There are two classifications of modulators, pneumatic and thermal. Initially, modulation was achieved by means of a resistively heated piece of capillary column that was coated with a conductive paint[1]. John Phillips, Derhsing Luu and Janusz Pawliszyn used this design, not for GCxGC, but for signal amplification in a one-dimensional GC system. This early work set the foundation for GCxGC and the various modulation techniques.

Valve Based Modulators. Synovec and coworkers developed non-thermal modulations strategies. A six-port diaphragm valve was used as a modulator[61]. Fast valve-switching creates pulses of the first column effluent that are injected onto the second column. The sample eluting from the first column is split after the valve and before the second column. Because only 10-20% of the injected sample reaches the detector, sensitivity is significantly lower than with thermal modulators. The valve-switching approach is simple in terms of experimental set-up compared with early thermal modulation techniques. However, the relatively high flow rate in the modulator can cause peak chopping and other artifacts. Also, temperature limitations of the switching valve have limited the sample analysis to components with boiling points below 200°C.

Seeley has developed a simple yet very powerful modification of Synovec's valve-diverting strategy. Seeley's differential flow modulation concept uses a sample loop with a diaphragm valve[62]. Sample is collected 80% of the time and transferred to the second column 20% of the cycle time. Column flow in the second column is 20 times higher than in the primary column. This approach is more sensitive than Synovec's approach because more sample is introduced to the second column. The considerable pressure difference between the columns also generates a sharp peak as it enters the second column. A limitation of this design is that the modulation period is restricted to 2.0 s or less. This restriction limits the resolving power that can be obtained from the second column.

Seeley and coworkers have made improvements to the differential flow modulator[63]. This approach has several advantages over diaphragm valve modulators. Foremost, 100% of the effluent from the primary column passes into the modulator and onto the second column. The use of low dead volume 3-way connectors remedies the temperature restrictions that were of concern with previous valve-based modulators. The switching valve is located outside the GC oven and is not in the sample path. Performance showed a peak width at half-height to be less than 100ms with a modulation period of 2.0 s. This approach has been applied to the analysis of volatile organic compounds and diesel-range hydrocarbons.

Thermal Modulation. John Phillips set the stage with his early work in the late 1980s with a single stage modulator, which uses a segment of fused silica column coated with an electrical conductive gold paint[1]. This design was further modified in the early 1990s into a two-stage device. It would become the first modulator used for GCxGC[58,64].

The two-stage modulator was designed to prevent mass transfer through the modulator during the cooling cycle of the modulation period, a condition observed in a single-stage modulator. To overcome sample breakthrough during the cooling stage, a second stage immediately following the first stage would collect and re-inject the focused plug a short time after the fist stage had completely cooled. By independently applying current pulses to the first and second stage, components could be trapped, released and re-trapped prior to their injection onto the second column. Evaluation of this design proved enhanced linearity, and reports showed peak widths, as measured at the detector, to be ~100ms for volatile and semi-volatile components. Although this approach enabled good separation of complex mixtures, the setup was rather unstable due to thickness variation in the gold paint and immediate failure of the modulation device was sometimes observed[65]. After initial experiments with a resistively heated trap[66,67], Philips and Ledford developed a rotation heating device to perform sample transfer[68]. Samples eluting from the primary column were collected on a short segment of thick-film capillary column and then released by application of a sweeping heat pulse by means of a slotted rotating heater.

Phillips et al. performed a thorough study on the operation of slotted heater prototypes[65]. Some failures were observed and were attributed to the alignment of the modulator. Redesign of the oven-mounted components helped overcome these problems and a reliable thermal modulation device was demonstrated. Thermal modulation with a sweeping heater led to an increase in signal amplification by a factor of 10-30 compared with conventional GC operation and a base peak width of 250 ms was reported[65].

Work on a resistively heated single-stage modulator was performed by De Geus, et al. in 1997[69]. His approached involved wrapping a piece of capillary tubing with a

solid wire. A current pulse, 300 ms, was sent through the wire resulting in a rapid temperature increase. Cooling of the modulator was limited to the oven temperature and therefore trapping efficiency was limited by the thickness of the stationary phase in the modulator. Limitations in design, robustness of the wire and marginal performance turned most modulator attention to dual-stage and cryogenic means of cooling.

Marriott and Kinghorn developed a cryofocusing approach for the thermal modulation termed the "longitudinal modulation cryogenic system" (LMCS)[70]. When the modulator is at the top position, a narrow zone containing analytes from the primary column is cold trapped and focused in the inlet of the second column. When the modulator moves to the bottom position the cold spot in the second column containing the trapped fraction is heated by the surrounding oven air and remobilized. The focus plug migrates into the cold modulator and undergoes further focusing. The modulator then moves to the top position releasing the narrow plug for separation on the second column and begins trapping another sample plug eluting from the primary column. The movement of the modulator is dependent on the modulation period. The chromatographic modulation period is typically 2.0 to 12.0 seconds depending on the methodology and sample.

Ledford and Billesbach introduced a new type of thermal modulator from which moving modulation parts were eliminated[71]. The primary column was kept in the GC oven and modulation was performed by use of "jet-cooled thermal modulation". The secondary column was placed inside its own oven chamber with a semi-open connection to the main GC oven. The temperature of the modulator tube was 100°C below the oven temperature. Ledford and Billesbach pointed out that the design could be furthered

improved by the inclusion of two jets capable of pulsing hot and cold gas and that no slotted heater would be needed[71].

All of the previous modulators have many limitations in field portable systems, moving parts and consumables being the main two limitations. This chapter will describe the development of a field portable GCxGC system that utilizes a consumable free modulator. Data will be shown with both a pneumatic modulator, which utilizes previous separation enhancement techniques[72,73], and a thermal modulator[74,75], which had been previously developed by Dr. Mark Libardoni, and micro-fabricated columns[76] that have been described in detail in previous chapters. A commercially available piece of stainless-steel wall coated capillary column is used as the modulator. Cooling of the modulator is provided by a two-stage refrigeration unit with an external heat exchanger and a recirculating air system. The modulator is resistively-heated by sending a current pulse through each stage of the modulator tube. In addition to the initial separation results, modeling work will be presented on the necessary redesign of the micro-fabricated columns.

Experimental Section

Apparatus. Figure 6.1 shows the schematic of the experimental systems. For the (a) pneumatic modulation system, free standing split/splitless inlet from an HP 6890 is used as the injector. Detection is obtained by a Varian flame ionization detector (FID) with a high-speed electrometer built in-house. With the thermal modulation system, an HP 5890 GC equipped with a split/splitless injector and an FID is used as the GCxGC platform. The primary column on both systems is a nonpolar, dimethyl(poly)siloxanes

(PDMS) 3-m-long microfabricated column. For the pneumatic modulation system, the second dimension column is a polar, triflouropropylmethyl(poly)siloxane, 1-m-long microfabricated column, whereas, in the thermal modulation system, the stationary phase remains the same but the length of the column is 25-cm. All columns are coated in-house using a previously described static coating method.

Pneumatic Modulator. The two micro-fabricated columns, C_1 and C_2, are connected to the inlet and detector using 100 µm i.d. fused silica connection lines. A low-dead-volume solenoid valve V_1 (stop-flow valve) (EC-2-24VDC, Clippard, Cincinnati, OH) is connected from the column junction point to the inlet end of the first column. Connections are made by use of low-dead-volume Y connectors (MXT "Y" Connectors, Restek Corp., Bellafonte, PA).

Thermal Modulator. Located inside the GC oven is the 2-stage thermal modulator. The modulator is a piece of stainless steel capillary tubing measuring 10 cm long x 0.18 mm i.d. x 0.20 µm film thickness, PDMS (MXT-1, Restek Corp, Bellefonte, PA). The modulator is divided into two stages, a 5.5cm primary stage and a 2.2 stage secondary stage. Although the modulator is one continuous piece of stainless steel capillary, a soldered junction point serves as the electrical contact between the two stages. Figure 6.2 shows the component pictures of the modulator housing and modulator cartridge.

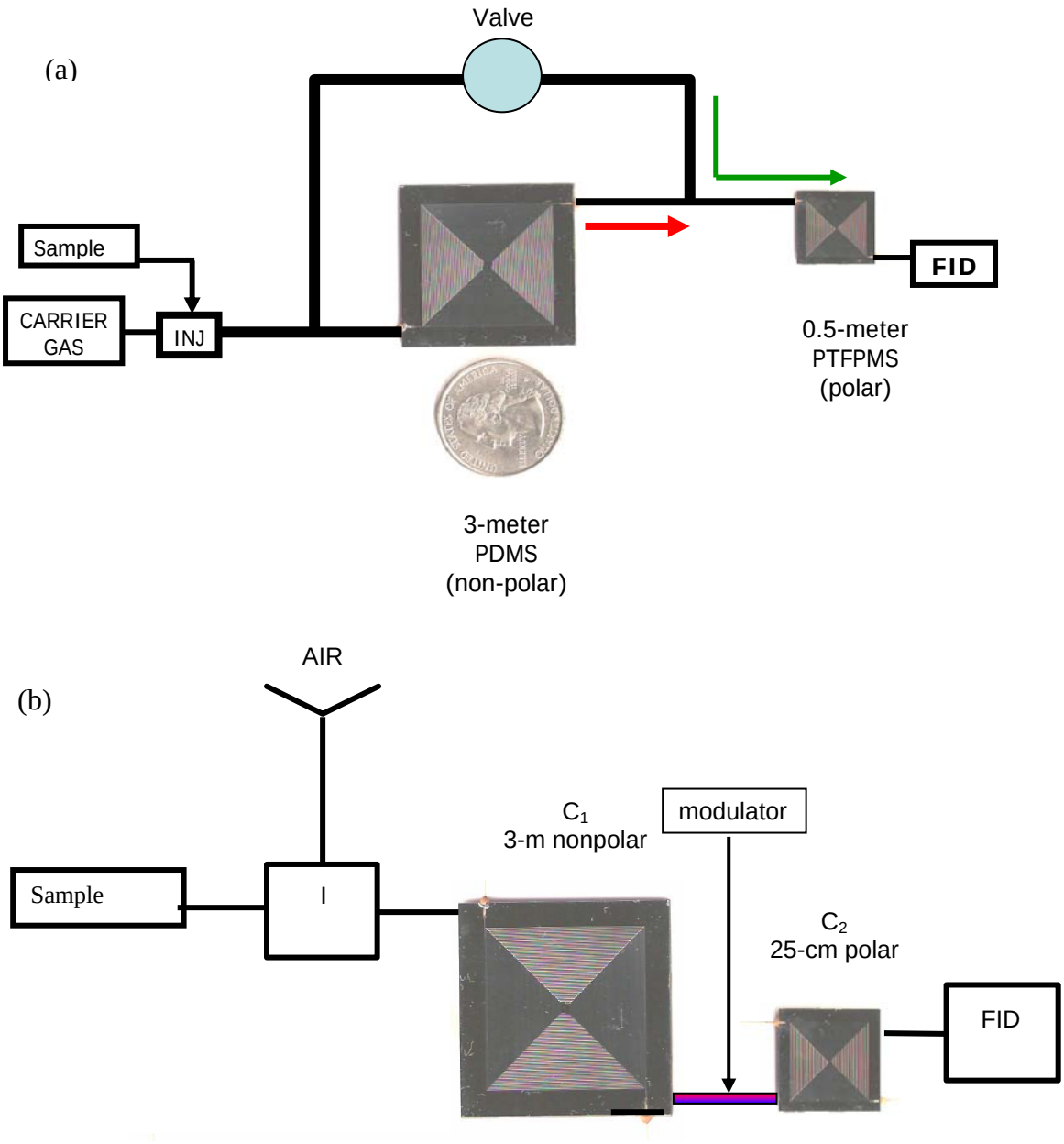

Figure 6.1 Instrument schematics of GCxGC systems. (a) Pneumatic modulation system. First dimension column is a 3-m nonpolar microfabricated column and the second dimension column is a 1-m polar microfabricated column. Modulation is obtained by opening and closing the junction point valve. (b) Thermal modulation system. First dimension column, is a 3-m nonpolar microfabricated column, and the second dimension column is a 0.25-m polar microfabricated column. Modulation is obtained by resistively heating capillary. Details of modulator in text.

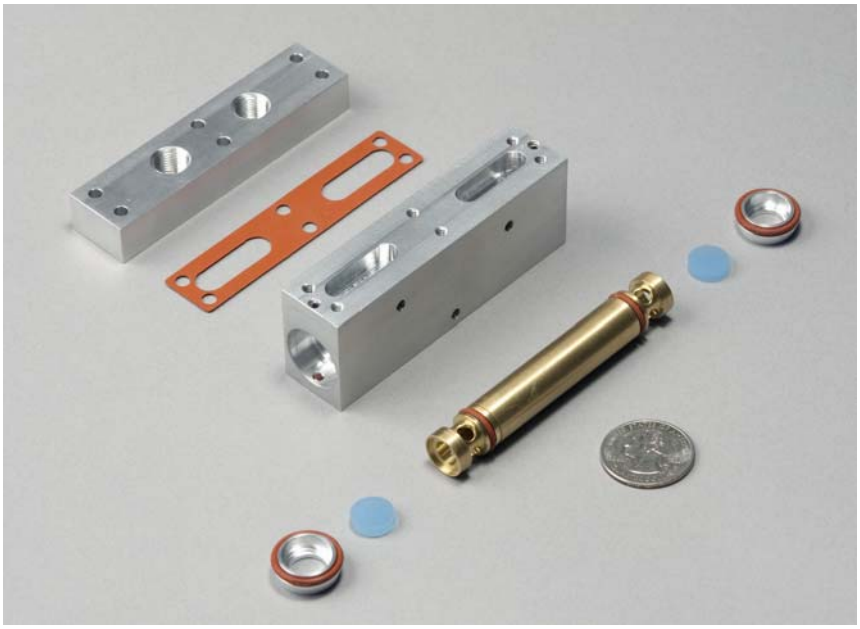

Figure 6.2. Components of thermal modulator housing and modulator cartridge. Photo courtesy of Bruce Block.

The modulator cartridge is 0.5 inches in diameter and 3.2 inches long, not including the end caps. A machined aluminum block, mounted on the inside of the GC oven, houses the modulator cartridge. The aluminum block is 3.4 inches long, 1.7 inches high and 0.8 inches wide. A center ground constructed from brass is used as the stage divider and electrical contact. The center ground ring is soldered directly to the metal column. The modulator is placed inside the cartridge and the end cap cartridge is threaded into place. The engineering of the cartridge provides electrical contact throughout the brass ring as well as the ends of the modulator tube. Once assembled, the modulator cartridge is inserted inside the aluminum block. Set screws are used to hold the modulator cartridge in place and provide electrical contact. Prior to mounting on the GC oven wall, the entire block is insulated. Design of the modulator was done by Dr. Mark Libardoni, Bruce Block, and Dr. Ernest Hasslebrink.

Materials and Procedures. Columns are interfaced to a conventional split/splitless injector and a FID for instrument evaluation. Compressed air, after passing through traps for water vapor and hydrocarbons, is used as carrier gas for the pneumatic modulation system and hydrogen was used for the thermal modulation system. Compounds used in the test mixture are listed in Table 6.1. All compounds are reagent grade or better. All chromatograms are obtained isothermally at ambient temperature (22-23^{o}C). Injections are typically 0.5 μL or less of individual components or mixtures with a split ratio of 300:1. No solvent is used. Carrier gas flow rate is controlled using an electronic pressure controller (EPC) and flow rate is calculated using methane hold up time and column length.

Pneumatic modulation is achieved by opening and closing of the stop-flow valve. When the valve is closed normal flow occurs from column one to column two. The valve is closed for 0.5 s to introduce some effluent from the first column onto the second. Then the valve is opened for 20s, bypassing the first column, and only allowing flow from the second column. This allows only a fraction introduced from the first column to be separated on the second column. Since the junction point of the two columns is connected to the inlet of the first column, when the valve is opened, there is an increase in head pressure at the start of the second column. This increases the flow rate on the second column causing the peaks to focus, and a faster second column analysis time. The process is then repeated throughout the entire separation.

For the thermal modulation, the modulator cooling is provided by cold air from a conventional refrigeration unit (Model CC-100 Cryocool Immersion Cooler, Neslab Instruments, Portsmouth, NH) by means of a heat exchanger built in-house and re-

circulating pump to prevent ice accumulation in the heat exchanger. The modulator tube is resistively heated by the current from two adjustable-voltage DC power supplies (Model DS-304M, Zurich MPJA, Lake Park, FL). A 100-ms heating pulse is applied to each stage of the modulator every 10s. The pulse voltages are 14.26 V and 8.58 V applied to the first and second stages, respectively. A one second offset is used between the first and second stage heating pulses. This delay allows for the first stage to cool completely and being trapping components that are eluting from the primary column. Once quantitative trapping has occurred, the second stage is heated and a narrow injection plug is introduced onto the second column from the second stage of the modulator. Heating pulse timing is controlled by a PC through two solid-state relays (RSDC-DC-120-000, Continental Industries, Inc., Mesa, AZ).

With both systems the FID is interfaced to a PC by means of a 16-bit A/D board (PCI-DAS 1602/16, Computer Boards, Inc., Marshield, MA). The board is controlled by LabTech Notebook software (Laboratory Technologies Inc., Wilmington, VA). Data are initially stored as a one-dimensional text file, and then processed, using MatLab Software (The Math Works, Natick, MA), into a matrix based on the modulation period.

Results and Discussion.

Pneumatic Modulation. Initial work with stop-flow was used in one-dimensional chromatography as a separation enhancement technique for high-speed separations with a dual column configuration. By opening and closing the valve during a specific time window for a specific length of time, co-eluting compounds can be separated. However,

this technique is limited to targeted component analysis. By continuously operating the stop-flow valve, modulation can be obtained.

A thirteen component mixture is separated using the same configuration as the pneumatic modulation set-up, however, the modulator was not actuated. A list of the components and their boiling points can be found in Table 6.1

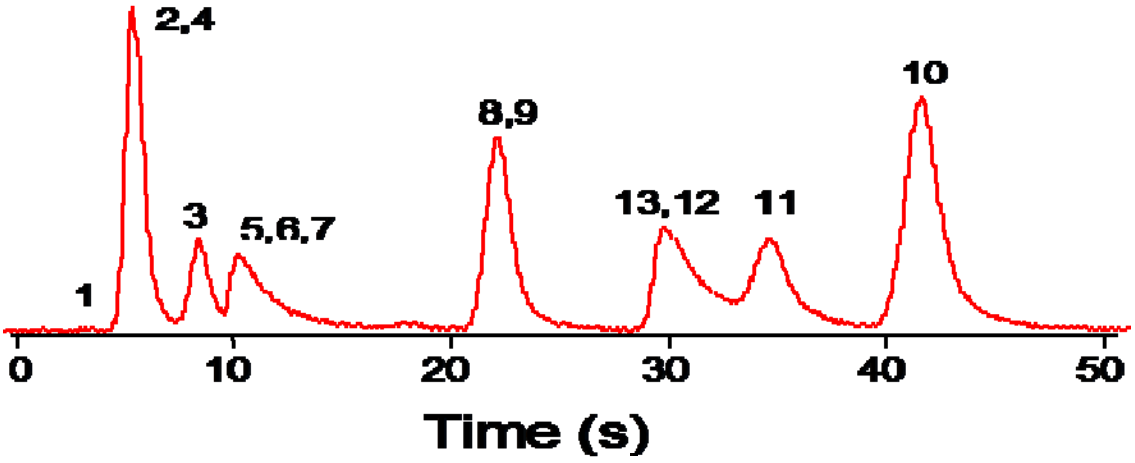

Figure 6.3. One-dimensional separation of a thirteen component mixture separated on two micro-columns. There are multiple co-elutions that occur, compounds 2:4, 5:6:7, 8:9, and 12:13.

Table 6.1. List of thirteen components and their boiling points (in °C).

1	ethanal	20.1	7	n-hexane	69
2	n-pentane	36.1	8	methylchloroform	74.1
3	dichloromethane	39.8	9	benzene	80.1
4	acetone	56.3	10	n-heptane	98.4
5	butanal	75	11	chloropentane	107
6	2-butanone	79.6	12	pentanal	102
			13	2-pentanone	101

There are multiple co-elutions that occur in the separation shown in Figure 6.3: 2:4, 5:6:7, 8:9, and 12:13. Each one of these co-elutions are between compounds of differing polarities, which means that they would be separated on a polar column. However, if the

mixture was separated on a single polar column there would be other co-elutions that would occur.

The same mixture was injected onto the columns and after a 10s delay to ensure all compounds were on the first column the valve was opened for 20s, bypassing flow on the first column. The valve was then closed for 0.5s introducing a small fragment of the analyte band onto the second column, the valve was opened again and flow increased on the second column. This process was continued throughout the entire separation.

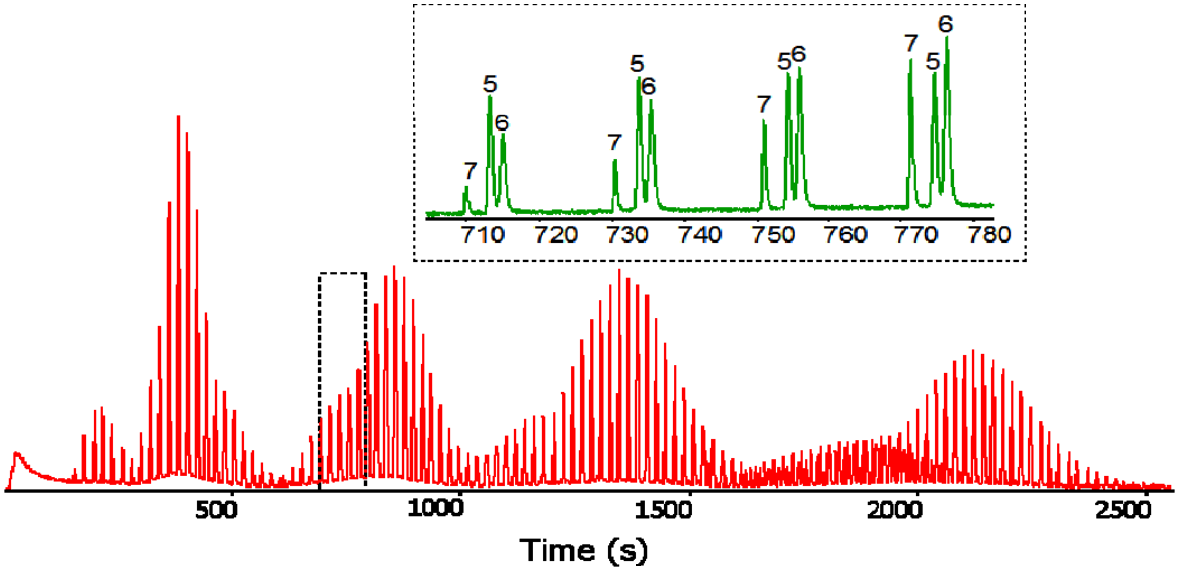

Figure 6.4. GCxGC separation as collected at the detector. A second dimension separation is taking place every 20.5 seconds. Inset shows four second dimension separation slices of three components that would co-elute in one-dimensional GC, but are separated on the second column.

Figure 6.4, shows the modulated GCxGC separation of the same 13 component mixture. There are multiple co-elutions that occur in the one-dimensional separation, but all 13 compounds are separated. The inset shows three compounds that co-elute in the one dimensional separation, but are separated by GCxGC. Every 20.5 seconds a second dimension separation takes place. There are 4 second-dimension separations in the inset.

Compounds 5,6 and 7 co-elute from the one-dimensional ensemble, but are baseline separated here. Using Matlab software, the one-dimensional representation of the GCxGC chromatogram was processed into a two-dimensional figure.

The same separation is then shown as a contour plot Figure 6.5. There is a clear separation of all 13 components. Compounds that have the same elution time on the x-axis would co-elute in a one-dimensional separation. There is an increase in peak capacity by adding the second dimension column. Instead of a separation axis there is now a separation plane. This place allows for the separation in both dimensions. This is again seen with the separation of compounds 5,6 and 7. These three peaks have overlapping first dimension retention times but very different second dimension retention times.

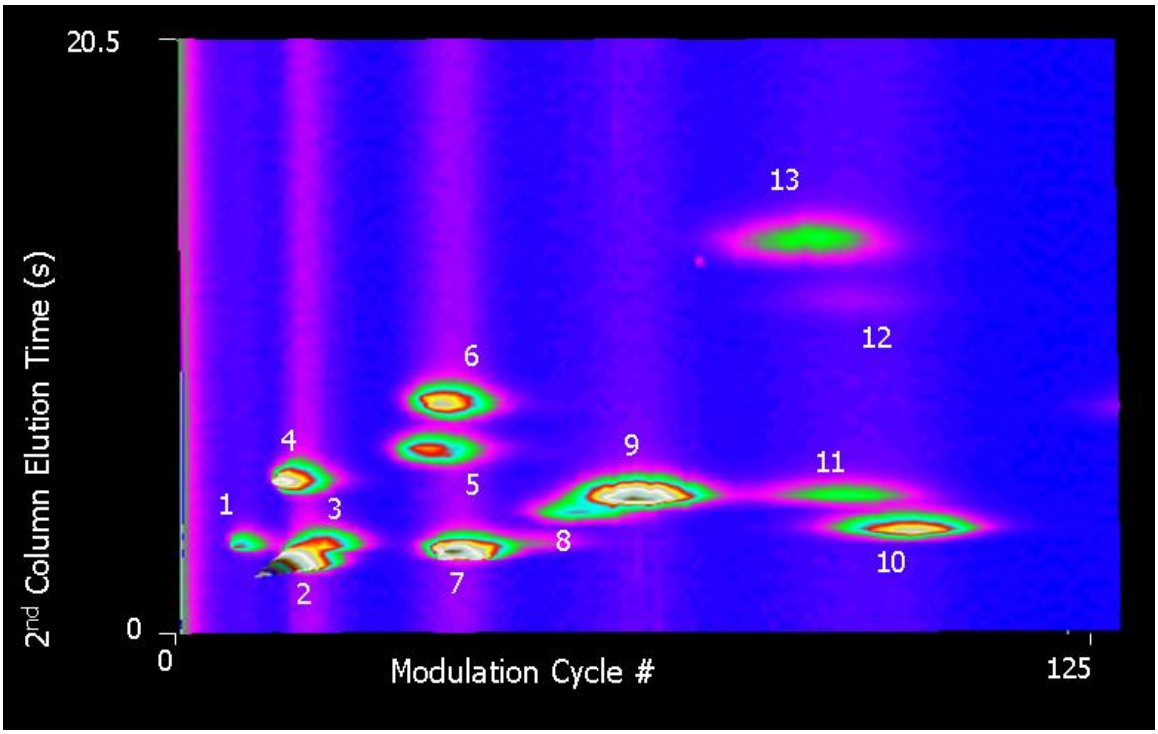

Figure 6.5. Contour plot of 13-component separation. All 13 components are separated over the separation plane. Peak intensity is illustrated by color.

There are some limitations to this method of modulation. Since flow stops on the first column while separation occurs on the second dimension column the overall separation time is the product of the first and second dimension separation times. However, one of the major advantages of pneumatic modulation is that there is no volatility limitation since modulation is occurring due to a difference in pressure. Compounds with very high volatility, for example methane, have been successfully modulated using this modulator. Also, since the valve is not in the fluidic path there is no upper temperature limit due to the valve as has been the case with previous valve-based modulators. The upper temperature limit restriction in this case would be that of the stationary phase.

Thermal Modulation

A meso-scale consumable free modulator has been previously developed. This modulator uses a thermo-electric cryo-cooler to cool recirculation air to -35°C. The modulator is constantly cooled and then resistively heated using a DC power supply to desorb the bands. The modulator has been designed as a both a single and dual stage modulator. The dual stage modulator is integrated with two microfabricated columns. The first dimension column is a 3-m-long nonpolar column. The second dimension column is a 0.25-m-long polar column. Sample is injected using a conventional split/splitless inlet and detected using a commercial flame ionization detector (FID) (Agilent 5890, Santa Clara, CA) with a high-speed electrometer.

A mixture of nC_6-C_{10} alkanes and C_3-C_7 ketones was injected onto the column with a head pressure of 17psi and a split flow of 20 mL/min. In a one-dimensional

separation all 10 compounds would perfectly co-elute. The modulator was heated every 11.0 seconds with a 0.5 second delay between the two stages. This corresponds to an 11.5 second modulation period for 3.25m total separation column. In the modulated one-dimensional chromatogram there is a clear separation of the ketones and the alkanes, Figure 6.6. The inset shows the separation of C_9 and pentanone which perfectly co-elute in the one-dimensional separation.

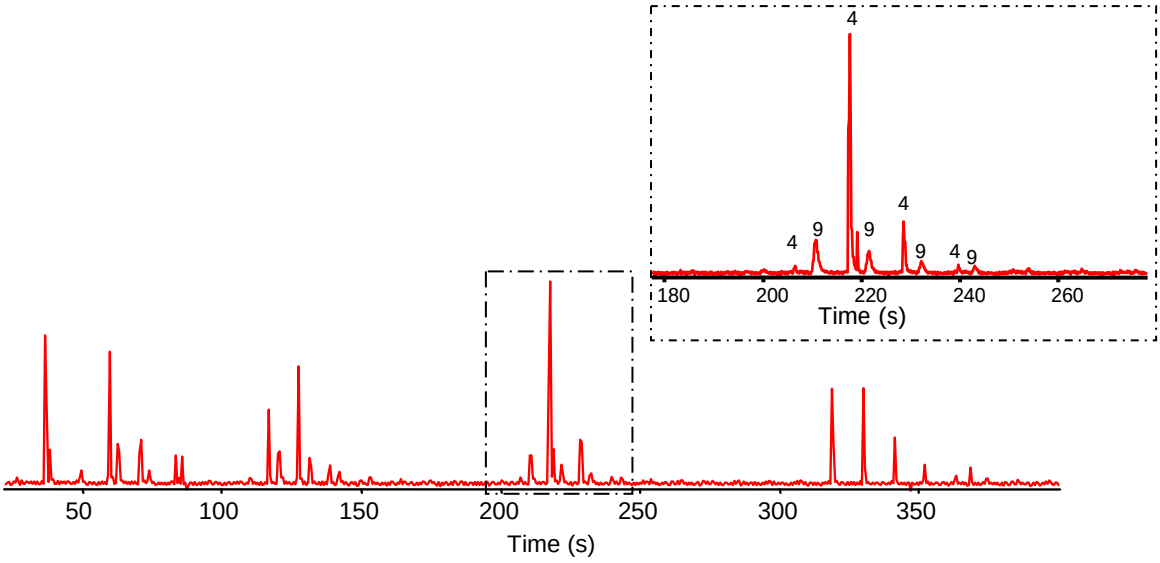

Figure 6.6. A thermally modulated one-dimensional chromatogram of the separation of normal alkanes, C_6-C_{10}, and ketones, C_3-C_7. Inset shows the separation of pentanone and n-nonane. When this separation is not modulated these two components would perfectly co-elute.

In the contour plot, Figure 6.7, it becomes quite easily visible the definite separation of all ten compounds. Also seen when the separation if viewed as a contour plot is the clear structure of the GCxGC chromatogram.

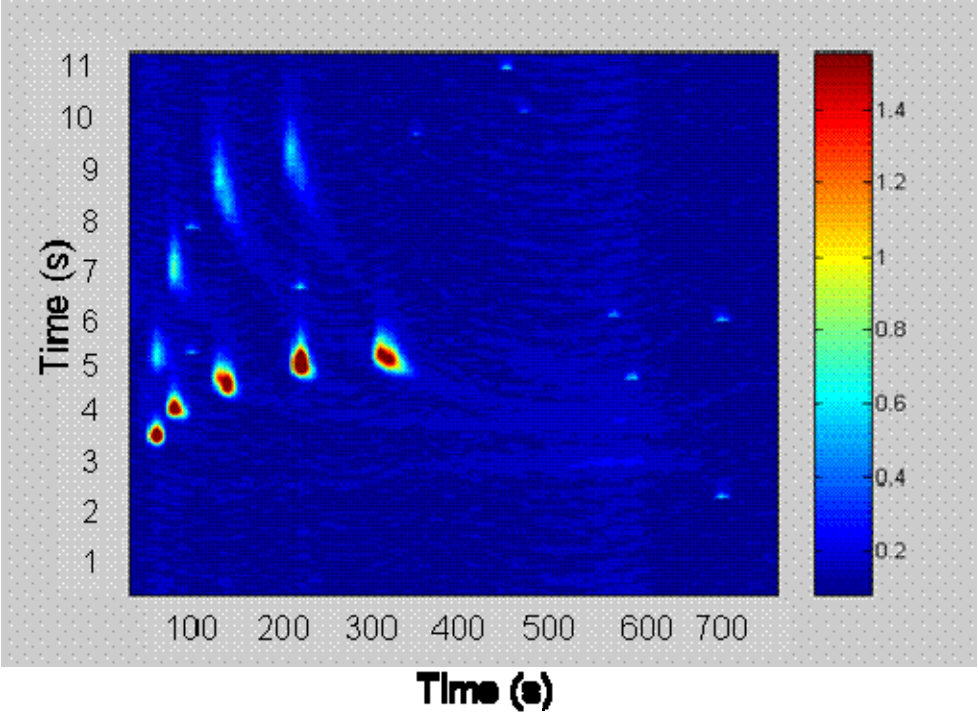

Figure 6.7. Contour plot of a thermally modulated separation. The contour plot shows the structure that result from a GCxGC separation. The peaks along the bottom are the nonpolar alkanes, and along the top are the polar ketones.

The nonpolar alkanes align along the bottom and the polar ketones align towards the top. With GCxGC, separations typically columns are completely orthogonal, the separation means of the two stationary phases are not dependent on each other. The separation therefore occurs over the entire plane instead of along the diagonal. Since the polar phase is only a moderately polar phase there is still some influence of the compounds boiling point on the second dimension separation.

Another benefit of GCxGC separations is the increase in detectibility due to the focusing effects of the modulator. This means there is an increase in detection in trace components. The ketones are in much lower concentration than the alkanes in this mixture. Without modulation the ketones were barely above the noise and almost undetectable. Typically the peaks in the second dimension are even more focused and more intense due to the increase in linear velocity from the decrease in column diameter

on the second column. With the current column configuration the peaks are not as intense as they can be because the second column has the same dimensions as the first column. Previous work has shown that with the appropriate columns peak widths can be as narrow as 30ms. Therefore it was concluded that a new second dimension column was needed.

Modeling work has been done utilizing Spangler's equation for height equivalent to a theoretical plate

$$H = \frac{2D_g f_2 f_1}{\bar{u}} + \frac{\left(0.9 + 2k + 35k^2\right) w^2 f_1}{96(k+1)^2 D_g f_2}\bar{u} + \frac{2}{3}k\frac{d_f}{D_s(1+k)^2}\bar{u} \qquad (6.1)$$

for a range of linear velocities as calculated from a given pressure drop to determine new column dimensions. Three dimensions were chosen because the aspect ratio most closely resembled the current column configuration and had the equivalent cross-sectional area to a 100 µm i.d. fused silica capillary which would allow for the increase in linear velocity needed. However, there are some advantages and disadvantages to each dimension. Based on Spangler's H equation, Equation 6.1, column performance was found to be greater with the smaller width, Figure 6.8, and have less variation over the wider range of pressures, Figure 6.9. By having less variation this means column performance will not vary drastically when operating at higher flow rates. As seen in Figure 6.9, the original columns had very little tolerance for operation off linear velocity. However, the narrower

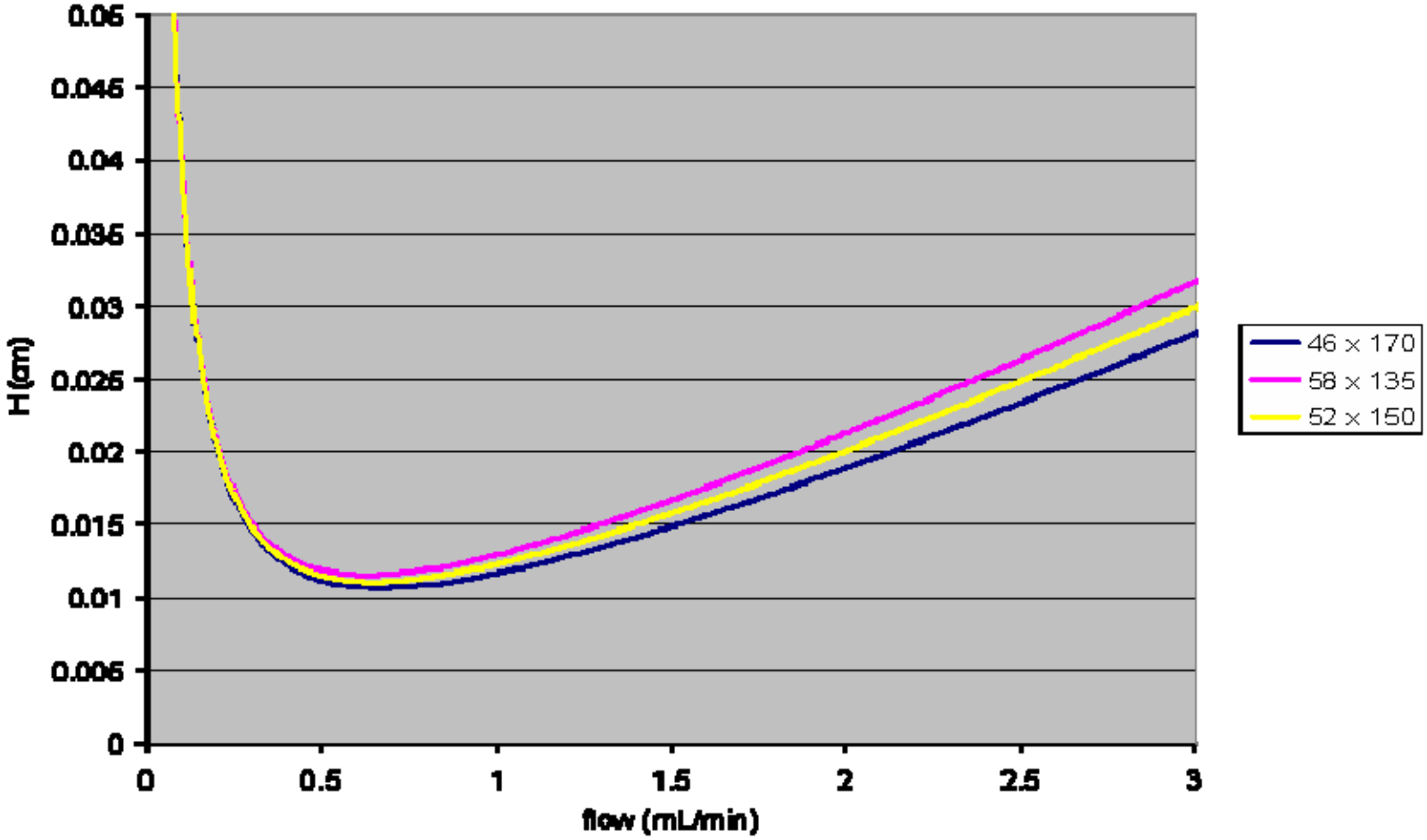

Figure 6.8. Column performance at different channel dimensions. All columns have the equivalent internal diameter of 100μm i.d. column. The narrower the column width, the better the column performance.

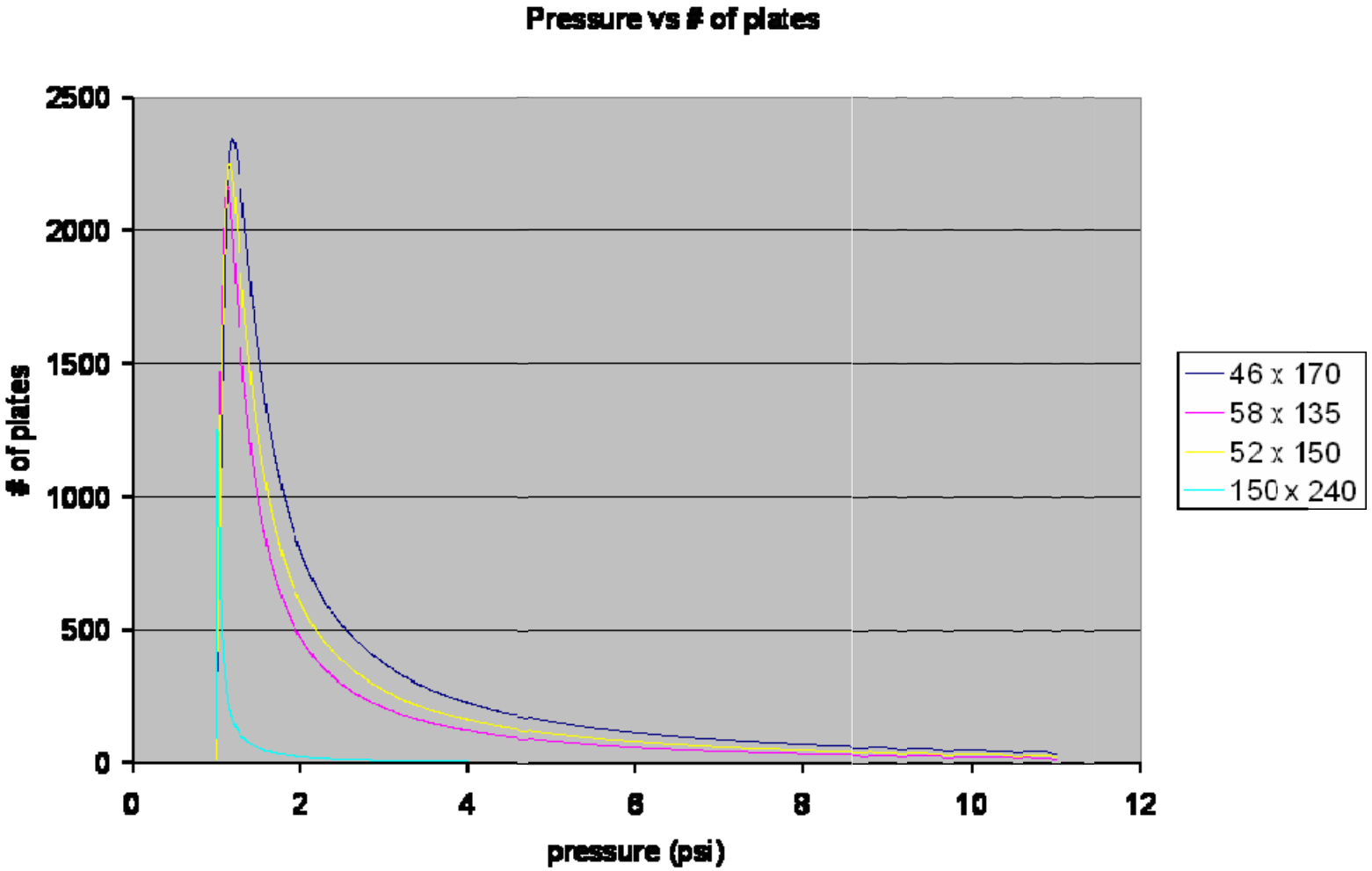

Figure 6.9. A plot of pressure versus number of theoretical plates at different column dimensions. The best column has the narrowest width, and the worst column is the current column configuration.

width of the columns have more of a pressure drop restriction which means that a greater head pressure is required to achieve the same flow rate. It was also found that there was little variation between column dimensions and its performance over a range of dead times.

The same evaluation was done on the first dimension column. It was compared to predicted performance of the original column dimensions. Minimum plate height between the two dimensions did not vary greatly, optimal velocity did however. Both columns yield approximately the same pressure tolerance. There is a great improvement in the pressure drop with the new column dimensions.

Another main advantage with the new column design is the change in inlet and outlet port design. In the original design of the columns, the inlet and outlet ports were 250µm deep and 250µm wide. This limited the capillary needed to fluidically connect to have an o.d. no greater than 250µm. This corresponds to an i.d. of 100µm. This decrease in i.d. acts as a very large pressure drop and causes band broadening.

The first dimension columns have larger connections to accommodate 250µm i.d. capillary which is the equivalent cross-sectional area of the columns. The smaller second dimension column uses the same 100 µm i.d. capillary; however, this now is a match in cross-sectional area and should not cause a decrease in system performance.

Conclusions.

GCxGC separations utilizing silicon MEMS columns have been achieved using both a pneumatic and a thermal modulator. Both modulators show great trapping and focusing effects and the columns show good separation in both dimensions. It appears

that separation in the second dimension can be improved by eliminating unnecessary pressure restrictions. For thermal modulation a narrower second dimension column is required.

Modeling work shows that having a smaller second dimension column will have a higher tolerance for operation at higher linear velocities. Based on the model a 25-cm column should generate approximately 2500 plates at a flow rate of 0.65 mL/min. Peak widths in the second dimension currently are between 100-250ms full width at half height. By going to a narrower second dimension column this number can be greatly improved.

Pneumatic modulation is particularly attractive for field portable instrumentation. There are no-consumables and is of low maintenance. Since the valve is outside of the flow path the upper temperature limit is regulated by the upper temperature limit of the stationary phase. Another advantage to pneumatic modulation is the fact that there is no limitation in terms of volatility of the target analytes. However, with pneumatic modulation there is not as much focusing that occurs in comparison to thermal modulation. The focusing that does occur is due to gas compression and depending on the column head pressure this could not be sufficient enough to increase the detectability of trace components.

Thermal modulation does have the increase in focusing capabilities that is lacking in pneumatic modulation. The thermal modulator used in this study uses no consumables. It was designed to be used for field-portable use. The modulator is capable of producing peak widths in the second dimension of 25ms. By obtaining narrower peaks in the second dimension there is an increase in peak capacity.

Using this modulator with the micro-fabricated columns there shows great separation in both the first and second dimensions. Either one of these modulators used in combination with the microfabricated columns will generate a very powerful portable analytical instrument. Also, by using the smaller cross-sectional area columns for the second dimension, there will be a higher linear velocity. This higher velocity means that the hold up time on the second dimension column would be significantly reduced. This would increase the peak capacity even more.

There is future testing that needs to be done on the new column dimensions and the performance of these columns when integrated to these modulators. Also, coating of a differently polar stationary phase will help utilize more of the separation plane.

Column efficiency on the new column dimensions has been modeled but empirical data has not yet been collected. In addition to changing the column dimensions the new columns also have corners that have been rounded off so there is no longer the 90° angle in the fluidic path. It is believed that the 90° angles cause band-broadening beyond that usually associated with longitudinal and non-equilibrium effects. Also, the inlet ports have been etched deeper to accommodate the appropriate size fused silica capillary. This should minimize much of the additional pressure restriction that was seen with previous columns. Testing of these columns is needed.

References

1. Phillips, J.B.; Luu D,; Pawliszyn, J.B.; *Anal. Chem.*, **1985**, 57, 2779-2787.
2. Phillips, J.B.; Beens, J.; *J. of Chromatogr.* **1999**, 856, 331-347.
3. Bertsch, W.; *J. High Resol. Chromatogr.* **2000**, 23, 167-181.
4. Frysinger, G.S.; Gains, R.B.; *J. High Resol. Chromatogr.*, **2000**, 23, 197-201.
5. Dimandja, J.M.; *American Laboratory*, **2003**, 2, 42-53.
6. Frysinger, G.S.; Gaines, R.B.; Ledford, E.B.; *J. High Resol. Chromatogr.*, **1999**, 22, 195-200.
7. M. Adahchour, J. Beens, R.J.J. Vreuls, A.M. Batenburg, U.A.Th. Brinkman, *J. Chromatogr. A*, **2004,** 47, 1054.
8. B.L. Winniford, K. Sun, J.F. Griffith, J.C. Luong, *J. Sep. Sci.*, **2006**, 29, 664.
9. L.L.P. van Stee, J. Beens, R.J.J. Vreuls, U.A.Th. Brinkman, *J. Chromatogr. A*, **2003**, 89, 1019.
10. R. Hua, J. Wang, H. Kong, J. Liu, X. Lu, G. Xu, *J. Sep. Sci.*, **2004**, 27, 691.
11. F.C.Y. Wang, W.K. Robbins, M.A. Greaney, *J. Sep. Sci.*, **2004**, 27, 468.
12. F. Adam, F. Bertoncini, N. Brodusch, E. Durand, D. Thi´ebaut, D. Espinat, M.-C. Hennion, *J. Chromatogr. A*, **2007**, 55, 1148.
13. C. von Muhlen, C.A. Zini, E.B. Caramao, P.J. Marriott, *J. Chromatogr. A*, **2006**, 39, 1105.
14. C. Vendeuvre, F. Bertoncini, L. Duval, J.-L. Duplan, D. Thiebaut, M.-C. Hennion, *J. Chromatogr. A*, **2004**, 1056, 155.
15. C. Vendeuvre, R. Ruiz-Guerrero, F. Bertoncini, L. Duval, D. Thiebaut, M.-C. Hennion, *J. Chromatogr. A*, **2005**, 1086, 21.
16. R. Edam, J. Blomberg, H.-G. Janssen, P.J. Schoenmakers, *J. Chromatogr. A*, **2005**, 1086, 12.
17. R.K. Nelson, B.M. Kile, D.L. Plata, S.P. Sylva, L. Xu, C.M. Reddy, R.B. Gaines, G.S. Frysinger, S.E. Reichenbach, *Environ. Forens.*, **2006**, 7, 33.
18. Ch.M. Reddy, R.K. Nelson, S.P. Sylva, L. Xu, E.E. Peacock, B. Raghuraman, O.C. Mullins, *J. Chromatogr. A*, **2007**, 1148, 100.
19. J.F. Hamilton, A.C. Lewis, M. Millan, K.D. Bartle, A.A. Herod, R. Kandiyoti, *Energy Fuels*, **2007**, 21, 286.

20. J. Blomberg, T. Riemersma, M. van Zuijlen, H. Chaabani, *J. Chromatogr. A*, **2004**, 1050, 77.
21. R.-G. Rosario, V. Colombe, Th. Didier, B. Fabrice, E. Didier, *J. Chromatogr. Sci.*, **2006**, 44, 566.
22. K.J. Johnson, B.J. Prazen, D.C. Young, R.E. Synovec, *J. Sep. Sci.*, **2004**, 27, 410.
23. C. Vendeuvre, F. Bertoncini, D. Espinat, D. Thiebaut, M.-C. Hennion, *J. Chromatogr. A*, **2005**, 1090, 116.
24. V.G. vanMispelaar, H.-G. Janssen, A.C. Tas, P.J. Schoenmakers, *J. Chromatogr. A*, **2005**, 1071, 229.
25. C. Debonneville, A. Chaintreau, *J. Chromatogr. A*, **2004**, 1027, 109.
26. C. Cordero, C. Bicchi, D. Joulain, P. Rubiolo, *J. Chromatogr. A*, **2007**, 1150, 37.
27. M. Adahchour, J. Beens, R.J.J. Vreuls, A.M. Batenburg, U.A.Th. Brinkman, *J. Chromatogr. A*, **2004**, 1054, 47.
28. M. Adahchour, L.L.P. van Stee, J. Beens, R.J.J. Vreuls, M.A. Batenburg, U.A.Th. Brinkman, *J. Chromatogr. A*, **2003**, 1019, 157.
29. M.S. Dunn, N. Vulic, R.A. Shellie, S. Whitehead, P. Morrison, P.J. Marriott, *J. Chromatogr. A*, **2006**, 1130, 122.
30. F. David, Ch. Devos, P. Sandra, *LC–GC Eur.*, **2006,** 602.
31. B.d'A. Zellner,A. Casilli, P. Dugo, G. Dugo, L. Mondello, *J. Chromatogr. A*, **2007**, 1141, 279.
32. T.C. Tran, P.J. Marriott, *Atmos. Environ.*, **2007**, 41, 5756.
33. F. Gogus, M.Z. Ozel, A.C. Lewis, *J. Sep. Sci.*, **2006**, 29, 1217.
34. C. Vendeuvre, F. Bertoncini, L. Duval, J.-L. Duplan, D. Thi´ebaut, M.-C. Hennion, *J. Chromatogr. A*, **2004**, 1056, 155.
35. S. de Koning, E. Kaal, H.-G. Janssen, Ch. van Platerink, U.A.Th. Brinkman, J. Chromatogr. A (in press).
36. M. Adahchour, E. Jover, J. Beens, R.J.J. Vreuls, U.A.Th. Brinkman, *J. Chromatogr. A*, 2005, 1086, 128.

37. N. Ochiai, T. Ieda, K. Sasamoto, A. Fushimi, Sh. Hasegawa, K. Tanabe, Sh. Kobayashi, *J. Chromatogr. A*, **2007**, 1150, 13.
38. S. Morales-Muñoz, R.J.J. Vreuls, M.D. Luque de Castro, *J. Chromatogr. A*, 2005, 1086, 122.
39. S. Penet, C. Vendeuvre, F. Bertoncini, R. Marchal, F. Monot, *Biodegradation*, **2006**, 17, 577.
40. G.F. Slater, R.K. Nelson, B.M. Kile, Ch.M. Reddy, *Org. Geochem*. **2006**, 37, 981.
41. M. Kallio, T. Hyötyläinen, *J. Chromatogr. A*, **2007**, 1148, 228.
42. M. Shimmo, T. Hyötyläinen, M. Kallio, P. Antifa, M.-L. Riekkola, *LC–GC Eur*., **2004**, 17, 640.
43. J.F. Hamilton, P.J. Webb, A.C. Lewis, J.R. Hopkins, S. Smith, P. Davy, *Atmos. Chem. Phys.*, **2004**, 4, 1279.
44. X. Xu, L.L.P. van Stee, J.Williams, J. Beens, M. Adahchour, R.J.J. Vreuls, U.A.Th. Brinkman, J. Lelieveld, *Atmos. Chem. Phys.*, **2003**, 3, 665.
45. X. Xu, J. Williams, C.P. D¨ulmer, H. Berresheim, G. Salisbury, L. Lange, J. Lelieveld, *Atmos. Chem. Phys.* **2003**, 3, 1461.
46. M. Kallio, M. Jussila, T. Rissanen, P. Anttila, K. Hartonen, A. Reissell, R. Vreuls, M. Adahchour, T. Hy¨otyl¨ainen, *J. Chromatogr. A*, **2006**, 234, 1125.
47. W.Welthagen, J. Schnelle-Kreis, R. Zimmermann, *J. Chromatogr.A*, **2003,** 233, 1019.
48. W. Welthagen, J. Schnelle-Kreis, R. Zimmermann, *J. Aeros. Sci*., **2004**,17,35.
49. L. Vogt, Th. Gröger, R. Zimmermann, *J. Chromatogr. A*, **2007**, 2, 1150.
50. M. McGuigan, J.H. Waite, H. Imanaka, R.D. Sacks, *J. Chromatogr. A*, **2006**, 280, 1132.
51. R.K. Nelson, B.M. Kile, D.L. Plata, S.P. Sylva, L. Xu, C.M. Reddy, R.B. Gaines, G.S. Frysinger, S.E. Reichenbach, *Environ. Forens.*, **2006**, 7, 33.
52. C.G. Johnson, G.S. Frysinger, R.K. Nelson, R.B. Gaines, N. Ohkouchi, C.M. Reddy, T.I. Eglinton, *Mar. Chem.*, **2003**, 5, 83.
53. H.C. Trap, M. van der Schans, *LC–GC Eur*., **2007**, 202.

54. J. Schnelle-Kreis,W.Welthagen, M. Sklorz, R. Zimmermann, *J. Sep. Sci.*, **2005**, 28, 1648.
55. Z. Parsi, T. G´orecki, J. Poerschmann, *LC–GC Eur.*, **2005**, 18, 582.
56. J.M. Sanchez, R.D. Sacks, *Anal. Chem.*, **2006**, 78, 3046.
57. M. Libardoni, P.T. Stevens, J. Hunter Waite, R. Sacks, *J. Chromatogr. B*, **2006**, 13, 842.
58. Lui, Z.; Phillips, J.B.; *J. Chromatogr. Sci.,* **1991**, 29, 227-231.
59. M. Adahchour, J. Beens, R.J.J. Vreuls, U.A.Th. Brinkman, *Trends Anal. Chem.*, **2006**, 438, 25.
60. Pursch, M.; Sun, K.; Winniford, B.; Cortes, H.; Weber, A.; McCabe, T.; Luong, J.; *Anal. Bioanal. Chem.,* **2002**, 373, 356-367
61. Bruckner, C.A.; Prazen, C.A.; Synovec, R.E.; *Anal. Chem.*, **1998**, 70, 2796-2804
62. Seeley, J.V.; Kramp, F.; Hicks, C.J.; *Anal. Chem.,* **2000**, 72, 4326-4352.
63. Seeley, J.V.; Bueno, P.A.; *J Chromatogr. A.,* **2004**, 1027, 3-10.
64. Lui, Z.; Sirimanne, S.R.; Patterson, D.; Needham, L.L.; Phillips, J.B.; *Anal.Chem.*, **1994**, 66, 3086-3092.
65. Phillips, J.B. et al., *J. High Resol Chromatogr.*, **1999**, 22, 3-10
66. Phillips, J.B.; Lui, Z., US Patent 5, 135, 549, **1992**.
67. Phillips, J.B.; Lui, Z., US Patent 5, 196, 039, **1993**.
68. Phillips, J.B.; Ledford, E.B.; *Field Anal Chem Tech*, **1996**, 1, 23-29.
69. de Geus, H.J.; de Boer, J.; Brinkmans, U.A.T.; *J Chromatogr. A.*, **1997**, 767, 137-151
70. Marriott, P.J.; Kinghorn, R.M.; *Anal. Chem.*, **1997**, 69, 2582-2588.
71. Beens, J.; Adahchour, M.; Vreuls, R.J.J.; van Altena, K.; Brinkmans, U.A.T.; *J. Chromatogr. A.,* **2001**, 919, 127-132.
72. Lambertus, G.R.; Sacks, R.D.; *Anal. Chem.*, **2005**, 77, 2078-2084.
73. Veriotti, T.; Sacks, R.; *Anal. Chem.,* **2001**, 73, 3045-3050.
74. Libardoni, M.J. et al. *J. Sep. Sci.*, **2006**, 29, 1001-1008.
75. Libardoni, M.J. et al. *Anal. Chem.*, **2005**, 77, 2786-2794.
76. Lambertus, G.R., et al. *Anal. Chem.*, **2004**, 76, 2629-2637.

Chapter 7
Conclusions

The research presented in the dissertation has been directed towards the development of high performance microfabricated separation columns for field portable and microfabricated instrumentation. This work describes the optimization of silicon/glass gas chromatography columns with numerous applications, including indoor and ambient air quality, industrial emissions control, breath analysis and homeland security. A static coating technique has been developed and optimized. Two static coated columns were connected in-series, utilizing the on-board heaters and temperature sensors, and separation enhancement has been achieved by varying the temperature programming ramps on each column independent of each other. Integration of these columns into two different testbed systems has been done. One system is comprised of completely microfabricated components and the other is a comprehensive two-dimensional gas chromatography system.

The static stationary phase deposition method relies on a positive pressure to fill the column. After filling, the inlet is sealed and the outlet of the column is connected to a vacuum pump. The solvent evaporates leaving behind a thin stationary phase film. Film thickness can be controlled by controlling the mass of stationary phase dissolved in the

solvent. Films also tend to be more uniform due to the lack of axial motion during the coating process.

A 3-m-long column coated with non-polar stationary phase generated ~12,500 theoretical plates and was thermally stable to at least 250°C in hydrogen and 200°C in air. Temperature programming for alkane vapors ranging from n-C_5 to n-C_{12} using a temperature programming rate of 10°C/min generated a peak capacity greater than 100 peaks in an analysis time of 500s. Complex mixture analysis of a 30-component test mixture and an air-phase petroleum hydrocarbon mixture were separated using a single 3-m nonpolar column.

Having a column that is coated with a thin uniform film allows for the separation of complex mixtures, and these columns do not need to be limited to targeted analysis. Through these new coating procedures, the microfabricated columns are achieving resolving powers comparable to commercially coated fused silica capillary columns.

One of the major challenges of the column coating procedure is finding an appropriate solvent for the moderately polar trifluoropropylmethyl(poly)siloxane and more work needs to be done on the development of better polar columns. This can be done by investigating new polar phases as well as surface pre-treatment. Polar columns have been coated but with limited success.

In Chapter 3 on-board heaters and temperature sensors have been used to temperature program separations without the need for a large convection oven. Using these heaters, temperature programming rates up to 1000°C/min have been achieved. This reduces overall analysis time and increases the vapor pressure range that can be sampled and separated. Also, by having the heaters and temperature sensors directly on

the columns, two columns connected in series can be temperature programmed at different rates. By having this separated temperature control over the columns, compounds that co-elute from the column ensembles can be separated. This has been achieved with two shorter columns and shows great potential to separate even more complex mixtures. This technique, however, is limited to targeted compound analysis.

After fully evaluating the columns on a component level, integration into a testbed system was performed. When integrating components, the system needs to be optimized to give the overall best performance. With both the Gen 0.6 system, as well as the GCxGC system, there were many more questions that came about when integrating all of the individual components. The Gen 0.6 system showed great initial results but the system has room for improvements. Many groundbreaking separations were obtained on this system. It was the first microfabricated system to ever utilize two microfabricated columns with independent temperature programming. Also, they were the most complex mixtures to be separated on a completely microfabricated system. It also has great potential to produce even better separations. By optimizing the polar column stationary phase, peak widths will be even narrower, and retention times will be reduced. Therefore, overall analysis times will decrease, and peak capacity on the system will increase. Investigation into surface deactivation needs to be done to help reduce tailing on very polar compounds. Determination of the sources of extra column band broadening on the integrated system and how to reduce them will also help increase overall system performance.

Then GCxGC system again shows great initial promise for the separation of complex mixtures. The initial separations show that the columns can be utilized in this

configuration. By narrowing the second dimension column, the long analysis times in the second dimension should be significantly reduced. Also, investigation of different polar stationary phase will allow for an increase in peak capacity by having a more orthogonal column pair. In connection with a low-resource modulator, a very powerful analytical instrument can be developed.

The work presented in this dissertation has demonstrated the use of microfabricated columns for the separation of complex mixtures. These columns will aid in the development of field portable microfabricated instrumentation that should be of use in a wide range of applications. Continued work towards the development and evaluation of a polar stationary phase will prove beneficial for increased performance of the testbed systems.